The mineralogy and isotope geochemistry of the Nopal I uranium deposit, Chihuahua, Mexico.

By

Alba Luz Saucedo Roacho

A Thesis submitted to the Faculty of Graduate Studies of

The University of Manitoba

In partial fulfilment of the requirements of the degree of

MASTER OF SCIENCE

Department of Geological Science

University of Manitoba

Winnipeg

Abstract:

The Nopal I uranium deposit located in northern Chihuahua Mexico has been the focus of study for the past 40 years. Information regarding to its formation and evolution through time demonstrate that it has a very complex history. Uranium mineralization occurs in two different styles: uranium oxide uraninite and a secondary phases of silicates (uranophane, soddyite) and oxyhydroxides (schoepite and ianthinite). Petrographic studies have revealed that uraninite is found encapsulated within the host rock (ignimbrites) as fine grains while secondary uranium minerals are filling fractures and micro-veins. Chemical dates from the uranium minerals give a wide range from 0 to 611 Ma; many of the ages may be overestimated since the host rock is 44 Ma. U/Pb isotopic studies demonstrate the presence of common Pb, and after a correction was applied, a new range of dates from 1< to 7 Ma was obtained.

Acknowledgments:

I would like to express my gratitude to the people who has been involved in many ways into this journey to discover another side of this beautiful discipline called Geology. I would like to thank to my advisors Dr. Mostafa Fayek and Dr. Alfredo Camacho to share their valuable knowledge, for supporting me with my studies and for their patience. I would also like to thank Dr. Panseok Yang for providing me assistance in the operation of the EMPA, Dr. Rong Liu with the operation of the SIMS and Sergio Mejía for his operation and help with the SEM. I would like to make a special thanks to my mother and brother for giving me the strength that I needed it to continue forward, and Alvaro López Picos for his support at the end of this road. Funding for this research was provided by a Natural Science and Engineering Research Council of Canada (NSERC), Discovery Grant to Fayek and the CRC program.

Tanto vivir entre piedras
yo he creído que conversaban
voces no sentí nunca,
pero el alma no me engaña
Algún algo han de tener
aunque parezcan calladas,
no de balde ha llenado Dios,
de secretos la montaña
Algo se dice en las piedras
a mí no me engaña el alma,
temblor, sombra o qué sé yo,
igual que si conversaran
¡Malhaya, pudiera un día,
vivir así, sin palabras!

Atahualpa Yupanqui

Table of Contents:

List of Figures:

Chapter 1. Introduction

Nuclear power generation (military and civilian) produces high-level radioactive waste in the form of spent nuclear fuel. This form of radioactive waste consists of several environmentally toxic, long-lived radionuclides with half-lives up to several hundred thousand years. Most countries agree that the safest and most cost-effective method of disposing of the spent nuclear fuel (SNF) is sub-surface disposal in a geologic repository. However, most geologic disposal concepts require that the spent fuel remain isolated from the accessible environment for more than 100,000 years (i.e., the time required for the fission and actinide products to reach safe levels). Therefore, one of the most challenging aspects of nuclear waste management is the extrapolation of laboratory data, collected over short periods of time (hours to years) to longer periods required in performance assessment calculations. Uranium deposits, by analogy, can provide important information on the long-term performance of radioactive waste forms and the radioactive waste repository because uraninite (UO_{2+X}), the most abundant uranium-bearing mineral in most uranium deposits, is similar in many ways to the UO_2 in spent nuclear fuel. For these reasons, detailed characterization of the uranium minerals provides information about the conditions under which uranium is mobile in sub-surface environments (Pearcy et al. 1994, Fayek et al, 2006).

In 1987, the U.S. Nuclear Waste Policy Act of 1982 (NWPA) designated Yucca Mountain, located in Nevada in the Western United States, as a candidate site

for the permanent disposal of high-level nuclear waste (HLNW). The HLNW to be stored at the Yucca Mountain repository consists mainly of spent fuel from commercial nuclear reactors (Pearcy et. al., 1994). This controversial storage site occurs within alternating layers of ignimbrite including welded, non-welded, and partially-welded tuff. Tuff has special physical, chemical and thermal characteristics that some experts believe make it a suitable material to entomb radioactive waste for the hundreds of thousands of years required for the waste to become safe through radioactive decay. Until recently, the Yucca Mountain Project (YMP) was the most advanced repository concept in the world. The U.S. Department of Energy (DOE) was in the licensing phase of the project and the YM site was scheduled to start receiving HLNW by 2017. However, the new Obama administration in 2009 has all but shut down the YMP (Ewing and von Hippel, 2009). Nevertheless some work on the geologic disposal of spent nuclear fuel (SNF) is still on-going.

The U.S. Department of Energy (DOE) has incorporated the study of natural analogues into the Yucca Mountain Project (YMP) to provide additional ways of testing process models that support the Yucca Mountain total system performance assessment (TSPA). The Peña Blanca uranium district is located approximately 50 km north of the city of Chihuahua, Mexico within a similar geologic environment that hosts the Yucca Mountain site and a similar climate. Exploration and development on the Sierra Peña Blanca was carried out between 1960 and 1978 by the Instituto Nacional de Energía Nuclear (INEN) and Uranio Mexicano (URAMEX) from 1978 to 1986 (George-Aniel et al., 1991, Goodell, 1981). Over a 100 uranium

anomalies where found, from which only three small low grade deposits were developed: Las Margaritas, El Puerto III, and El Nopal I (George-Aniel et al., 1991).

One of the first studies on the uranium district reported K-Ar ages that ranged from 54 Ma to 38 Ma for the volcanic sequences (Alba & Chávez, 1974). Calas (1977) published a brief description and proposed three genetic models for the three largest deposits (Nopal I, Las Margaritas and Nopal III) in the region. Goodell et al. (1979) and Goodell (1981) summarized the regional geology and gave generalized descriptions of the largest uranium deposits. Aniel (1983), Aniel et al. (1985), and George-Aniel et al. (1991) described the uranium and alteration mineral paragenesis of the largest deposits and identified three genetically different types of deposits. Magonthier (1984) showed how the volcanic sequence in Peña Blanca district is associated with the volcanic sequences in the Sierra Madre Occidental and Chaulot-Talmon (1984) was able to link Cenozoic tectonics in Sierra Madre Occidental with tectonic features observed in the vicinity of the largest uranium mines in Peña Blanca district. More recently investigators from Mexico (Reyes-Cortés, 1997), U.S.A. (Pearcy et al., 1994, 1995), and Europe (Calas et al., 2008) have worked on the Nopal I deposit, primarily to address questions pertaining to radionuclide transport in the unsaturated zone (UZ). Although Reyes-Cortés (1997) documented many structural and stratigraphic features associated with uranium mineralization from the Peña Blanca uranium district, he did not develop a tectonic model that included the formation of uranium deposits. Angiboust et al. (2012) refined the tectonic model of the district and identified four major tectono-magmatic fault and fracture systems

with uranium occurrences localed at the intersection of two or more of these fault systems. Based on the tectonic history, sulphur isotopic composition of sulphides and uranium mineralization, Angiboust et al. (2012) suggested that these deposits were part of a large uraniferous geothermal system that was mediated by bacteria. The periodic reactivation of the structures associated with regional tectonic events resulted in the precipitation of several generations of minerals where each new generation of minerals appears to have partially overprinted previous mineral assemblages.

Although there have been numerous studies on the uranium deposits from the Sierra de Peña Blanca including structural relations, mineralization, alteration and migration of uranium within these deposits, the age of these deposits is poorly constrained and documenting the mobility of uranium associated with near-surface uranium deposits such as the Nopal 1 deposit is essential to using these deposits as natural analogues for subsurface disposal of SNF (Pearcy et al., 1994, 1995; Goodell, 1985, 1981; Ildefonse et al., 1990; Reyes-Cortés, 1997; Fayek et al., 2006). The proposed models for the genesis of the Nopal I deposit and the fluid evolution suggest that the Nopal I deposit has had a protracted and complex fluid history (Bell, 1981; Pilcher, 1981; Goodell, 1985; Calas et al., 2008; George-Aniel et al., 1991; Reyes-Cortés, 1997; Fayek et al., 2006; Angiboust et al., 2012).

Therefore, the purpose of this study is to: 1) characterize the uranium minerals and refine their paragenesis from the Nopal I deposit, 2) determine the ages

of these minerals, and 3) based on the ages, relate the oxidation and precipitation of uranium minerals to tectonic or paleoclimatic events. The information from this study can be used to identify the geologic and paleoclimatic events that are responsible for uranium oxidation and migration in subsurface environments most similar to the YMP.

Chapter 2. Regional Geology

Mexico has been characterized into several tectono-stratigraphic terranes, basically composed of Precambrian basement, accretionated terranes and superjacent assemblages (Figure 2.1). Campa and Coney (1982) suggested three major divisions for the basement: 1) the north-western zone, characterized by autochtonous North American cratonic Precambrian basement mainly composed by an extensive suite of greenschist-facies of phyllite with sub-ordinate marble, metaconglomerate, quartzite and metagraywacke (Salas, 1968) with their Paleozoic-Mesozoic cover; 2) the eastern zone, surrounding the Gulf of Mexico, of late Paleozoic age with material accreted to the North American craton during the Appalachian-Ouachita Marathon orogeny, and 3) the western zone, characterized by assemblages of submarine volcanic and sedimentary rocks of late Mesozoic age deposited on unknown basement. This basement is covered by assemblages represented by the mid-Tertiary volcanic plateau of the Sierra Madre Occidental (SMO) and the late Tertiary trans-Mexican volcanic belt (TMVB).

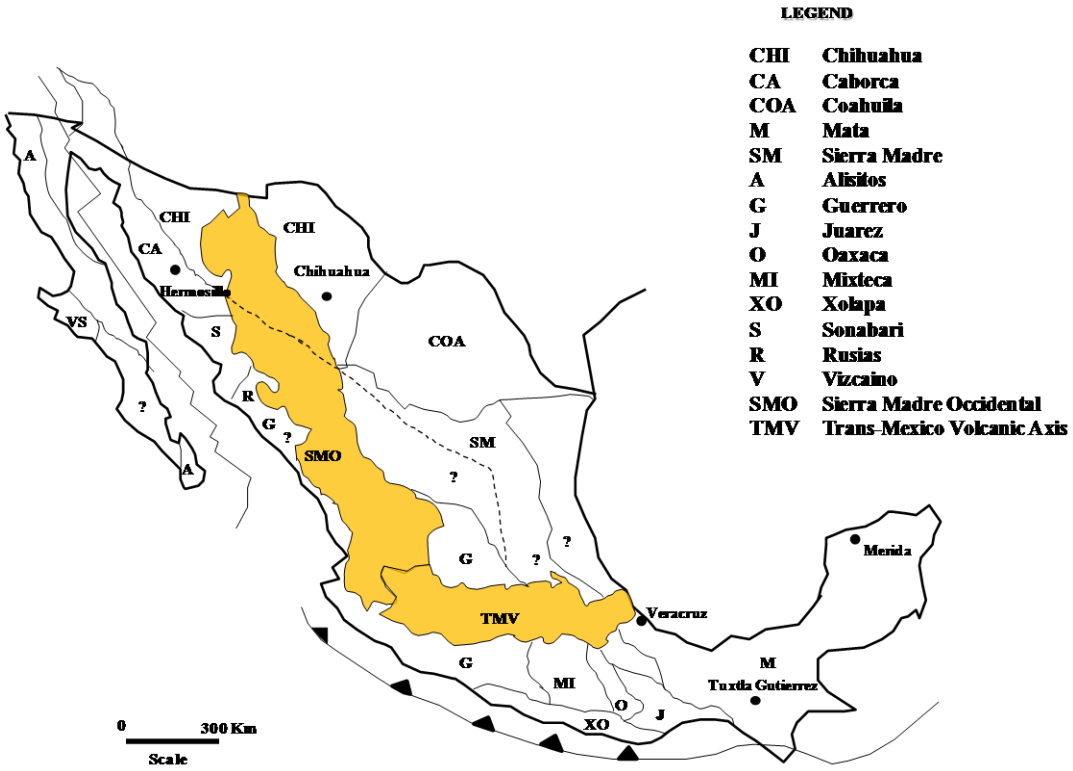

Figure 2.1. Tectono-stratigraphic terranes of Mexico from Campa and Coney (1982). Basement terrane boundaries are shaded thin black lines and superjacent assemblages (SMO and TMV) are colored in orange.

The north western zone can be further subdivided into the Chihuahua and Caborca terranes (Figure 2.1). The Chihuahua terrane is composed by the cratonic North America Precambrian basement rocks and overlain by 3000 m Paleozoic sandstones, shales, and limestones whose lithology is similar to those exposed in well known sequences in Arizona and New Mexico (Campa and Coney, 1982; Malpica and De la Torre, 1980). In the south eastern margin of the terrane, detrital sequences from the upper Paleozoic are close to the south western margin of the

Appalachian-Ouachita-Marathon orogenic belt (Figure 2.2) (Bridges, 1964). The north western frontal zone of the Paleozoic-Ouachita Marathon orogen is defined by deep-seated faults whereas the south western boundary is defined by a tectonic discontinuity described as Mojave-Sonora megashear separating Precambrian age belts and Paleozoic-early Mesozoic sedimentary sequences (Silver and Anderson, 1974). Younger sequences related to the transgression out of the Gulf of Mexico of late Jurassic and early Mesozoic age cover the terrane (Campa and Coney, 1982).

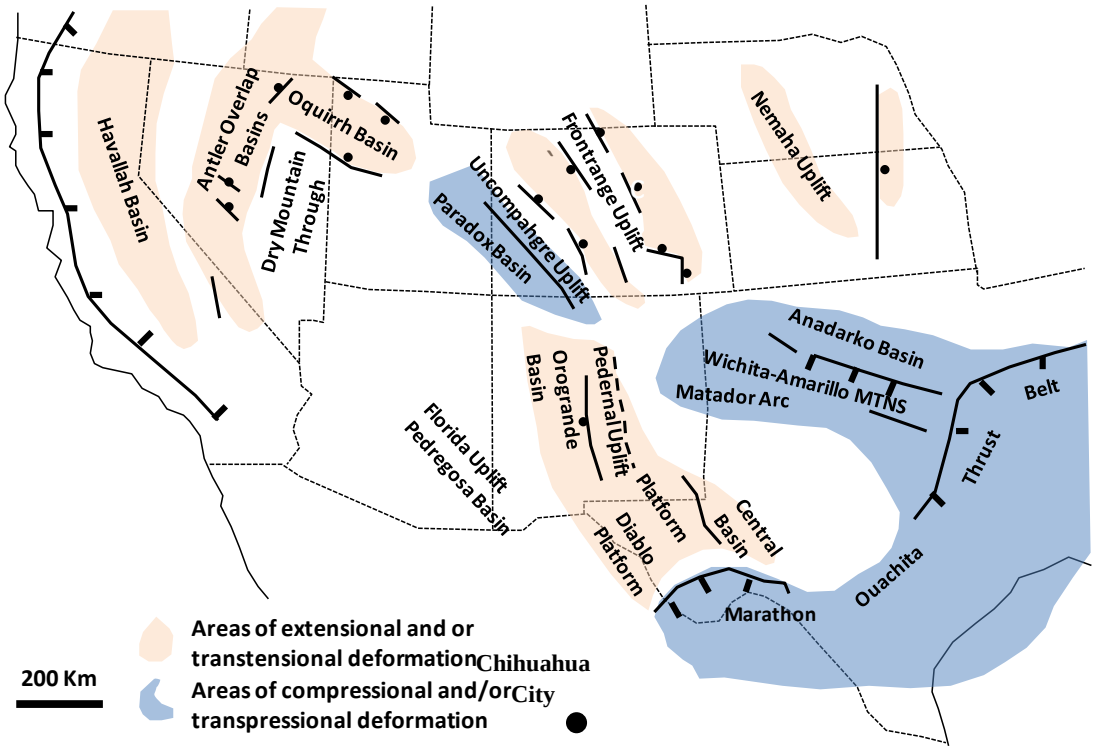

Figure 2.2. Distribution of extensional/transtensional deformation and compressional/transpressional deformation of the south western United States. In blue, continuation of the western Marathon Ouachita Thrust (from:http://www.colorado.edu/GeolSci/Resources/WUSTectonics/AncestralRockies/ouachita.html).

The Chihuahua terrain is located in the state of Chihuahua, north-central Mexico. The state can be divided in 2 physiographic regions: the Western half which is part of the Sierra Madre Occidental (SMO) province, and the Eastern half which corresponds to the Basin and Range (B&R). The SMO is a 2000 km long by 200-500 Km wide volcanic plateau that extends from the US-Mexico border to Guadalajara along the Western Mexican coast (Figure 2.1). The plateau consists mainly of silicic ignimbrites and, to a lesser extent, rhyolitic domes that cover about 393,000 km² with an average thickness of 1 km (Aguirre-Díaz and Labarthe-Hernández, 2003). The thick SMO volcanic sequence is the result of Cretaceous-Cenozoic magmatic and tectonic episodes related to the subduction of the Farallon plate beneath North America and to the opening of the Gulf of California (Campa and Coney, 1982). The highest elevation of the SMO in Chihuahua State is ~3000 m while moving eastward, the average graben elevation decreases from 2000 m to 700 m in the Rio Grande Valley, at the Texas border. These ranges commonly contain sedimentary rocks, mostly Cretaceous limestones and represent the northern extension of the Laramide folds of the Sierra Madre Oriental (Tardy, 1980). This 'thin-skinned' fold-and-thrust belt known as the Mexican fold belt is oriented in a NW-SE to NNW-SSE direction and controls the orientation of subsequent extensional basins. This folded system is covered by the SMO volcanics (Tardy, 1980).

The Laramide orogeny (Mesozoic to early Tertiary) produced folding, thrusting, uplift and calc-alkaline plutons and dikes (Livaccari, 1991). This dramatic compression event (between 80 Ma and 45 Ma) was accompanied by a thickening of the continental crust in western US and northern Mexico (Livaccari, 1991). In the Late Eocene-Oligocene significant uplifting and extension affected the entire volcanic sequence collapsing it and creating the Basin and Range province, but in discontinuous phases and rotation of least principal stresses.

Chaulot-Talmon (1984) and Aguirre-Díaz and Labarthe-Hernández (2003) showed that extensional tectonism occurred during deposition of SMO volcanic (around 38 and 23 Ma), coeval with NW striking dykes and faults could have served as conduits for the eruptions of large volumes of volcanic material; this extensional deformation is considered part of the pre-Basin and Range occurring between 36-30 Ma. The pre-Basin and Range has been also reported in the western U.S. along closely spaced listric normal faults, and produced highly tilted strata (Zoback et al., 1981). Classic Basin and Range structures date from Early Miocene ~ 22 to 5 Ma (Eaton, 1982).

Early Cenozoic tectonic events in Mexico are accompanied by widespread magmatism and McDowell and Clabaugh (1979) estimated that the total volume of ignimbrites is approximately 587,000 km^3 extruded by more than 200 calderas. Most ignimbrites of the SMO are related to numerous caldera complexes and fissure eruptions that formed between the Eocene-Oligocene 51 to 17 Ma (Aguirre-Díaz and

McDowell, 1991; Aguirre-Díaz and Labarthe-Hernández, 2003; Nieto-Obregón et al., 1981). The thickest ignimbrite unit erupted between 38-28 Ma (Aguirre-Díaz and McDowell, 1991). This voluminous ignimbritic flare-up coincides with the extensional Basin and Range tectonics (Figure 2.3).

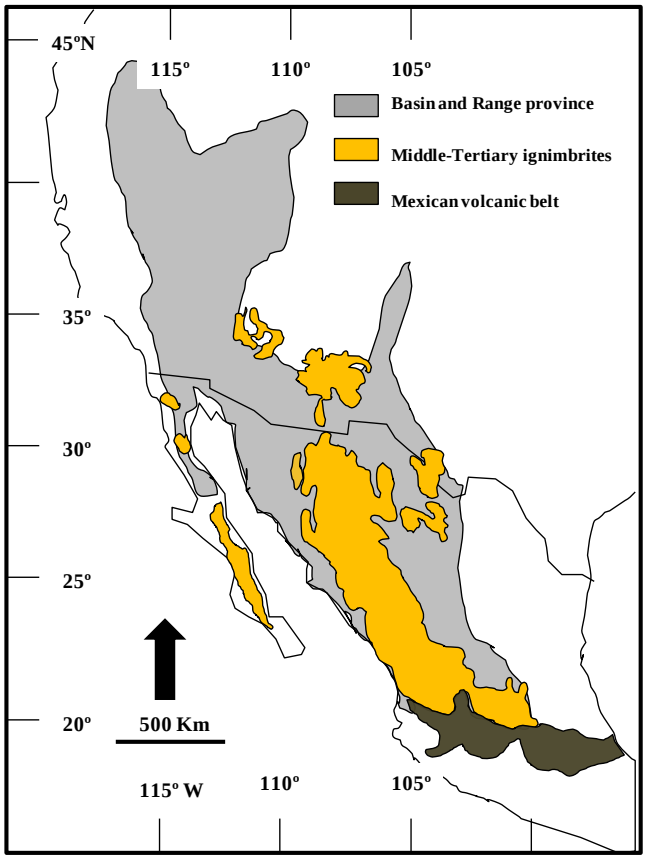

Figure 2.3. Distribution of middle Tertiary ignimbrite outcrops (SMO) in Mexico and south western United States, Basin and Range and Mexican volcanic belt structural provinces. In this figure can be notice that SMO ignimbrites and Basin and Range province overlap in space and time (from Aguirre-Díaz and Labarthe-Hernández, 2003).

The north-eastern part of the state of Chihuahua is at the boundary between the Basinand Range *s.s* tectonic province and the Rio Grande Rift (RGR). The RGR

is a series of deep *en echelon* grabens extending over 1000 km from central Colorado to New Mexico and most likely extending into west Texas and northern Chihuahua, Mexico (Chapin, 1979; Henry et al., 1983). Regional faulting is associated with the RGR extension which probably began ~32 Ma in New Mexico. Reverse rotational stresses located within the rift echelon fault along the Eastern Rockies-Great Palin boundary may have contributed to the development of the RGR in the late Cenozoic. In the southern part of the RGR, Seager et al (1984) reported two episodes of rifting: early rifting at ~20 Ma producing broad basins and a late, more intense episode of rifting at 10-3 Ma, which increased extension and modified the topography.

Stretching and thinning of the crust (i.e., development of the Basin and Range s.s and RGR) during the late Cenozoic was accompanied by warping and shallow upwelling of the asthenosphere, the emplacement of dykes, and the formation of volcanic complexes. There is a sharp compositional contrast between early and late volcanism, where the latter spans a range from basalt to high silica and peralkaline rhyolites (Christiansen and Lipman, 1972).

Tardy (1980) described two strike-slip crustal scale tectonic features in the region; the Texas lineament and Caltam lineament. Evidence of the Caltam lineament existence is the shifting and rotation of Laramian trends along eastern Chihuahua. This lineament (axis: N 120-130) is cut by the Sierra Peña Blanca horst, which is located 50 km to the northeast of Chihuahua City and is sinistrially shifted. The trace of this lineament disappears westward, covered by the thick SMO volcanic

sequence. This lineament did not influence Cenozoic graben formation. Moreover, this lineament could have provided an easy path for the emplacement of intrusive complexes (Chaulot-Talmon, 1984). The Texas lineament is a structure that traverses the southwest of the United States from Arizona, New Mexico, Texas and northern margin of Mexico. This lineament is composed by a number of strands and important breaks similar to a wide fracture or shear zone up to several miles wide at some places, with an *en echelon* pattern or discontinuous fractures. The importance of this lineament is that numerous occurrences have been form along its pattern from Bisbee to Cananea (northern Sonora).

Most of the units located at the northern portion of Chihuahua State dip to the north and are linked to Rio Grande Rift formation. Rocks corresponding to the Sierra Peña Blanca horst become progressively younger to the north (Calas, 1977); with the exception of a few small outcrops of Paleozoic metamorphic shales near Aldama, the basement is mostly made of gently folded early to middle Cretaceous limestones (Stege et al., 1981).

At the north east of Sierra Peña Blanca the dominant unit is made up of volcanics and volcano-clastic units (Cuervo Fm.), which are characterized by recumbent westward folds (anticlinal axis: N 145 – 170) and syn-sedimentary sequences formed during the late Laramide event (Calas, 1977). Sanidine phenocrysts from the Cuervo Fm gave an average age of 53 Ma (Reyes-Cortés, 2002).

The K-Ar ages on sanidines range from 37 to 44 Ma from Alba & Chávez (1974) for the volcanic rocks from the Nopal rhyolite; however, these ages are questionable because they are older when compared with ages obtained recently for similar rocks from West Texas (38-32 Ma) and Southern New Mexico (35-27.5 Ma) using the ^{40}Ar-^{39}Ar method (McIntosh and Bryan, 2000). The older K-Ar ages may be due to excess Ar and other problems intrinsic to the K-Ar method such as Ar loss, the presence of foreign inclusions and hydrated or devitrified glass.

The Peña Blanca district is also host to the largest number of uranium occurrences (up to 105 airborne anomalies) and the largest uranium deposits in Mexico. Many uranium occurrences also occur throughout the state of Chihuahua, including: (1) the "Mexican fold belt" (e.g., Placer de Guadalupe in Paleozoic formations; (Calas, 1977); (2) remobilized secondary uranium minerals in fractures or in the volcanics in the Sierra de Gomez; and (3) near the boundary between Peña Blanca, La Gloria, and San Marcos.

The Peña Blanca area is affected by several regional structural features (Reyes-Cortes, 1997; Angiboust et al., 2012). Fault and fracture orientations indicate four generations of extension (Figure 2.4). The first set or so-called stage 0 faults are confined to underlying limestones and have orientations of N 40 to N 70 and is considered the oldest event. This set does not affect the Pozos conglomerate. The second set of faults and fractures (stage 1) is along the western margin of the Peña Blanca area most noticeably striking to N 150 to N 175 and dip towards the east. The

third set of faults (stage 2) is more dominant along the eastern margin of the Sierra and is characterized by *en echelon* N-S faults. The latest fault network (stage 3) has an orientation of N 90 to N 120 and offsets the previous three stages of faults.

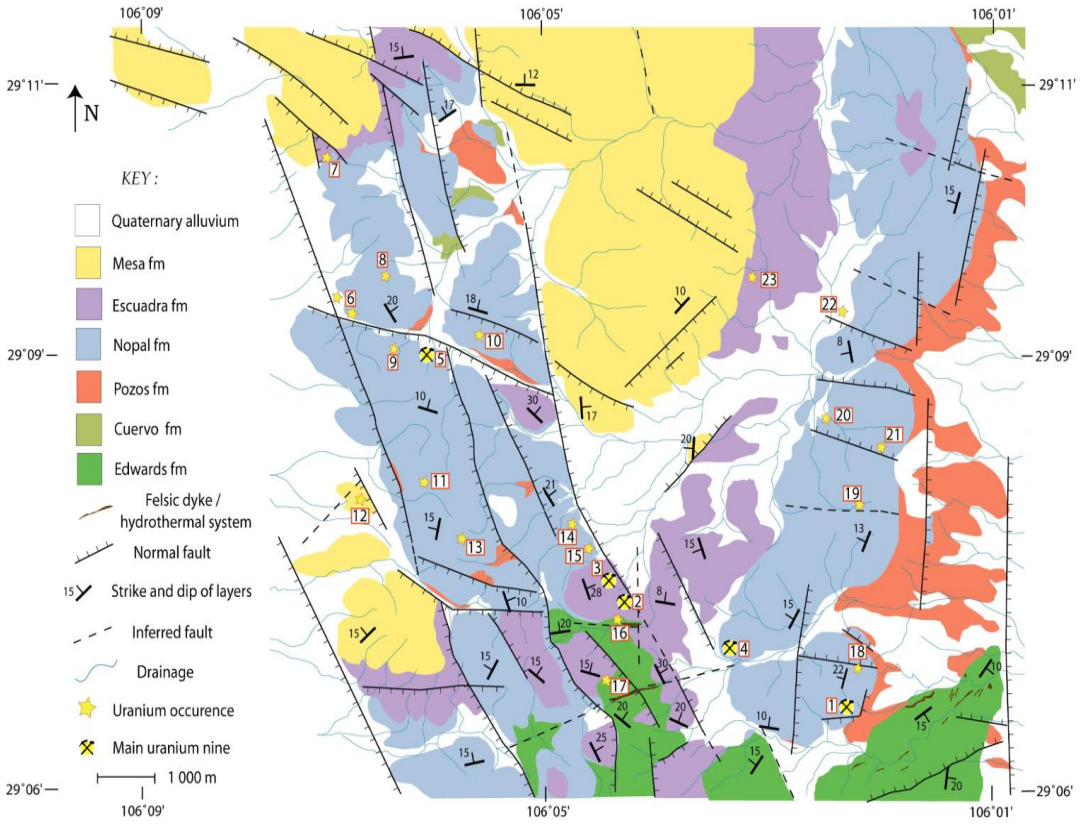

1 : Nopal I, 2 : Las Margaritas, 3 : Puerto III, 4 : Nopal III, 5 : Puerto II, 6 : Puerto 0, 7 : Cueva amarilla, 8 : unnamed, 9 : Puerto I, 10 : unnamed, 11 : Tascates II, 12 : Laguna del Diablo, 13 : Tascates I, 14 : Puerto V, 15 Puerto IV, 16 : Domitila, 17 : unnamed, 18 : Nopal II, 19 : unnamed.20 : Boquillas, 21 : Peña Blanca XVII, 22 : unnamed, 23 : unnamed (names from Aniel, 1982 based on Uramex internal report)

Figure 2.4. Structural map of the Peña Blanca District from Angiboust et al., (2012). Major lineaments on the western portion of the block correspond to the stage 1. N-S *en echelon* structures on the eastern side correspond to stage 2.

2.1 Deposit Geology

The Nopal I deposit is located ~50 km northeast of Chihuahua City (Figure 2.5). The deposit is hosted in a stratified series of felsic ignimbrites that unconformably overlie Cretaceous limestones (Angiboust et al., 2012). These ignimbrites include the lower part of the Nopal Fm which consists of an ash flow tuffs and a red vitrophyre (Reyes-Cortés, 1997, Dobson et al., 2008) (Figure 2.6).

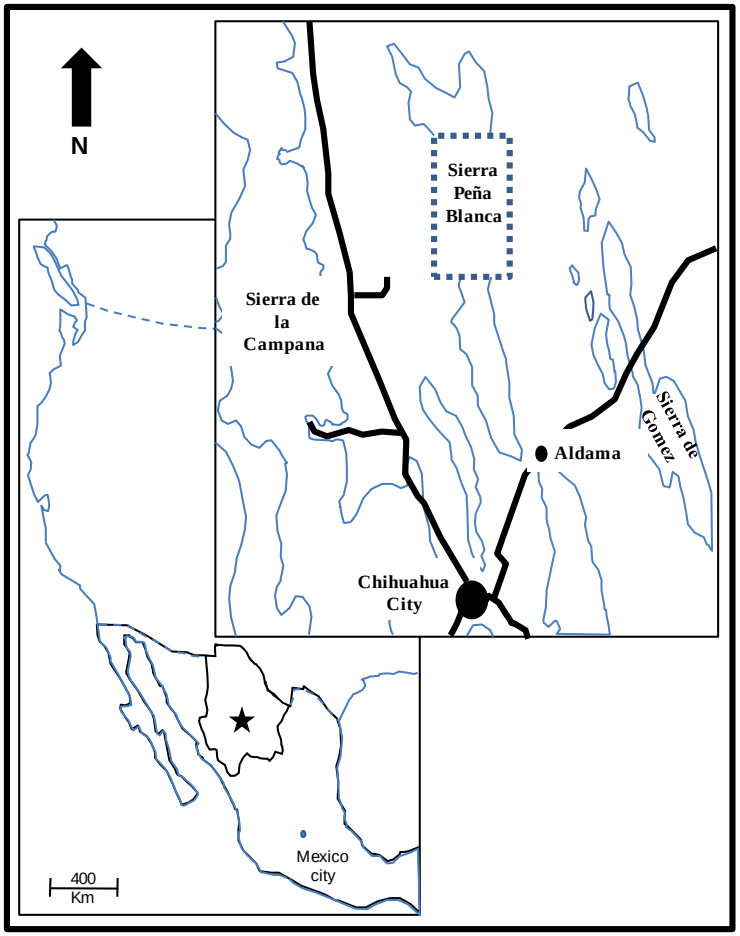

Figure 2.5. Location of the Sierra de Peña Blanca, Chihuahua, Mexico.

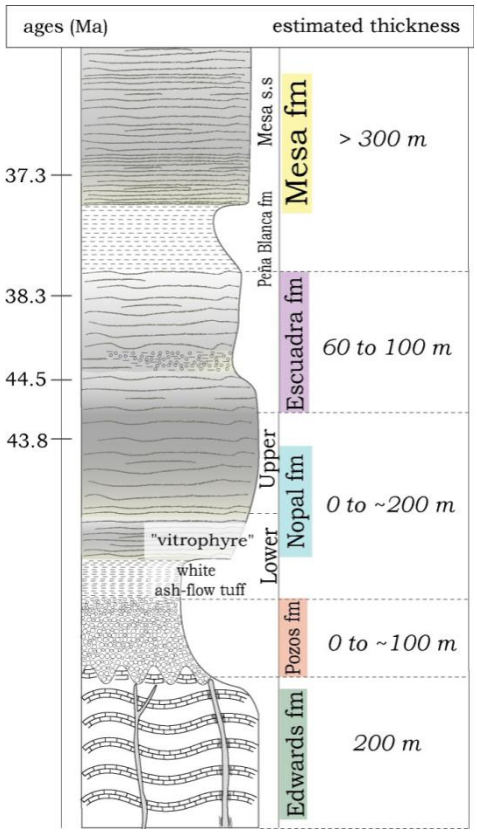

Figure 2.6. Stratigraphic column of the Peña Blanca area from Alba and Chavez (1974) and modified by Angiboust (2012).

Most of the uranium deposits, including the Nopal I deposit are associated with the Nopal Fm. Petrographic characterization of the Nopal Formation (Nopal Fm.) was carried out by Magonthier (1984, 1985) and George-Aniel et al. (1991). Recent petrographic characterization between unaltered samples from the Nopal Fm. and altered samples from to the Nopal I uranium deposit performed by Angiboust et al. (2012) revealed that upper Nopal rhyolite consists of welded pumice fragments and glass shards within an ash matrix. Features observed within the

unaltered rhyolite are replacement of glass shards by cristobalite and alkaline feldspars coupled with deformation while the vertical load increased. Devitrification of the glass and subsequent alteration of alkaline feldspars to kaolinite occurred when fluids (CO_2, H_2O) circulated throughout the units of ash-flows accompanied by cooling (Angiboust et al., 2012; George-Aniel et al., 1991). Breccia samples are altered to kaolinite, hematite and goethite.

The Nopal I uranium deposit is 20 m wide and 40 m in length. It extends approximately 100 m below the surface and 130 m above the water table. The Nopal I deposit formed at the intersection of two prominent fault and fracture systems (Figure 2.7; Fayek et al., 2006; Angiboust et al., 2012). Field relations indicate that two dominant fault and fracture systems bound the southwestern and north-eastern margins of the Nopal I deposit. The south-western fault is nearly vertical and strikes 305^o. Slickensides on the fault plunge dip 20^o to the southwest. The fracture system that bounds the north-eastern margin of the deposit strikes ~350^o and shows very little vertical or horizontal movement. A third fault system is exposed along the +10 level (the top) of the deposit. This fault is sub-horizontal, and dips ~20^o to the west, and has slickensides that trend 260^o. The south-west and north-east bounding fault and fracture systems occur throughout the Nopal I deposit and appear to have channelled subsequent fluid flow. Detailed mapping of the Nopal I deposit shows that brecciation intensifies towards the south, where the west and east bounding fault and fracture systems intersect. Movement along the southwest bounding fault

appears to have increased brecciation, which in turn enhanced permeability. As a result, the deposit is zoned, with increasing oxidation towards the southern portion. Other minor and younger fault and fracture systems (e.g., E-W fracture system described by Pearcy et al., 1994; 1995) also occur throughout the deposit. These younger fracture systems appear open and permeable to meteoric fluids. The young fractures are lined with secondary U^{6+} minerals where they intersect the main ore body.

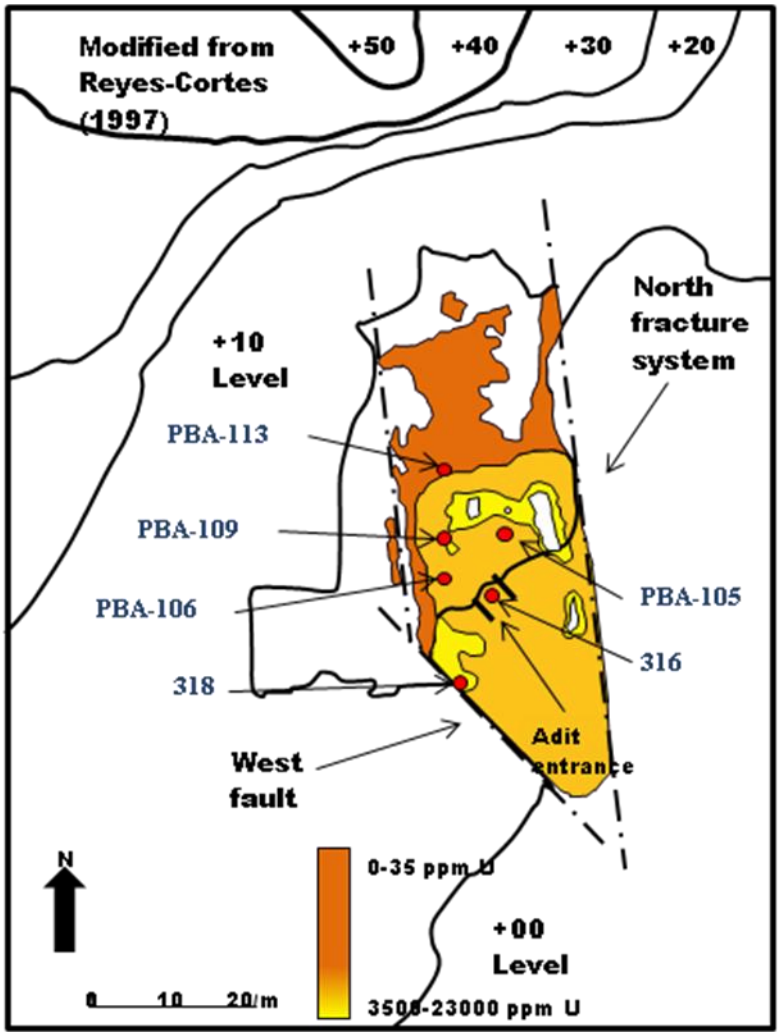

Figure 2.7. Plan view of the El Nopal I from the +00 to +50 levels. Color indicates uranium concentration. Deposit limits are characterized by a north fracture system and a vertical fault located at the western side. Red dots correspond to samples located inside of the adit.

Chapter 3: Methodology

3.1 Overview

A total of 40 hand samples from the Nopal rhyolite, Nopal vitrophyre and across the breccia along the face between the +00 and +10 levels were taken to document and understand the degree of alteration of the breccia. Twelve hand samples from inside the breccia along the adit between levels +00 and +10 were also characterized.

Seventeen samples were chosen for more detailed petrographic characterization and microprobe analyses. Radiogenic isotopic analyses were performed on five samples. Samples correspond to different zones: 1) highly silicified and insulated main body, 2) at the surface of the breccia, and 3) located at the west fault or west limit.

Polished thin sections were prepared to identify the uranium minerals, their alteration products and their paragenesis. Minerals were identified using transmitted and reflective light microscopy, and scanning electron microscopy (SEM) backscatter electron imaging (BSE). Chemical composition of uranium minerals was determined using electron microprobe (EMP).

3.2. Analytical techniques

3.2.1 Scanning Electron Microscopy

Polished thin-sections were analysed using a Cambridge Stereoscan 120 scanning electron microscope (SEM) at the University of Manitoba. The samples were cleaned and carbon coated to ensure sample surfaces would be conductive. The samples were then mounted and placed under vacuum and analyzed with a 15 keV electron beam. Backscattered electron images were collected and electron dispersive spectroscopy (EDS) was used to characterize the samples.

3.2.2 Electron Microprobe

The composition of uranium minerals from all samples was obtained by electron microprobe (EMP) wavelength-dispersive spectroscopy and an automated CAMECA SX-100 X-ray microanalyzer. Analyses were performed using the following analytical conditions: 15 keV, a beam diameter varied from 10 μm and 1 μm, with counting times of 40 seconds per element. The following elements were analyzed: sodium (Na), aluminum (Al), silicon (Si), potassium (K), calcium (Ca), iron (Fe), titanium (Ti), lead (Pb), vanadium (V) and sulphur (S). To calibrate Ca, diopside was used as standard, pyrite for S, sphene for Ti, UO_2 for U, fayalite for Fe, TePb for Pb, andalusite for Al, ThO_2 for Th, orthoclase for K and V_2O_7 for V. Detection limits in uranium minerals is 0.1 wt%. Matrix corrections were made using

ZAF. Oxygen content of uraninite and secondary uranium minerals were calculated by stoichiometry assuming an ideal composition.

Chemical Pb ages of uranium minerals were calculated using the method by Bowles (1990) which is based on the U/Th, and Pb concentrations measured using the EMP. The assumptions are: 1) all Pb is radiogenic, 2) the Pb concentration increases with time, and 3) the mineral was closed to Pb loss or U gain. A problem arising from this method is that not all Pb is radiogenic in origin and that the contribution of common lead can cause an error in age determination due to the difficulty in differentiating lead origin. Common lead contribution will increase Pb concentration and the total Pb within minerals, that is common lead and radiogenic lead will give an erroneous age. Equation [1] described below was used to calculate chemical Pb ages:

$$\mathbf{Pb} = \frac{Th}{232} x \left(e^{(\lambda^{232} x t x 10^6)} - 1 \right) x 208 + \frac{U}{238.04} x 0.007196 \left(e^{(\lambda^{235} x t x 10^6)} - 1 \right) x 207$$

$$+ \frac{U}{238.04} x 0.99276 \left(e^{(\lambda^{238} x t x 10^6)} - 1 \right) x 206$$

[1]

where Pb, U and Th are the atom wt% measured and converted into ppm by multiplying atom wt% by 10^4; $\lambda^{232} = 4.95x10^{-11}$, $\lambda^{235} = 9.85x10^{-10}$, and $\lambda^{238} = 1.55x10^{-10}$, are the decay constants of ^{232}Th, ^{235}U and ^{238}U. The values 0.007196 and 0.99276 are the natural abundances of ^{235}U and ^{238}U, respectively. Analytical

precision for each analytical point is ±0.1 wt% for U, Th and Pb, which is roughly equivalent to ±10 Ma.

3.2.3 Secondary Ion Mass Spectrometry (SIMS)

3.2.3.1 Radiogenic Isotopes

The isotopes of lead and uranium in Nopal I uranium mineral samples were measured by secondary ion mass spectrometry (SIMS) using a CAMECA IMS 7F ion microprobe. Operating conditions for U and Pb analysis were ~5.5-nA primary ion beam of O^- accelerated at 12.5 keV. The secondary accelerating voltage was set to 8 kV. A voltage offset of -50 V in conjunction with a mass resolving power of 1400 was used to eliminate isobaric interferences. Ions were detected with an ETP electron multiplier coupled with an ion-counting system. A typical analysis lasted ~45 minutes, comprising 100 cycles per analysis. The following isotopic ratios were calculated: $^{206}Pb^+/^{204}Pb^+$, $^{207}Pb^+/^{204}Pb^+$, $^{207}Pb^+/^{206}Pb^+$, $^{235}U^+/^{238}U^+$, $^{206}Pb^+/^{238}U^+$, $^{207}Pb^+/^{235}U^+$, $^{238}UO^+/^{238}U^+$ and $^{238}U^+/\ ^{238}U^+ + {}^1H^+$, $^{234}U/^{238}U$. $^{230}Th/^{238}U$, $^{230}Th/^{234}U$ and reported in %.

U/Pb and U/Th isotopic ratios were corrected for instrumental mass fractionation (IMF) using a similar method described by Fayek et al. (2005) and for common lead. Corrected ratios of $^{206}Pb/^{204}Pb$ and $^{238}U/^{204}Pb$ were used to calculate U-Pb ages for minerals that show enough radiogenic ^{206}Pb by using the following equation [1]:

$$\frac{^{206}Pb}{^{204}Pb} = \left(\frac{^{206}Pb}{^{204}Pb}\right)_i + \frac{^{238}U}{^{204}Pb}\left(e^{\lambda^{238} x\, t} - 1\right) \quad [1]$$

where $^{206}Pb/^{204}Pb$ is the isotopic ratio of Pb measured by ion probe in minerals, $(^{206}Pb/^{204}Pb)\mathbf{i}$ is the initial isotopic ratio (18.7), $^{238}U/^{204}Pb$ is the isotopic measured by ion probe in minerals and $\lambda^{238} = 1.55125 \times 10^{-10} y^{-1}$ is the decay constant of ^{238}U.

Age calculation based on U-Th Disequilibria Series was applied by using the activity ratios of $^{234}U/^{238}U$, $^{230}Th/^{238}U$ and $^{230}Th/^{234}U$. The activities can be calculated in two ways: 1) using the counts per second of each species (e.g., ^{234}U) and multiplying them by their respective decay constant or 2) correct the mass bias of the isotopic ratios and divided them by their respective abundances. Activities obtained were used to calculate the age using the following equation:

$$\mathbf{t} = \left\{\frac{-1}{\lambda^{230}}\right\} x\ \ln\left(1 - \left(\frac{^{230}Th}{^{234}U}\right)_A\right) \quad [1]$$

where ($^{230}Th/^{234}U$)A and ($^{234}U/^{238}U$) are the activity ratios of the respective mineral, t stands for time, $^{230}\lambda = 9.19x10^{-06}$ and $^{234}\lambda = 2.83x10^{-06}$ are the decay constants of ^{230}Th and ^{234}U, respectively.

Chapter 4. Results

4.1 Field Observations

The Nopal Fm is characterized by layers of pumice intercalated with lithic fragments. The Nopal Fm is typically brecciated and highly oxidized with altered (bleached) zones along the margins of fractures (Angiboust et al., 2012). The alteration of feldspar into clay and the presence of hematite is usually associated with voids and fractures. A highly altered ash-rich silicified zone of approximately 35 m occurs at the base of the Nopal Fm.

Four alteration zones, which mainly relate to the size of breccia clasts and degree of alteration of the Nopal Fm, were identified by mapping the exposures between the 0+00 and the 0+10 level of the Nopal I deposit (Figure 4.1 and Figure 4.2). These are,

Zone one is characterized by fragments that are >1 m in size with little or no matrix. Uranium minerals such as uraninite (black) and secondary uranium minerals (yellow and green) are abundant (Figure 4.3). Although the rocks from this zone are extensively altered to kaolinite and hematite, unaltered phenocrysts of K-feldspar are still preserved (Figure 4.4).

Zone two fragments are <1m in diameter within a matrix of oxide and clay minerals (Figure 4.5). This zone is devoid of uraninite and contains only secondary uranium minerals.

Zone three contains fragments that are <30 cm in size and is highly oxidized and kaolinitized (Figure 4.6). This zone is distinct from the other three in that green opal is found as a coating on the surface of outcrops (Schindler et al., 2010). The uranium minerals in zone three are largely secondary.

Zone four, which is proximal to the south-western fault, is characterized by small (~5 cm) highly oxidized breccia fragments from the Nopal rhyolite (Figure 4.7). Uranophane is the only uranium mineral observed in outcrop. Uranium concentrations are highest (~35,200 ppm) in zone one decreasing values away from zone one (Figure 4.8).

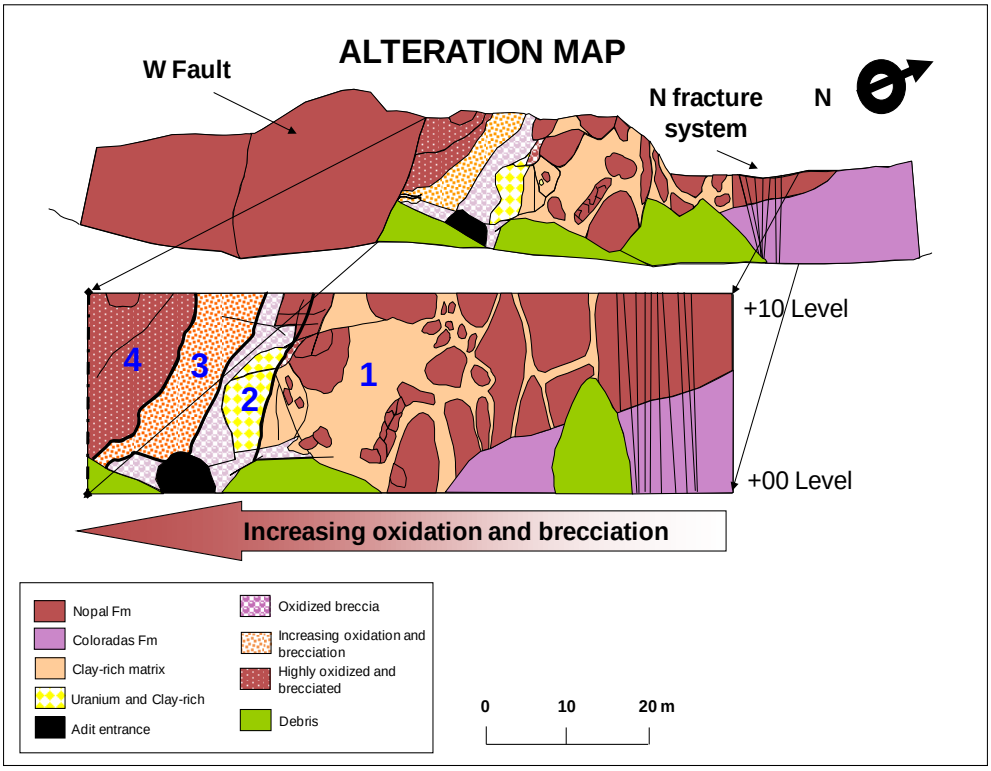

Figure 4.1 A map of the alteration zones at the Nopal I Uranium Deposit. Large numbers 1 to 4 correspond to the alteration zones described in text.

Figure 4.2 Outcrop sample location along the face of the breccia zone between the 0+00 and the 0+10 levels.

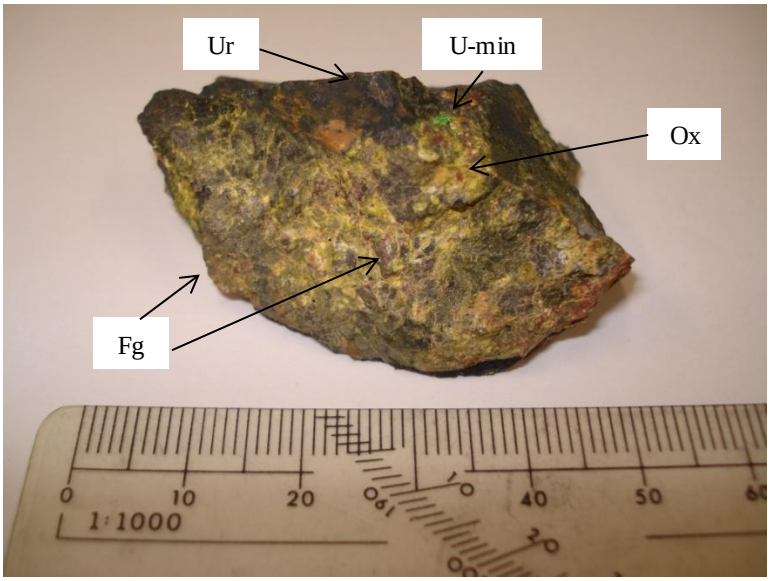

Figure 4.3 Sample PBA-105 from zone one from inside the adit between levels 0+00 and 0+10. Uraninite (Ur) and secondary uranium minerals (U-min) cement highly silicified rock fragments (Fg). Oxides (Ox) are present mostly within the rock fragments.

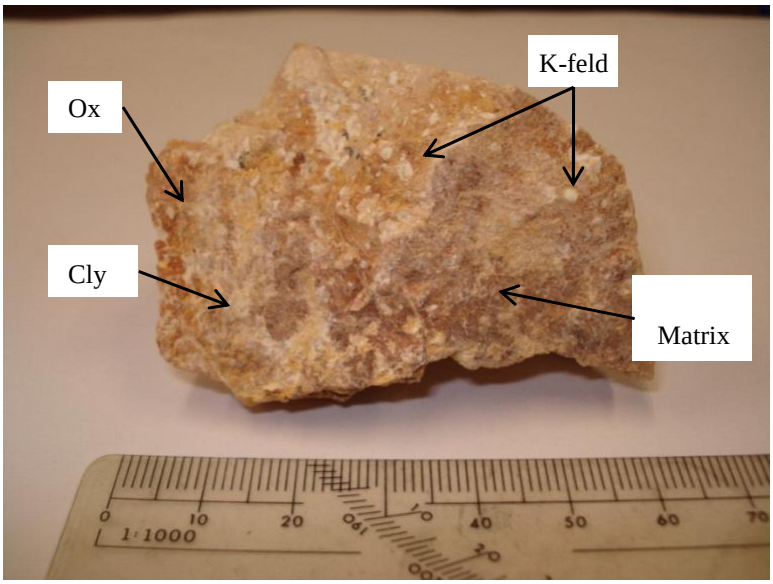

Figure 4.4 Sample 311 from zone of brecciation in the eastern margin (zone 1) of the Nopal Deposit along the face between the 0+00 and 0+10 levels. Phenocrysts of K-feldspar have been partially altered into clay (Cly) along with oxides (Ox).

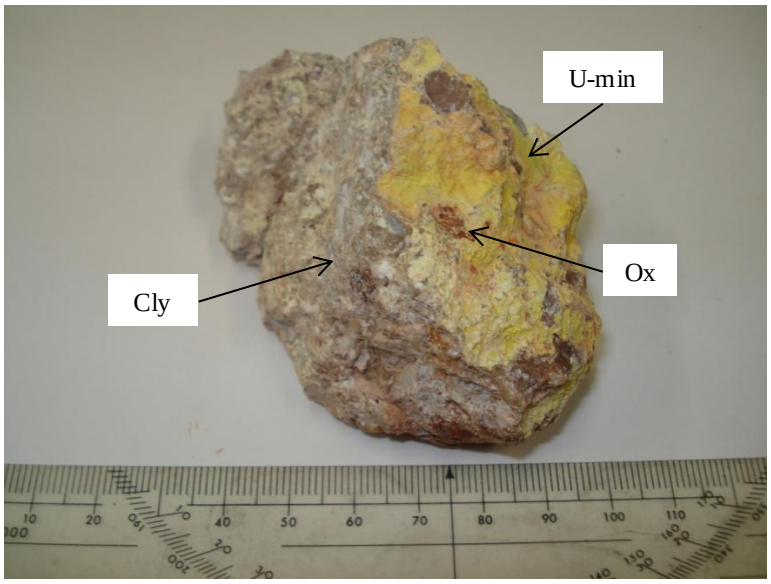

Figure 4.5 Sample 317 from the face of the breccia (zone 2) between 0+00 and 0+10 levels. Rock fragments are partially silicified and argillized (Cly). Oxide (Ox) and uranium minerals (U-min) are associated with fractures.

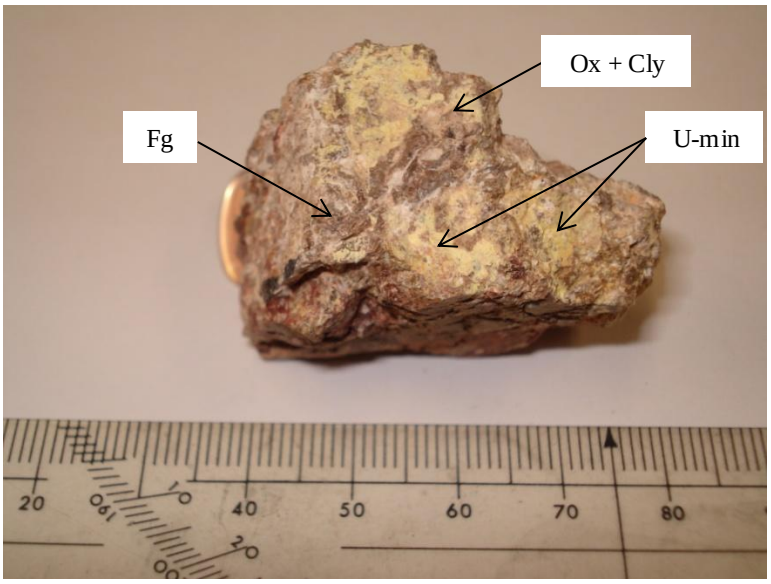

Figure 4.6 Sample PBA-106 is from zone three. The rocks corresponding to zone three are usually made up of strongly silicified rock fragments from the Nopal rhyolite (Fg); oxide (Ox) and clay minerals (Cly) occur within fragments and along micro-fractures.

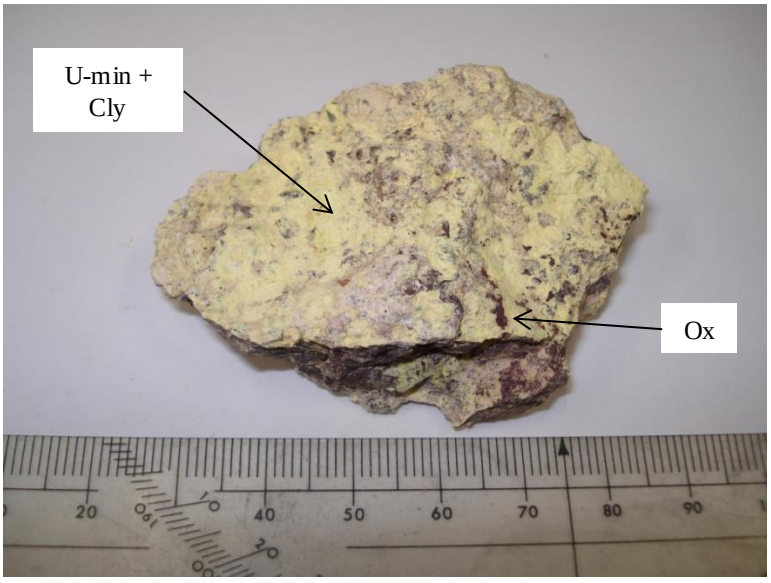

Figure 4.7 Sample 328 is from zone four. Rocks from zone four are extensively altered to cly minerals (Cly) and secondary uranium minerals (U-min).

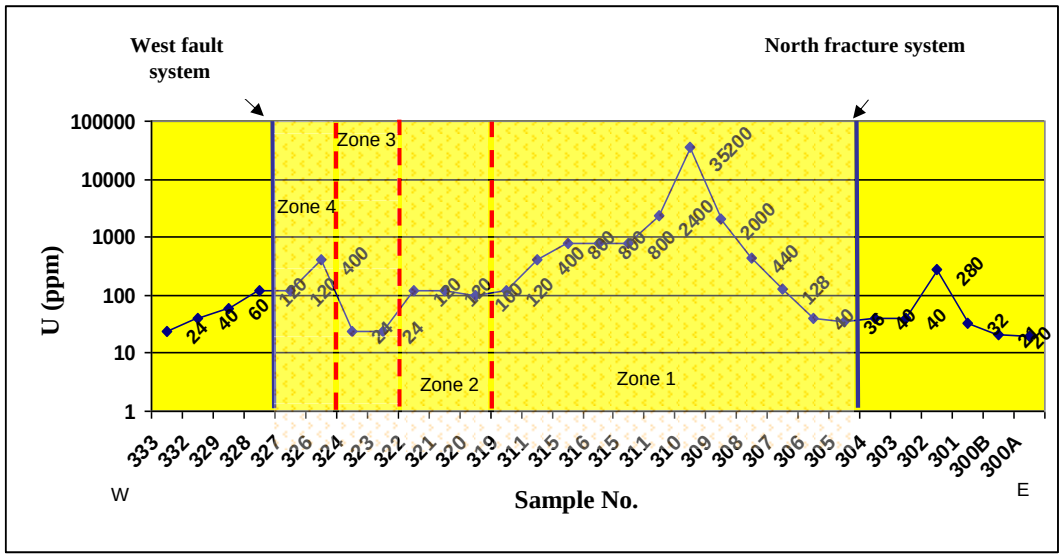

Figure 4.8 A plot of the sample location along the face of the Nopal I deposit, alteration zones and U concentrations in ppm. This graph shows that the highest concentration (up to 35,200 ppm U) is located in zone 1, whereas at the limits of the deposit concentrations decrease to values lower than 100 ppm. X axis represents sample location along the breccia and Y axis represents U concentration in ppm.

Two main fracture systems have been identified in the 0+00 level: a NNE-SSW trending system with an average strike of N 12º and a second NNW-SSE system with an average strike of N 118º (Figure 4.9). On the 0+10 level a preferential EW trending (N77º) fracture system was mapped (Figure 4.10). Near the west fault, a NNW-SSE set of fractures occur with an average strike of N159 º (Figure 4.11).

It has been observed that the three fracture systems had controlled the alteration within the deposit because most of these fractures show alteration halos with a strong presence of clay minerals and oxides with variable widths from a few mm to 3 meters in areas with stronger fracture intersections.

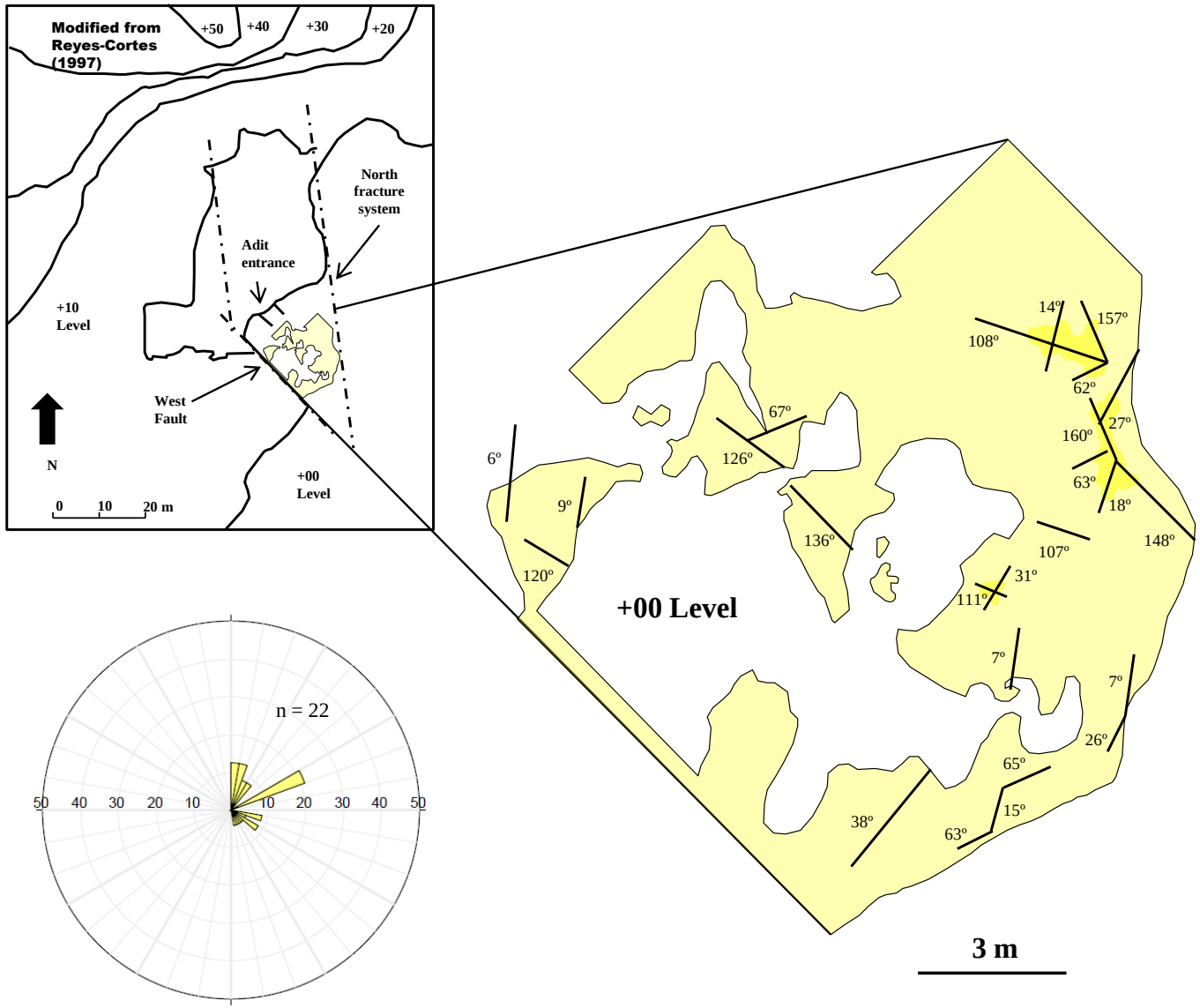

Figure 4.9. Structural map of exposed surface within the Nopal I Deposit 0+00 level. The rose diagram (inset) shows that there are two dominant sets of fractures; one that trend E-W and a second set of fractures that trend NNE-SSW. A third set of fractures trend NNW-SSE, modified from Reyes-Cortés, 1997.

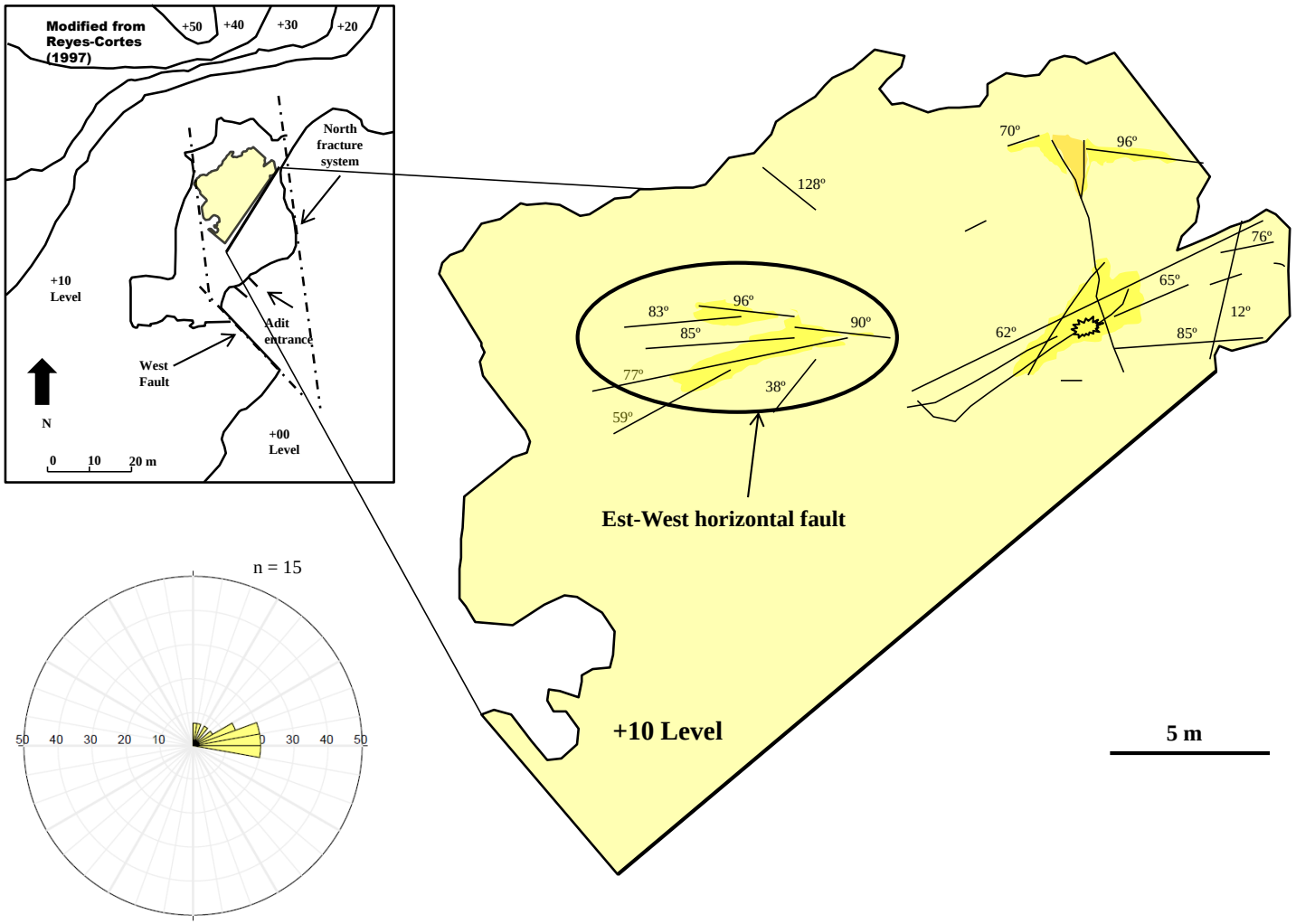

Figure 4.10. Structural map of the exposed area located within the Nopal I Deposit on 0+10 level. The rose diagram (inset) shows that there is one dominant set of fractures that trend E-W and a second set of fractures that trend NNE-SSW, modified from Reyes-Cortés, 1997.

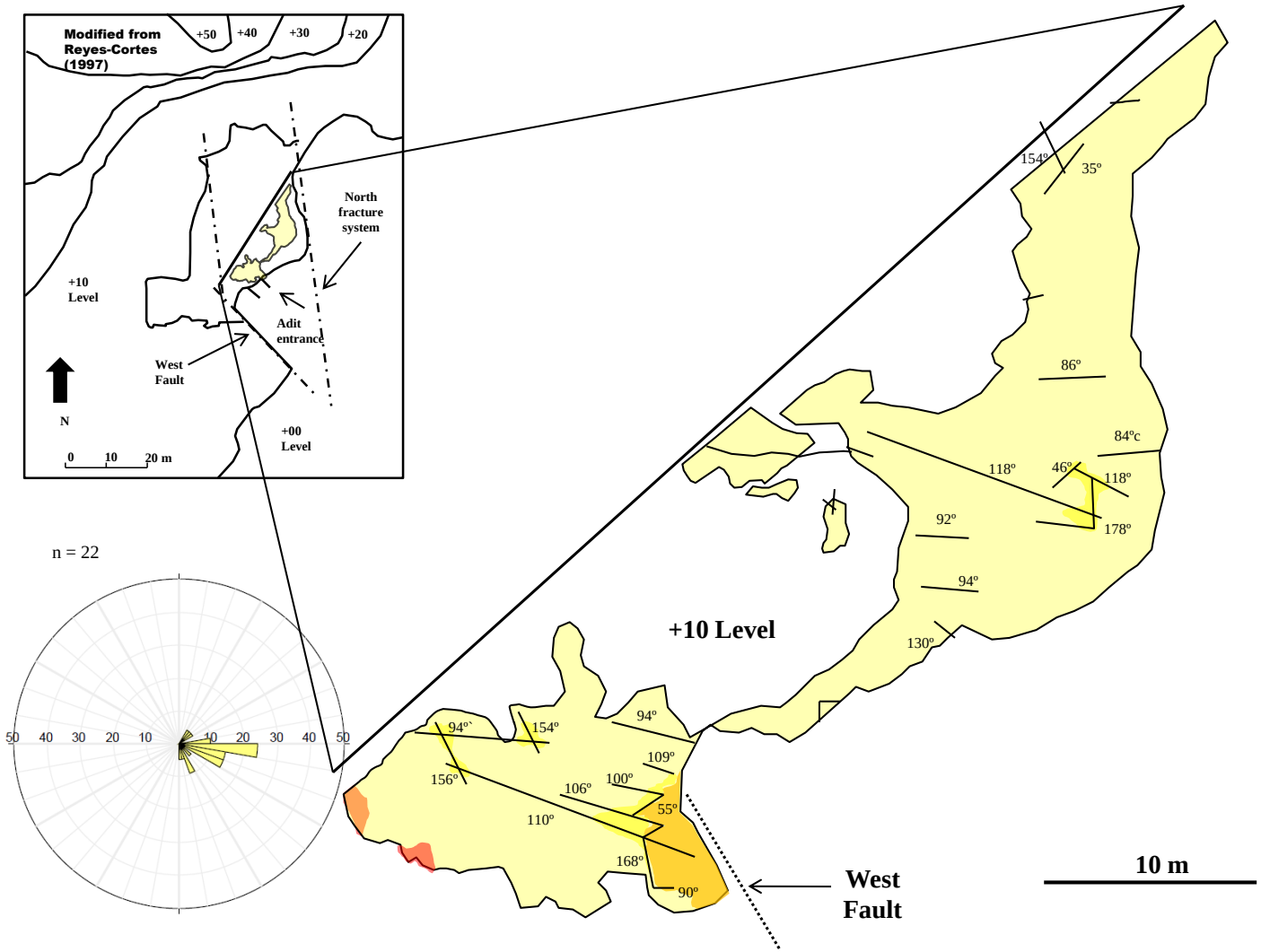

Figure 4.11. Structural map of the exposed area from the Nopal I Deposit located on the 0+10 level. The rose diagram (inset) shows that there is one preferential set of fractures NNE-SSW and a second minor set E-W, modified from Reyes-Cortés, 1997.

4.2 Petrography

On the basis of petrographic evidence, Angiboust et al; 2012 divided the Nopal Fm in two different units: the lower Nopal and the upper Nopal. Unaltered upper Nopal Fm is a pink to brownish rhyolitic ignimbrite with 20-30% phenocrysts, biotite more common than plagioclase and K-feldspar the most abundant mineral within the rock. The ignimbrite is characterized by the recrystallization of primary eutaxitic texture consisting of welded pumice fragments and glass shards within an ash matrix.

Later cooling of the Nopal Fm and fluid circulation caused devitrification of the glass (to me, is the same as above) and produced alteration in K-feldspars into kaolinite (Angiboust et al, 2012). This alteration destroyed the texture of the rock leaving most of the accessory minerals such as ilmenite ($Fe^{++}TiO_3$), magnetite ($Fe^{++}Fe^{+++}{}_2O_4$), titanite ($CaTiSiSO_5$), apatite ($Ca_5(PO_4)_3(OH,F,CL)$) and zircon ($ZrSiO_4$) disseminated.

The lower Nopal Fm is different from upper Nopal Fm in terms of matrix characteristic. It has been mentioned above that the upper Nopal Fm consists of welded pumice fragments and shards within an ash matrix while the lower Nopal consists of a groundmass of a very fine-grained recrystallized pumice with kaolinite, quartz and iron-titanium oxides (ash flow tuffs) with a slightly different underlying rock corresponding to the red vitrophyre (Angiboust et al., 2012). Reyes-Cortés (1997) and Dobson et al., (2008) differentiate this lower Nopal Fm into three different units: an upper ash flow tuffs (Lower Nopal Fm) unit followed

by a red vitrophyre at its base overlaying a unit composed by lithic tuffs corresponding to the Coloradas Fm.

Rocks located at the eastern part of the breccia from to the upper Nopal Fm (rhyolitic ignimbrite) and in contact with the north fracture/fault system show that are the least altered, conserving their initial rock characteristics: a vitric matrix and phenocrysts that have partially altered into clay minerals. Quartz phenocrysts are common within the matrix and are associated with refractory minerals such as ilmenite, ilmeno-magnetite and zircon (Figure 4.12).

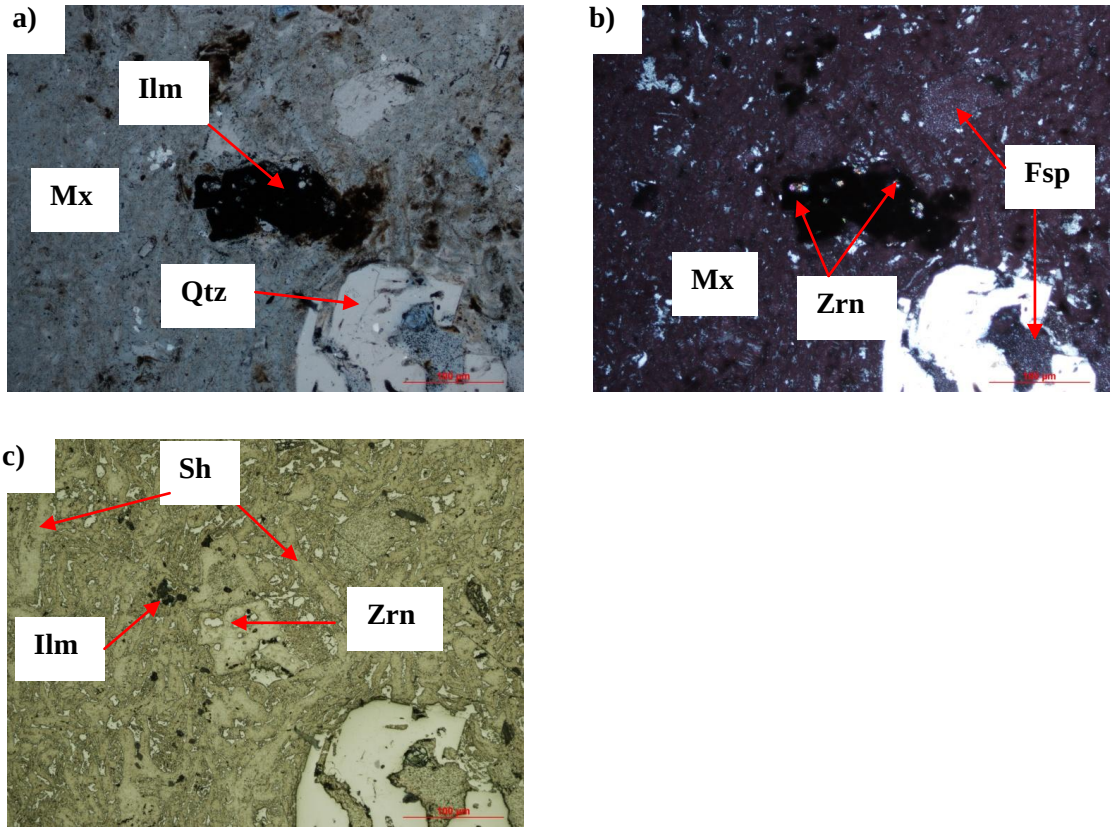

Figure 4.12 Sample 309 located at the eastern margin of the deposit (upper Nopal Fm.). a) This microphotograph was taken with transmitted light; it shows dark minerals consisting basically of ilmenite (Ilm) and a large quartz (Qtz) phenocryst. b) The image is presented under cross Nichols and contains abundant vitric matrix (Mx) with some altered feldspar (Fsp) included within matrix and quartz. Small zircon (Zrn) inclusions are present within ilmenite. c) This picture using reflected light demonstrates dark minerals (Ilm) and shards (Sh) structures. Eutaxitic texture has been modified leading to shards (Sh) flattening. High reflectivity corresponds to iron-rich minerals (Ilm), altered material with iron content and zircons (Zrn).

In the direction to the centre of the deposit samples of the ignimbrite (upper Nopal Fm) show an increase in fragmentation that enhanced fluid flow and consequently the degree of alteration (Figures 4.13 and 4.14). Rock fragments are strongly silicified, quartz phenocrysts are still preserved and K-feldspar is mostly altered into clay minerals

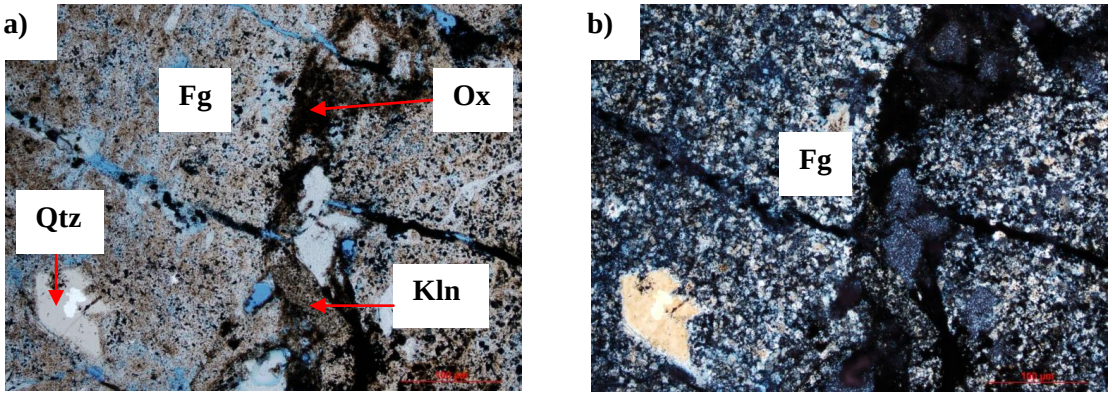

Figure 4.13 Sample 314. This sample is located at the center of the breccia between +00 and +10. a) This picture under transmitted light shows large rock fragments (Fg). Oxidation (Ox) is present mainly within fracture patterns and vugs. Quartz (Qtz) and kaolinite (Kln) can be observed within the fragments. b) Same image using crossed Nichols showing high degree of silicification of the fragments.

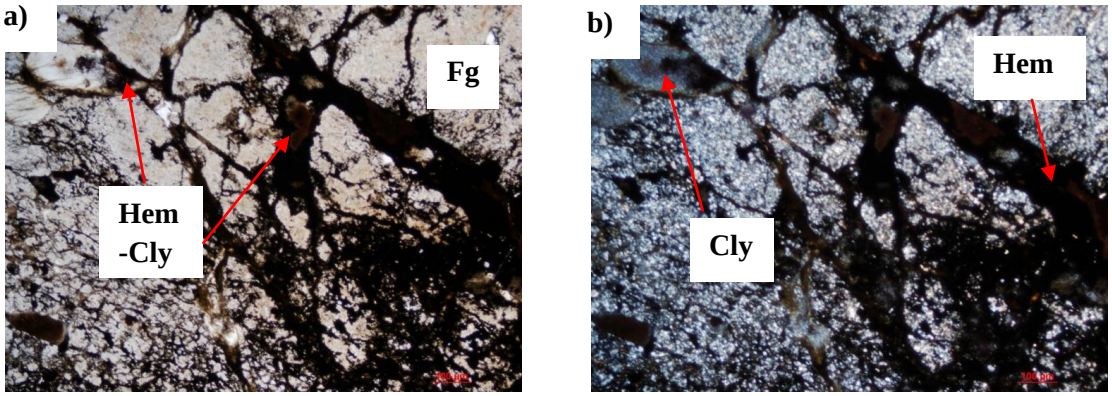

Figure 4.14 Sample PBA-105. This sample is located at the center of the breccia inside of the adit. a) This image in transmitted light shows highly silicified breccia fragments (Fg) fractured and filled by hematite (Hem) and clays (Cly) minerals. b) Same image but now is presented under crossed Nichols. The high degree of silicification and argilization of the fragments can be observed.

Towards the western margin of the deposit, the rocks are strongly fragmented and silicified. Clay alteration and oxidation correlates to this zone due to fragmentation. However, minerals such as ilmenite resisted fragmentation and can be observed disseminated within the matrix (Figure 4.15).

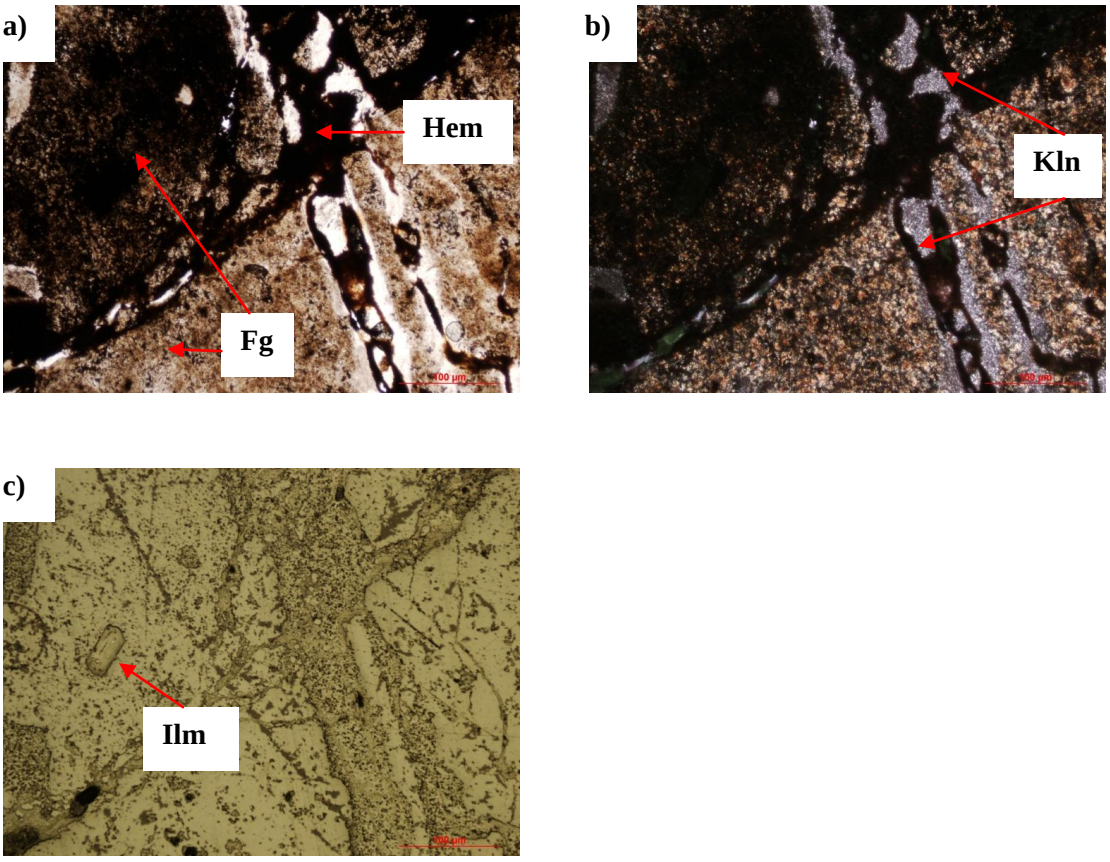

Figure 4.15 Sample PBA-106. This sample has been collected at the western margin of the deposit inside of the adit. This zone is characterized by its intense alteration to oxides and clays. a) This image in transmitted light shows oxidized (Hem) breccia fragments. b) This picture depicts same area now under crossed polar light, the upper part shows high oxidation (Ox) of breccia fragments along with clay minerals like kaolinite (Kln) preferentially located along fractures. c) Transmitted light allows the recognition of some hard minerals such as ilmenite (Ilm).

4.3 Uranium minerals

To identify the uranium minerals in the Nopal I uranium deposit qualitative and quantitative analyses were done on 21 polished thin sections (Table 1).

Table 1. List of uranium minerals identified at the El Nopal I deposit.

Mineral	*Chemical formula*
Uraninite	UO_{2+X}
Uranophane-β	$Ca(UO_2)_2Si_2O_7 \cdot 6H_2O$
Schoepite	$UO_3 \cdot 2H_2O$
Dehydrated Schoepite	$UO_3 \cdot nH_2O$ (n<2)
Soddyite	$(UO_2)_2SiO_4 \cdot 2H_2O$
Ianthinite	$U^{4+}(U^{6+}O_2)_5(OH)_{14} \cdot 3H_2O$
Becquerelite	$Ca(UO_2)_6O_4(OH)_6 \cdot 8H_2O$
Weeksite	$K_2(UO_2)_2SiO_6O_{15} \cdot 4H_2O$
Compreinagcite	$K_2(UO_2)_6O_4(OH)_6 \cdot 8H_2O$

4.3.1 Uraninite

Three different types of uraninite were identified on the basis of textural differences (Figure 4.16). Uraninite occurs as well-formed cubic crystals (~5-10 µm) in rock fragments and with pyrite (Figure 4.16a) is the least common. Granular uraninite is the most abundant form and represents clusters as big as 20 µm in size of fine intergrown anhedral crystals that are approximately ~5 µm in size. Granular uraninite and kaolinite are commonly found filling fractures and voids resulting from the alteration of phenocrysts (Figure 4.16b). Colloform uraninite is found as rims along secondary uranium minerals. These rims consist of multiple layers of colloform uraninite that approximately 10-20 µm thick (Figure 4.16c).

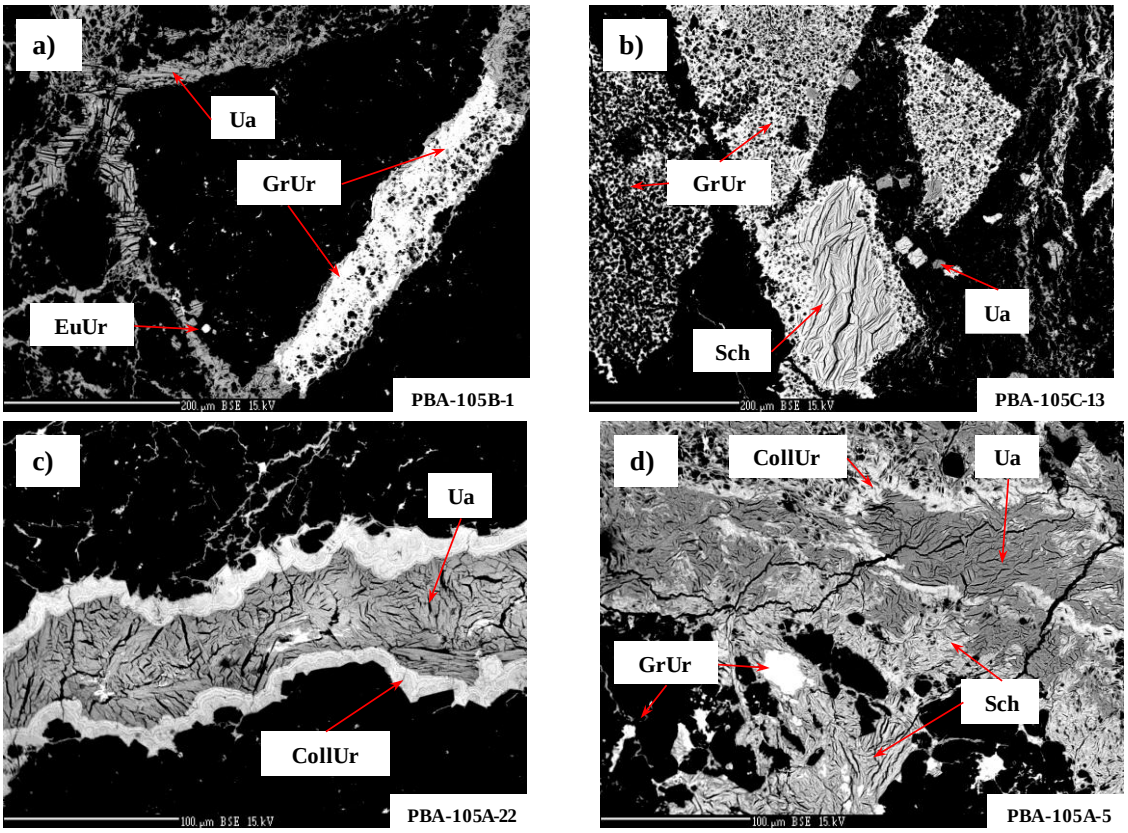

Figure 4.16. Back-scattered electron images from sample PBA-105B-1, PBA-105C-13, PBA-105A-22, and PBA-105A-5. Samples correspond to zone 1 of the deposit. a) Breccia fragment surrounded by uranium infilling material such as uranophane-β (Ua) and granular uraninite (GrUr). A euhedral uraninite (EuUr) can be observed within the fragment. b) This image shows granular uraninite filling and/or replacing k-feldespar pseudomorphs. Schoepite and small uranophane-β crystals are found replacing pseudomorphs or filling open spaces c) The image illustrates a fracture filled by uranophane-β and colloform uraninite (CollUr); d) Back-scattered image shows the complex mineralogy of several uranium phases. A large uranophane crystal has been altered into colloform uraninite, schoepite appears to be formed after uranophane and granular uraninite as the latest mineral to form.

4.3.2 Uranyl Oxyhydroxides

Four different types of uranyl oxyhydroxide minerals were identified in thin section with schoepite $(UO_2)_8O_2(OH)_{12}\cdot 12(H_2O)$ and dehydrated (D) schoepite $UO_3\bullet 0.8H_2O$ being the most common at the Nopal I uranium deposit. Both types of schoepite infill open spaces. Schoepite and D. schoepite occur as equigranular to acicular crystals (Figure 4.17).

Ianthinite $(UO_2)\cdot 5(UO_3)\cdot 10(H_2O)$ is the second most abundant uranyl oxyhydroxide mineral and occurs as large crystals (up to 100 μm) within opens spaces and fractures. This mineral is commonly associated with uranophane-β or intergrown with schoepite (Figure 4.17b). Other minor secondary uranium oxyhydroxide minerals include becquerelite $(Ca(UO_2)_6O_4(OH)_6\cdot 8(H_2O))$, and compreignacite $(K_2(UO_2)_6O_4(OH)_6\cdot 8(H_2O))$.

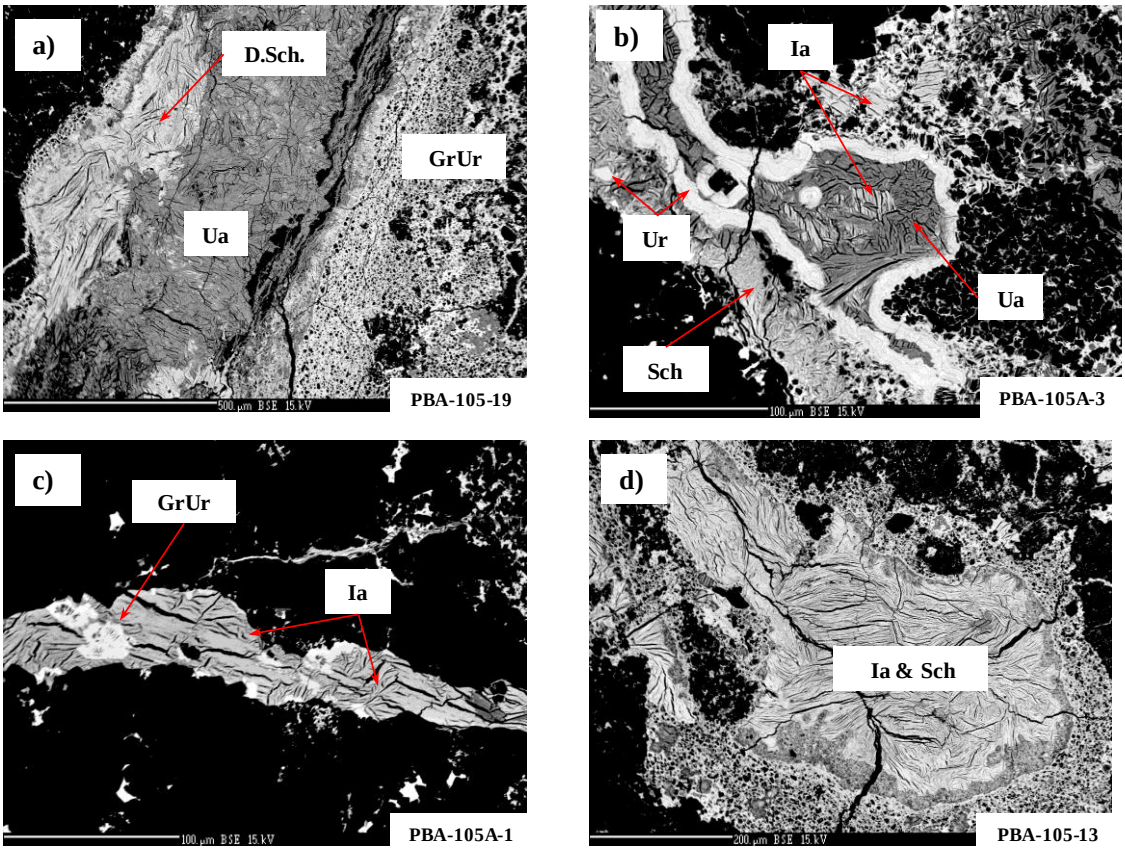

Figure 4.17. Back-scattered electron images from samples PBA-105 and PBA-105A located inside the adit in the main ore (zone 1). a) The image illustrates a vein filled by schoepite altering to uranophane; granular uraninite is present within the vein, along breccia fragments and schoepite/uranophane. b) Ianthinite fragment almost completly altered to uranophane. Colloform uraninite altering to ianthinite/uranophane. Schoepite formed after Ianthinite alteration. c) Open-space filled by microcrystals of ianthinite with secondary granular uraninite. d) A large ianthinite crystal formed in an open space and altering to schoepite.

4.3.3 Uranyl silicates

Soddyite $(UO_2)_2SiO_4 \cdot 2(H_2O)$ occurs as 20-30µm, euhedral rhombic and lathe-like soddyite crystals within vugs and open spaces, and is commonly associated with both varieties of schoepite, uranophane, and colloform uraninite (Figure 4.18).

Uranophane $Ca[(UO_2)SiO_3\,(OH)]_2 \cdot (H_2O)$ and its polymorph uranophane-β are the most abundant uranyl silicate minerals throughout the Nopal I deposit and occur in fractures and vugs. Textures indicate that uranophane forms at the expense of soddyite, granular and colloform uraninite (Figure 4.18). In zones 3 and 4 of the deposit, which are the most oxidized zones, uranophane is the only uranium mineral observed and occurs as ~50 µm needle shaped microcrystals infilling open spaces and associated with hematite nodules. Weeksite $(K_2(UO_2)_2SiO_6O_{15} \bullet 4H_2O)$ occurs in trace amounts in the these oxidized zones in association associated with uranophane and hematite close to the west fault.

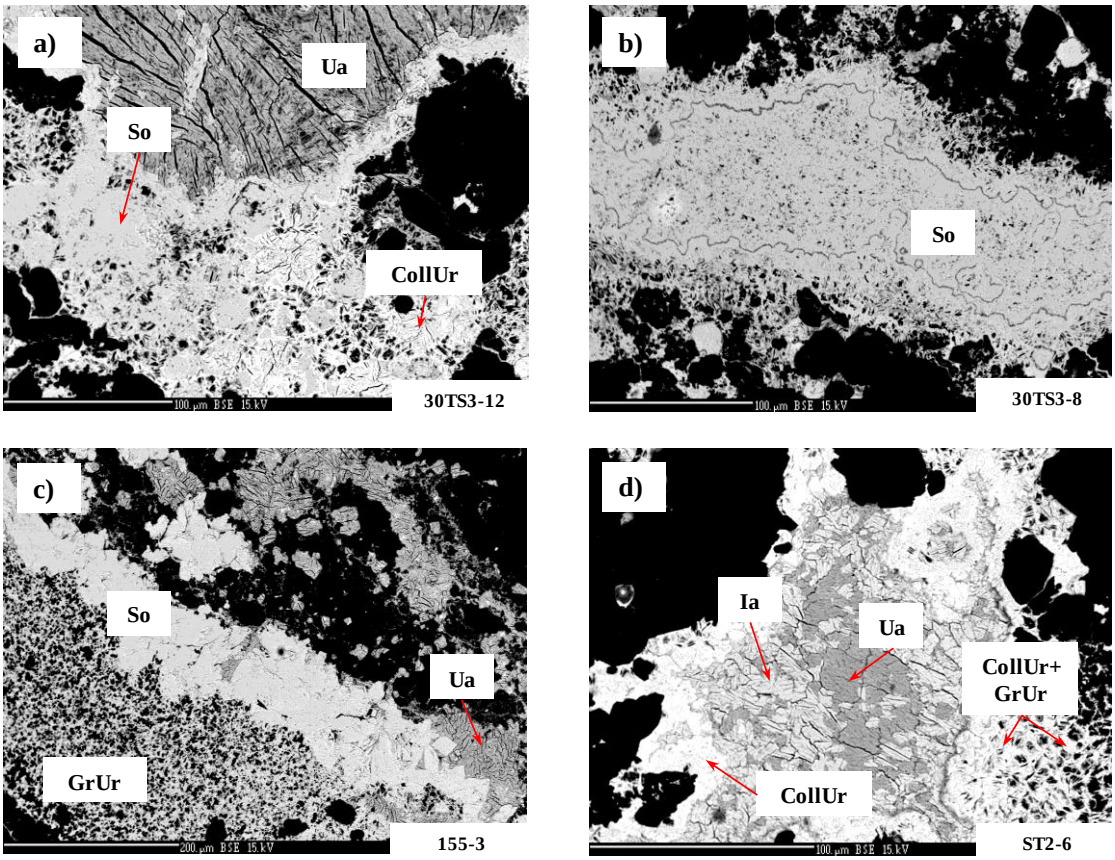

Figure 4.18. Back-scattered electron images of samples ST3-12, 30TS3-12, 155-3 and ST2-6. a) This image shows uranophane altering to soddyite and colloform uraninite. b) The image shows a vein filled with soddyite. c) This image demonstrates the relation between soddyite and uranophane growing along the edges of breccia fragments. Soddyite shows well developed euhedral crystals with smooth surfaces.. d) An image of ianthinite being replaced by uranophane. Colloform and granular uraninite occur along vein margins.

4.4 Major element chemistry

A total of 414 chemical analyses of uranium minerals were obtained using the electron microprobe (Appendix A: Table 2). All three textural varieties of uraninite have high and variable UO_2 concentrations (86.0 to 96.3 wt %) and low to moderate concentrations of PbO (from ~0.1 to 6.9 wt %). The SiO_2 and CaO contents are low and variable (0.1 to 4.1 wt % and up to 3.2 wt %, respectively). Figure 4.19 shows the relation of increasing SiO_2 with increasing CaO content for both colloform and granular uraninite. Total iron content (expressed as Fe_2O_3T) in uraninite is very low from ~0.1 to 0.4 wt %. Al_2O_3, K_2O, and SO_4 contents are near or below the detection limit of the electron microprobe.

Schoepite and D. schoepite have UO_2 concentrations that vary widely from ~25.2 to 89.8 wt %. Concentrations of PbO are up to 1.4 wt %. In addition, SiO_2 and CaO concentrations are low (up to 1.6 wt %, up to 0.2 wt %, respectively). Other elements such as iron, aluminum, potassium, and sulphur have variable concentrations (up to 5.7 wt % Fe_2O_3, up to 25.8 wt % Al_2O_3, and up to 1.6 wt % K_2O, and SO_4 up to 0.1 wt %).

Ianthinite has UO_2 concentrations that are high (85.7 to 93.4 wt %) and low PbO contents (up to 0.48 wt %). Iantihinite also incorporates SiO_2 (up to 4.2 wt %) and CaO from 0.9 to 2.8 wt %, Fe_2O_3T (up to 1.1 wt %), Al_2O_3 (up to 0.04 wt %), K_2O (0.5 wt %) and SO_4 (up to 0.1 wt %). The uranyl silicate weeksite has moderate UO_2 concentrations ranging from 50.5 to 59.9 wt % and has the lowest measured PbO content (up to 0.22 wt %) of all uranium minerals. It has high SiO_2

contents ranging from 27.8 to 34.0 wt % and low to moderate CaO contents (0.03 to 3.8 wt %). Both Fe_2O_3T and SO_4 are present in low concentrations up to ~0.1 wt %. Al_2O_3 and K_2O range from 0.1 to 5.5 wt % and 0.9 to 4.8 wt %, respectively. Uranophane and soddyite have similar variable UO_2 contents (up to 84.5 wt %) and low PbO contents (up to 2.2 wt %). The SiO_2 contents of uranophane ranges from 12.0 to 17.7 wt % whereas soddyite contains 5.2 to 10.6 wt % SiO_2. CaO concentrations in uranophane ranges from 2.5 to 7.0 wt % and for soddyite they range from 0.1 to 3.0 wt %. Uranophane, when compared to all uranium minerals, has high concentrations of Fe_2O_3T, Al_2O_3 and K_2O (up to 15.9 wt %, up to 7.8 wt %, and up to 3.3 wt %, respectively), and low contents of SO_4 (up to 1.7 wt %).

Compreignacite has low and variable SiO_2, CaO, SO_4, and Fe_2O_3T contents (0.6 wt %, 0.2 wt %, 0.01 wt % and 0.3 wt %; respectively).

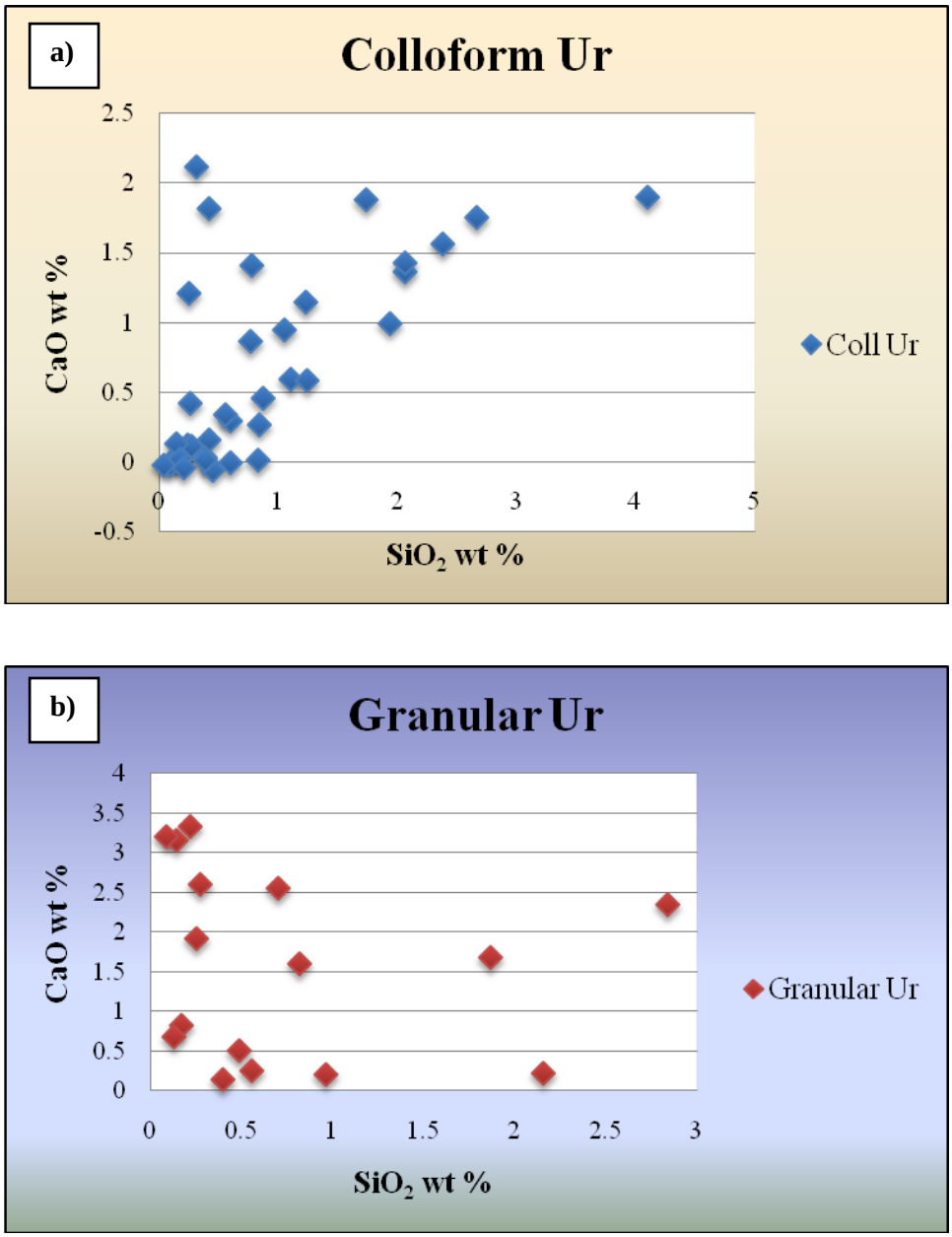

Figure 4.19. Plot of SiO_2 vs. CaO showing a weak positive correlation between SiO_2 and CaO for colloform uraninite (a) and no correlation for granular uraninite (b).

4.5 Paragenesis

The overall uranium mineral paragenesis is shown in Figure 4.20. At the Nopal I deposit, the primary stage of mineralization crystallized euhedral, granular and colloform uraninite (predominantly U^{4+}). Textural relationships among them suggest that granular uraninite crystallized after euhedral uraninite and at the same time as colloform uraninite (Figure 4.16b and 4.16c).

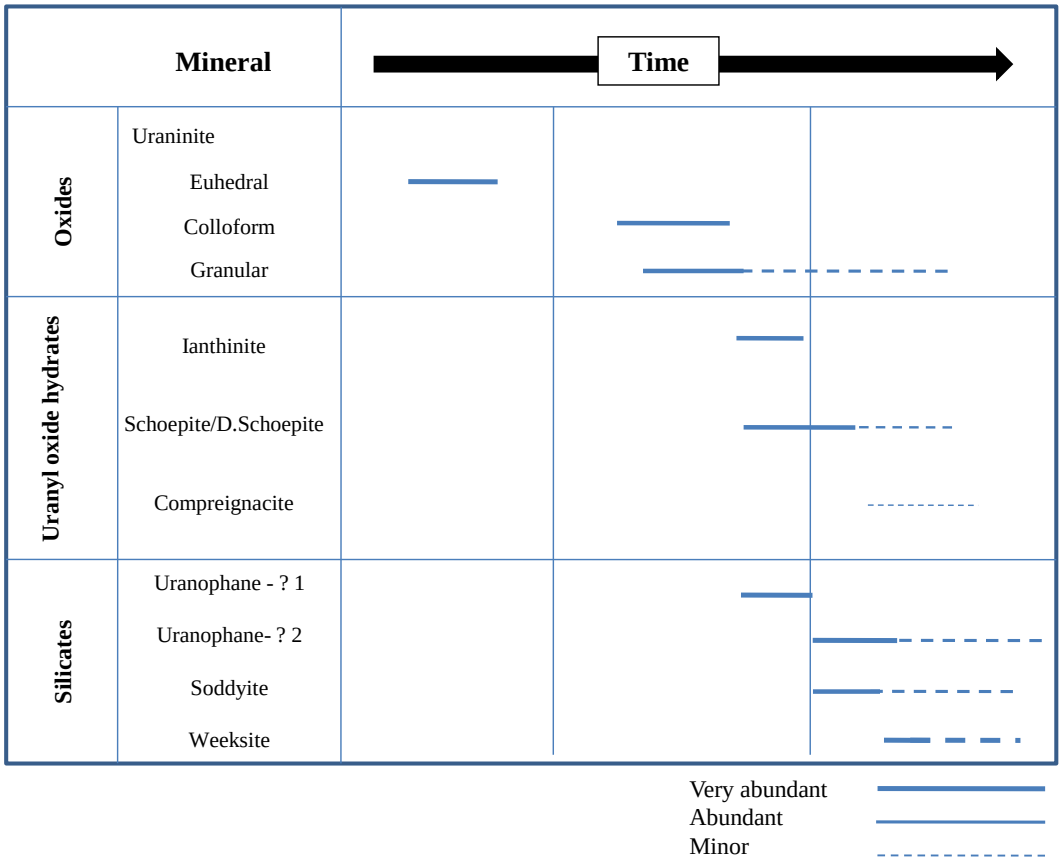

Figure 4.20. Paragenesis of U minerals from the Nopal I uranium deposit.

The secondary stage mineral assemblage (uranyl oxyhydroxides) with uranium predominantly in the +6 state is complex and replaces the primary stage

uraninite (Figure 4.20). Uranyl silicates are generally the latest uranium minerals to precipitate. Soddyite is generally concentrated in the central part of the deposit and formed after ianthinite and before uranophane. Weeksite formed after soddyite and uranophane. Compreignacite commonly replaces uranophane and schoepite.

4.6 Geochronology

4.6.1 Chemical Pb Ages

The chemical lead dating method is based on measuring the total concentration of U, Th and Pb with an electron microprobe (EMP). The main disadvantage of this method over other *in-situ* techniques (e.g., secondary ion mass spectrometry [SIMS]) is that common Pb cannot be differentiated from radiogenic Pb. That is all the measured Pb is assumed to be radiogenic, which can lead to anomalously old ages.

In minerals from the Nopal I, PbO contents of uraninite and secondary uranium minerals are as high as 6.9 wt % (Appendix A; Table 2). Chemical Pb ages obtained from uraninite generally give the oldest ages up to ~610 Ma. Figure 4.21 shows a histogram for each uranium minerals from the Nopal I deposit. Sixty analyses of uraninite give ages that are ~50 Ma or younger (similar to the age of the host rocks ~44 Ma; Alba and Chávez, 1974). Analyses on ianthinite, schoepite, uranophane, and soddyite give much younger ages (~10 Ma).

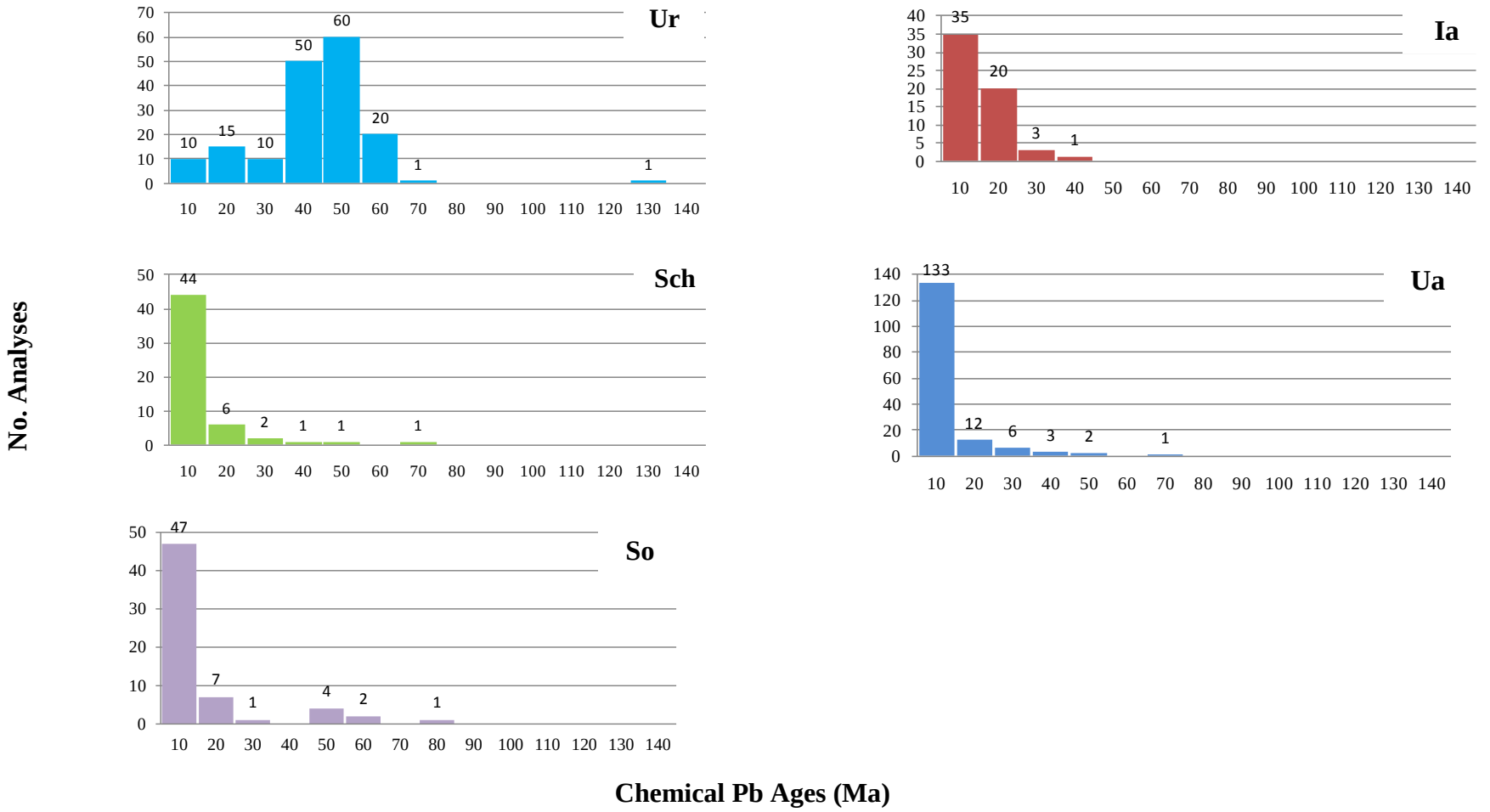

Figure 4.21. Histogram of chemical Pb ages of uraninite (Ur), ianthinite (Ia), schoepite (Sch), uranophane (Ua) and soddyite (So) from Nopal I.

4.6.2 SIMS Analysis

Here I use the SIMS technique to measure the isotopes of U, Th and Pb in uranium minerals from the Nopal I deposit to determine more precisely the ages of these minerals. These minerals were analyzed *in situ* (i.e., in thin sections) and contextual information was preserved. This approach provides the best possible chance to unravel the complex fluid history of the Nopal I deposit.

4.6.2.1 $^{207}Pb/^{206}Pb$ Isotopic Ages

The amount of common Pb in uranium minerals was determined by measuring $^{206}Pb/^{204}Pb$ isotopic ratio. $^{206}Pb/^{204}Pb$ ratios above 30 indicate that radiogenic Pb predominates over common Pb, whereas $^{206}Pb/^{204}Pb$ ratios less than 30 are considered to be dominated by common Pb (Holk et al., 2002). The results obtained from two colloform uraninite grains give $^{206}Pb/^{204}Pb$ ratios of 67 ± 14 and 93 ± 16. Twelve analyses of uranophane give $^{206}Pb/^{204}Pb$ ratios in the range of 7 ± 8 to 68 ± 30. Ianthinite has $^{206}Pb/^{204}Pb$ ratios ranging between ~23 (Appendix B; Table 3).

For the most part, the majority of the analyses have $^{206}Pb/^{204}Pb$ ratios below 30 and only a few samples were datable by this method (Appendix B; Table 3). Using a modern day $^{206}Pb/^{204}Pbn$ ratio of 18.7 to correct for common Pb, colloform uraninite gives the oldest ages ranging from 8 ± 2 Ma and 2 ± 2 Ma (Appendix B; Table 4; Appendix C for calculation). The low Pb contents in

uranophane and ianthinite suggests that these minerals are better dated using U-series.

4.6.2.2 U Series

Uranium minerals that are less than 1 Ma are not in secular equilibrium and thus have U-Th activity ratios that are less than 1 and must be dated by the U-series method (Faure and Mensing, 2005). Twenty-five U-series isotope ratios were obtained and activity ratios were calculated for the uranium minerals from the Nopal I deposit (Table 5; Appendix B). $^{234}U/^{238}U$ isotope ratios range from $1.19 \times 10^{-5} \pm 17$ to $1.20 \times 10^{-4} \pm 15$, and $^{230}Th/^{238}U$ from $1.40 \times 10^{-8} \pm 15$ to $7.47 \times 10^{-6} \pm 15$. $^{234}U/^{238}U$ and $^{230}Th/^{238}U$ activity ratios show that only four of the analyzed samples were in secular equilibrium ($^{234}U/^{238}U_A = 1$ and $^{230}Th/^{238}U_A = 1$). The samples that are in secular equilibrium correspond to colloform uraninite (section 4.6.2.1; Table 4).

Using the U-series dating method, the ages for the uranium minerals from the Nopal I deposit range from 4 ± 12 to 136 ± 12 ka. Six analyses could not be used for dating because of excess ^{230}Th. In-situ analyses of uranium minerals show a heterogeneous distribution of ages (Figure 4.22). Ianthinite gives ages ranging from 13 ± 15 to 81 ± 17 ka (sample PBA-105B8) and uranophane from sample 3165 gives an age of 16 ± 12 ka. Uranophane from sample 3161 gives an age of ~90 ka, and uranophane from 328A16 gives ages between 7 ± 12 to 109 ± 10 ka.

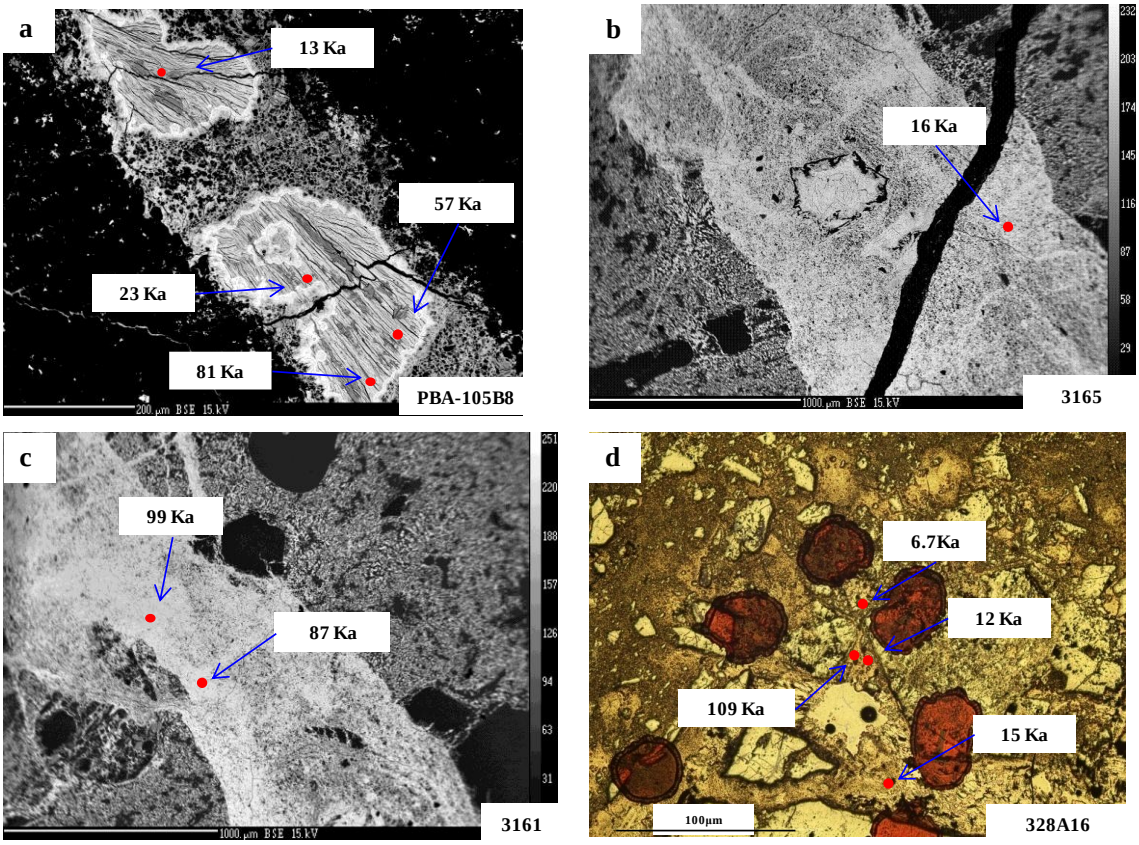

Figure 4.22 Ages calculated using U-Th disequilibrium series. a) Backscatter electron image of sample PBA-105B8 showing different ages for ianthinite from 13 to 81 Ka. b) Backscatter electron image of sample 3165, age obtained of 16 Ka is from a uranophane vein. c) Uranophane from the same sample (3165) gives older ages (87 and 99 Ka). d) Reflective image from sample 328A16, analyses were performed on uranophane. Ages obtained from this sample range from 7 Ka to 109 Ka.

$^{234}U/^{238}U_A$ and $^{230}Th/^{238}U_A$ activity ratios were used to identify the possible sources of disequilibria. Figure 4.23 shows the distribution of activity ratios reported in Table 5. Sixteen activity ratios plot in the first quadrant and four plot in the third quadrant within the forbidden zone. The activity ratios suggest that the

uranium minerals were experiencing uranium accumulation due to discontinuous processes (removal and addition). Four activity ratios plot in the fourth quadrant and suggest that uranium was remobilized during the alteration of these minerals (Figure 4.23).

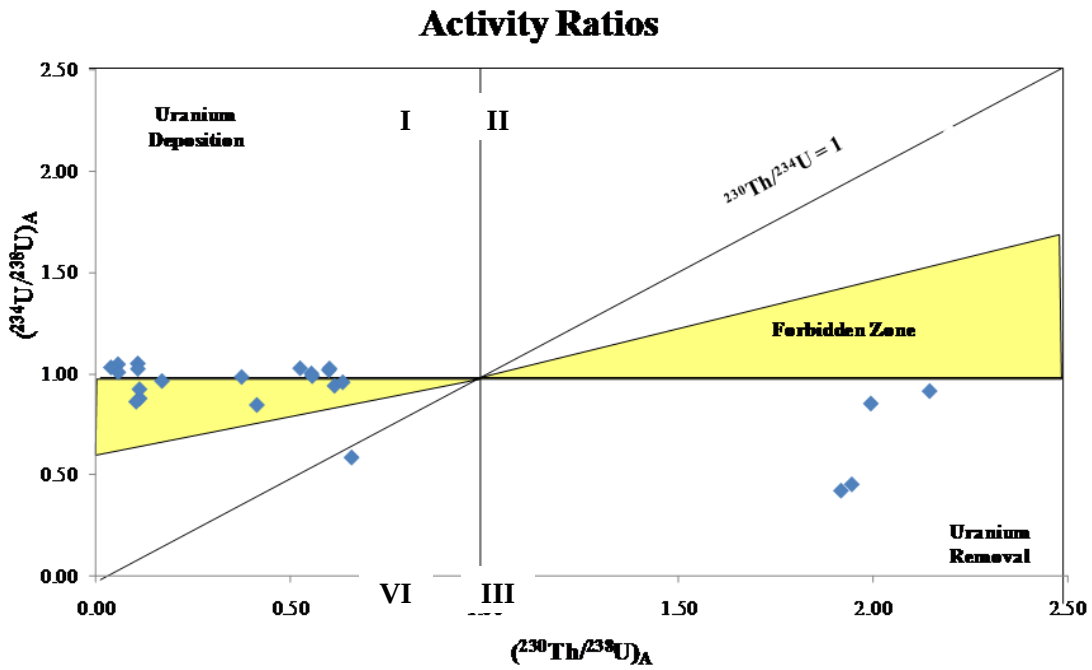

Figure 4.23 Activity ratios of a suite of samples from the Nopal I, data are from Table 8. Nineteen out of twenty four samples plot between the first and third quadrants. Those samples with $(^{234}U/^{238}U)_A$ equal to one are experiencing uranium deposition, however, those samples located within the third quadrant are experiencing uranium deposition and a few are located in the forbidden zone. This area is characterized by continuous alteration processes of uranium deposition/removal. Four analyses are found in the fourth quadrant, these minerals experienced uranium removal.

Chapter 5. Discussion

The Nopal I deposit is characterized by a series of fracture systems and faults that define the uranium mineralized zone and reflect a protracted tectonic and fluid history. Early uranium mineralization consists of the three types and stages of uraninite. Numerous studies have suggested several models for the formation of the Nopal I uranium deposit. These models include volcanic vent (Pilcher, 1981), hydrothermal (Bazan, 1980), collapse breccia (Bell, 1981), deuteric and low temperature processes (Goodell, 1985) and high temperature magmatic processes (Aniel and Leroy, 1985; George-Aniel et al., 1991). A recent study by Angiboust et al. (2012) has shown that the Nopal I uranium deposit was part of a large geothermal system where uraninite was a byproduct of microbial activity. Late oxidizing fluids have subsequently altered the uraninite to a variety of uranyl minerals.

Despite numerous studies over the past 30 years, the age of the uranium mineralization at the Nopal I deposit has remained elusive because the uranium mineralogy is fine-grained and complex (Pearcy et al., 1994; Picket and Murphy, 1997; Murphy, 2000; Fayek et al., 2006). An extensive study by Pearcy et al. (1994) reported chemical Pb ages that range from 3.7 Ma to 13.31 Ma. In this study, chemical Pb ages of several minerals including early uraninite and late-stage uranyl minerals range from <1 Ma to 611 Ma whereas the rocks that host the Nopal I deposit are 44 Ma (K-Ar, Alba and Chavez, 1974). The old chemical Pb ages suggest that the concentration of Pb in the uranium minerals is a mixture between radiogenic and common Pb.

The amount of common Pb in uranium minerals was determined by measuring the $^{206}Pb/^{204}Pb$ isotopic ratio. The majority of the analyses have $^{206}Pb/^{204}Pb$ ratios below 30, which indicates that common Pb dominates over radiogenic Pb (Holk et al., 2002).

Consequently, only a few samples were datable by the lead-lead method (Figure 5.1a; Appendix B; Table 3). A plot of $^{206}Pb/^{204}Pb$ ratios vs. chemical Pb for uranophane (Figure 5.1b) shows a weak correlation and shows that the chemical Pb age technique is not a reliable method for dating very young uranium mineral deposits.

a)

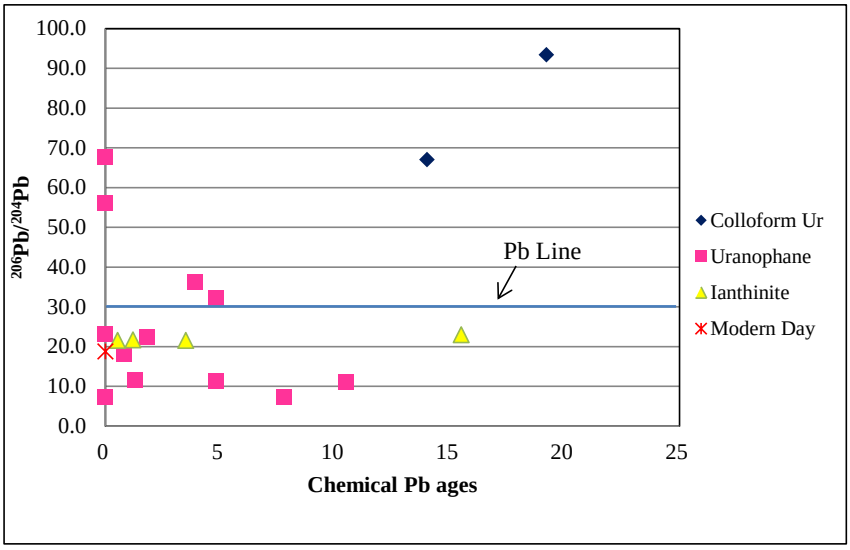

b)

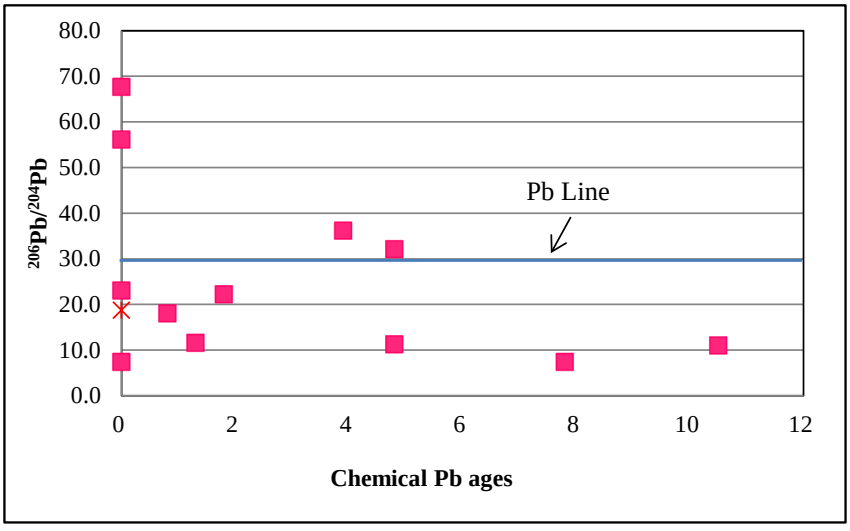

Figure 5.1. Chemical Pb ages vs $^{206}Pb/^{204}Pb$ isotopic ratios. a) This graph shows the isotopic distribution from selected uranium minerals from the Nopal I with their respective chemical Pb ages. b) A plot of $^{206}Pb/^{204}Pb$ isotopic ratios vs. chemical Pb ages for uranophane, which shows a weak inverse correlation.

According to Eaton (1982), earlier extensional deformation related to the pre-Basin and Range (B&R) tectonics was active within the southwest United States and northern Mexico at approximately 29 to 30 Ma with local deformations as early as 36 to 37 Ma. The early euhedral uraninite that was dated by Fayek et al (2006) gave an age of ~36 Ma, which suggests that primary uranium mineralization may have been related to this early extensional regime. Crystallization of the uraninite took place soon after the ignimbrite deposition (~38 Ma; Fayek et al., 2006) when hot silicic and reduced fluids rose from the chamber (rhyolite source) followed by devitrifiction of the glassy shards, which promoted the exolution of uranium (Angiboust et al., 2012). The lack of euhedral uraninites within the deposit and their weak presence only within strongly silicified rhyolitic fragments as small grains (~5µm in size) suggests that euhedral uraninite formed prior to brecciation. Granular uraninite mostly developed within fractures associated with kaolinite. This stage of alteration did not produce widespread uranium mineralization.

The dates of ~20 Ma obtained from uranium minerals and the orientations (west fault N 145° and north fracture system N 170°) of most of the structures that host the uranium mineralization at the Nopal 1 deposit indicate that the circulation of geothermal fluids was triggered by extension of the crust associated with the Basin and Range tectonic and magmatic events (Angiboust et al. 2012) at ~20-10 Ma. These fluids were responsible for brecciation and precipitation of low-temperature (~50 ^{o}C), biogenic, and granular uraninite.

At ~10 Ma, the Nopal I was affected by the Rio Grande Rift (RGR) tectonic event, which further brecciated the deposit, which facilitated the circulation of acid sulphur rich fluids that reacted with euhedral and granular uraninite releasing uranium and re-precipitating it again as a colloform uraninite at ~8 and 2 Ma. Colloform uraninite is the most common form of uraninite

and occurs throughout the deposit. Continued activity along the RGR resulted in meteoric waters circulating through the highly porous breccia zone promoting alteration/oxidation of previous uraninites (euhedral, granular and colloform) to secondary uranyl complexes: ianthinite, schoepite, uranophane, soddyite, weeksite, and compreignacite. U-series ages of these minerals suggest that progressive alteration of uraninite occurred within a million year period, ranging from the 406.0 ka to 4.1 ka (ianthinite to uranophane minerals, respectively, Appendix B, Table 4 and 5).

Chapter 6. Conclusion

The purpose of this study is to characterize the minerals that are formed in the Nopal I and their paragenesis as well as redefine the geochronology. The first mineralizing event at the Nopal I uranium deposit is characterized by the precipitation of the euhedral uraninite by highly sulphidic solutions. Subsequent tectonic events associated to Basin and Range (with a characteristic orientation of NNW-SSE) and Rio Grande Rift (mostly related to extensional processes with a strike of EW) enhance uranium alteration and mobilization.

Petrography reveals that uraninite is present in three textural forms: 1) euhedral uraninite, 2) granular uraninite, and 3) colloform uraninite. Secondary oxyhydrates and uranyl silicates are the alteration product of euhedral uraninite. Backscatter-electron images show that oxyhydrates such as ianthinite and schoepite/dehydrated schopeite form directly from the alteration of euhedral uraninite. Ianthinite only occurs in the center of the deposit where silicification is most dominant. The next minerals to appear are uranophane, soddyite and weeksite. These minerals are formed after ianthinite/schoepite alteration; however, sometimes it can be observed that uranophane, soddyite and weeksite are contemporaneous with the oxyhydrates. Secondary colloform uraninite post-dates schoepite/ianthinite as well as some uranophane crystals. Granular uraninite is late in the paragenesis and is commonly associated with kaolinite.

Uranium, lead and thorium contents of uranium minerals were used to calculate their chemical Pb ages. Dates obtained from minerals of the Nopal I show a wide distribution from 0 to 611 Ma. Some of these ages are older than the host volcanic unit, which has an age of ~44 Ma. Pb isotopic analysis showed that these old ages are a result of large quantities of common Pb. Therefore, the chemical Pb method cannot be used reliably to date the uranium mineralization of the Nopal I deposit. Six analyses of uranophane give $^{207}Pb/^{206}Pb$ isotopic ages from 2.1 ± 20 Ma to 7.6 ± 20 Ma. These ages correlate to the tectonic events of the B&R, Rio Grande, and to dramatic climate changes that occurred during the late Miocene-early Pliocene (Petit et al., 1991).

U-series ages on secondary uranium minerals showed that that there are four main mineral formation stages: 1) around 407 Ka, 2) between 240 and 254 Ka, 3) between 87 and 132 Ka, 4) between 4 to 20 Ka; these stages can be related to climatic oscillations that occurred within the past 420 Ka, at 80 and 110 Ka and between 4 to 20 Ka.

Recommendations:

- U/Pb isotopic studies are suitable to determine common Pb concentrations in young U mineral deposits; therefore, a proper dating technique can be applied.

Chapter 7. References

Aguirre-Díaz, G.J., and Labarthe-Hernández, G., 2003. Fissure ignimbrites: Fissure-source origin for voluminous ignimbrites of the Sierra Madre Occidental and its relationship with the Basin and Range faulting. Geology, v. **31(9)**, p. 773-776.

Aguirre-Díaz, G.J., and McDowell, F.W., 1991. The volcanic section at Nazas, Durango, Mexico, and the possibility of widespread Eocene volcanism within the Sierra Madre Occidental: Journal of Geophysical Research, v. **96**, p. 13,373–13,388.

Alba, L.A. and Chavez, R., 1974. K-Ar ages of volcanic rocks from the Central Sierra Peña Blanca, Chihuahua, Mexico. Isochron West. v. **10**, p. 21-23.

Angiboust, S., Fayek, M., Power, I.M., Camacho, A., Calas, G., and Southam, G., 2012. Structural and biological control of the Cenozoic epithermal uranium concentrations from the Sierra Peña Blanca, Mexico. Mineralium Deposita, v. 47, p. 859-874.

Aniel, B., and Leroy, J., 1985. The reduced uraniferous mineralizations associated with the volcanic rocks of the Sierra Peña Blanca, Chihuahua, Mexico. *American Mineralogist*, v.**70**, p. 1290-1297.

Aniel, B., 1983. Les gisements d'uranium associés au volcanisme acide tertiaire de la Sierra Peña Blanca (Chihuahua, Mexico). Géologie et Géochimie de I'Uranium, Mémoire Nancy, 2, 291 p.

Bazan, B.S., 1980. Depósitos de uranio en faja tipo cordillerano: Simposium sobre Exploracion de Uranio, Hermosillo, Sonora, Mexico. Nov. 24.

Bell, R.C., 1981. Geology of central Sierra Pena Blanca, M.S. thesis, University of Texas at El Paso, 57 p.

Bowles, J.F.W., 1990. Age dating of individual grains of uraninite in rocks from electron microprobe analyses. *Chemical Geology*, **83**, 47-53.

Bridges, L.W., 1964. Stratigraphy of Mina Plumoses – Placer de Guadalupe area. West Texas Geological Society, Guidebook, Midland, TX, Publication 64-50, p. 50-59.

Calas, G., 1977. Les phénomènes d'altération hydrothermale et leur relation avec des minéralisations uranifères en milieu volcanique: le cas des ignirnbrites tertiaires de la Sierra de Peña Blanca, Chihuahua (Mexique). Sciences Géologiques Bulletin Strasbourg, **30**, p. 3-18.

Calas, G., Agrinier, P., Allard, T., and Ildelfonse, P., 2008. Alteration geochemistry of the Nopal I Uranium Deposit (Sierra Peña Blanca, Mexico), a natural analogue for a radioactive waste repository in volcanic tuffs. Terra Nova, v. 20, p. 206-212.

Campa, M.F. and Coney, P.J., 1982. Tectono-stratigraphic terranes and mineral resource distributions in Mexico. Can. J. Earth Sci. v. **20**, p. 1040-1051.

Chapin, C.E., 1979. Evolution of the Rio Grande rift - A summary, In *Rio Grande Rift: Tectonics and Magmatism, R.E. Riecker, Editor*. American Geophysical Union. Washington, D.C.

Chaulot-Talmon, J.F., 1984. Geologic and structural study of the Tertiary ignimbrites of the Sierra Madre Occidental between Hermosillo and Chihuahua, Mexico, *Ph.D. Dissertation, University of Paris South, Orsay*, France.

Christiansen, R. L., and Lipman, P. W., 1972. Cenozoic volcanism and plate-tectonic evolution of the western United States, II, Late Cenozoic. Philos. Trans. R. Soc. London Ser. A 27 1 :249-84.

Dobson, P.F., Fayek, M., Goodell, P.C., Ghezzehei, T.A., Melchor, F., Murrell, M.T., Oliver, R., Reyes-Cortés, I.A., de la Garza, R., and Simmons, A., 2008. Stratigraphy of the PB-1 well, Nopal I uranium deposit, Sierra Peña Blanca, Chihuahua, Mexico. International Geology Review, v. **50**, p. 959-974.

Eaton, G.P., 1982. The Basin and Range Province; Origin and. tectonic significance: Annual Reviews Earth and Planetary Science, v. **10**, p. 409-440.

Ewing, R.C., and von Hippel, F.N., 2009. Nuclear waste management in the United States—Starting over, Science, v. **325**, p. 151-152.

Faure, G., and Mensing, T.M., 2005. Isotopes Principles and Applications, Third Ed. John Wiley & Sons, Inc. Hoboken, New Jersey.

Fayek, M., Ren, M., Goodell, P., Dobson, P., Saucedo, A., Kelts, A., Utsunomiya, S., Ewing, R.C., Riciputi, L.R., and Reyes, I., 2006. Paragenesis and geochronology of the Nopal I Uranium Deposit, Mexico. Proceedings, 2006 International High-Level Radioactive Waste Management Conference, April 30-May 4, 2006, Las Vegas, NV, American Nuclear Society, La Grange Park, IL, p. 55-62.

Fayek, M., and Kyser, T.K., 1997. Characterization of multiple fluid-flow events and rare-earth-element mobility associated with formation of unconformity-type uranium deposits in the Athabasca Basin. Canadian Mineralogist, v. **35**, p. 627–658.

George-Aniel, B., Leroy, J.L., Poty, B., 1991. Volcanogenic Uranium Mineralizations in the Sierra de Peña Blanca District, Chihuahua, Mexico: Three Genetic Models. *Economic Geology*, v. **86**, p. 233-248.

Goodell, P.C., 1981. Geology of the Pena Blanca Uranium Deposits, Chihuahua, Mexico. In: P.C. Goodell and A.C. Waters, Eds., Uranium in Volcanic and Volcaniclastic Rocks. AAPG Studies in Geology, v. 13, p. 275-291.

Goodell, P.C., 1985. Chihuahua City uranium province, Chihuahua, Mexico. In: Uranium deposits in volcanic rocks, Panel Proceedings Series IAEA-TC-490/19, International Atomic Energy Agency, Vienna, p. 97-124.

Goodell, P.C., Trentham, R.C., and Carraway, K., 1979. Geologic setting of the Peña Blanca uranium deposits, Chihuahua, Mexico. Chapter IX in: Formation of uranium ores by diagenesis of volcanic sediments, C.D. Henry and A.W. Walton, eds., U.S. Department of Energy Open-File Report GJBX-22 (79), 38 p.

Henry, C.D., Price, J.G., & Hutchins, M.F., 1983. Mineral resources areas of the Basin and Range Province of Texas: U.S. Geol. Survey Open-File Report 83-709, 7 p.

Holk, G.J., Kyser, T.K., Chipley, D., Hiatt, E.E., Marlatt, J., 2002. Mobile Pb isotopes in Proterozoic sedimentary basins as guides for exploration of uranium deposits. Journal of Geochemical Exploration. v. **80**, issues 2-3, p. 297-320.

Ildefonse, P., Muller, J.P., Clozel, B., and Calas, G., 1990. Study of two alteration systems as natural analogues for radionuclide release and migration. *Engineering Geology*, v. **29**, p. 413-439.

Livaccari, R.F., 1991. Role of crustal thickening and extensional collapse in the tectonic evolution of the Sevier-Laramide orogeny, western United States: *Geology*, v. **19**, p. 1104-1107.

Magonthier, M.C., 1984b. Contribution a la petrographie et à la gèochimie des ignimbrites de la Sierra Madre Occidentale et de la province uranèfire de la Sierra Peña Blanca, Mexique. Mém. Thèse d'Etat, Paris 6, 354 p.

Magonthier, M.C., 1985. Características petrográficas y geoquímicas de las unidades ignimbríticas portadoras de mineralización de uranio de la Sierra Peña Blanca, México. In: Uranium deposits in volcanic rocks, Panel Proceedings Series, IAEA-TC-490/7, International Atomic Energy Agency, Vienna, p. 137-150.

Malpica, C., De la Torre, G., 1980. Integración estratigráfica del Paleozoico de México. Parte I Cámbrico-Ordovícico: Instituto Mexicano del Petróleo, Subdirección de Tecnología de Exploración, Reporte Inédito 148 p.

McDowell, F.W., & Clabaugh, S.E., 1979. Ignimbrites of the Sierra Madre Occidental and their relation to the tectonic history of Western Mexico, In: Ash-Flow Tuffs, C.E. Chapin and W.E. Elston, eds., Geol. Soc. Am. Special Paper, v. **180**, p. 113-124.

McIntosh, W.C. and Bryan, C., 2000. Chronology and geochemistry of the Boot Heel volcanic field, New Mexico; in Lawton, T. F., McMillian, N. J, and McLemore, V. T. (eds.), Southwest passage— a trip through the Phanerozoic: New Mexico Geological Society, Guidebook **51**, p. 157–174.

Murphy, W.M., 2000. Natural analogs and performance assessment for geologic disposal of nuclear waste. *Materials Research Society-Symposium Proceedings*, **608**, 533-544.

Nieto-Obregón, J., Delgado-Argote, L.A., and Damon, P.E., 1981. Relaciones petrológicas y geocronológicas del magmatismo de la Sierra Madre Occidental y el Eje Neovolcánico en Nayarit, Jalisco y Zacatecas: Asociación de Ingenieros de Minas Metalurgistas y Geólogos de México, Memoria, XIV Convención Nacional, p. 327–361.

Pearcy, E.C., Prikryl, J.D., Murphy, W.M., and Leslie, B.W., 1994. Alteration of uraninite from the Nopal I deposit, Pena Blanca District, Chihuahua, Mexico, compared to degradation of spent nuclear fuel in the proposed U.S. high-level nuclear waste repository at Yucca Mountain, Nevada, Applied Geochemistry, v. **9**, p. 713-732.

Pearcy, E.C., Prikryl, J.D., and Leslie, B.W., 1995. Uranium transport through fractured silicic tuff and relative retention in areas with distinct fracture characteristics, *Applied Geochemistry*, **10**, p. 685-704.

Petit, J.R., Jouzel, J., Raynaud, D., Barkov, N.I., Barnola, J.-M., Basile, I., Chappellaz, J., Davis, M., Delaygue, G., Delmotte, M., Kotlyakov, V.M., Legrand, M. Lipenkov, V.Y., Lorious, C., Pépin, L., Ritz, C., Saltzman, E., Stievenard, M., 1999. Climate and atmospheric history of the past 240,000 years from the Vostok ice core, Antarctica. Nature, vol. **399**, p. 429- 436.

Pickett, D.A., and Murphy, W.M., 1997. Isotopic constrains on Radionuclide Transport at Peña Blanca. *Seventh EC Natural Analogue Working Group Meeting: Proceedings of an international Workshop held in Stein a, Rhein, Switzerland form 28 to 30 October 1996. Von Maravic, H. and Smellie, J., eds. EUR 17851 EN. Pages 113-122. Luxembourg, Luxembourg: Office for Official Publications of the European Communities.*

Pickett, D.A., and Murphy, W.M., 2002. Uranium chemistry and isotopy in waters and rocks at Peña Blanca, Mexico. Eighth EC Natural Analogue Working Group Meeting, H. von Maravic and W.R. Alexander, eds., European Commission Nuclear Science and Technology, EUR19118, p. 333-337.

Pilcher, 1981. Exploration guide for uranium in volcanic environments. AAPG Bull., v.65, p. 65.

Prikryl, J.D., Pickett, D.A., Murphy, W.M., and Pearcy, E.C. 1997. Migration behavior of naturally occurring radionuclide at the Nopal I uranium deposit, Chihuahua, Mexico. *Journal of Contaminant Hydrology*, 26, 61-69.

Reyes-Cortés, I.A., 1997. Geologic Studies in the Sierra de Peña Blanca, Chihuahua, Mexico, unpublished Ph.D. thesis, University of Texas, El Paso, 344 p.

Reyes-Cortés, I.A., 2002. Geologic setting and mineralisation: Sierra Peña Blanca, Chihuahua, México, 2002, Eighth EC Natural Analogue Working Group Meeting, H. von Maravic and W.R. Alexander, eds., European Commission Nuclear Science and Technology, EUR19118, p. 321-331.

Salas, G.A., 1968 (1970). Areal geology and petrology of the igneous rocks of the Santa Ana region, Northwest Sonora: Bol. Soc. Geol. Mexicana, v. **31**, p. 11-63.

Schlinder, M., Fayek, M., and Hawthorne, F.C., 2010. Uranium-rich opal from the Nopal I uranium deposit, Peña Blanca, Mexico: Evidence for the uptake and retardation of radionuclides. Geochimica et Cosmochimica Acta, v. **74**, p. 187-202.

Seager, W.R., Shapiqullah, M., Hawley, J.W., and Marvin, R., 1984. New dates from basalts and the evolution of the southern Rio Grande Rift. Geol. Soc. Amer. Bull.,v. **95,** p. 87-99.

Tardy, M., 1980. Contribution à l'étude géologique de la Sierra Madre Orientale du Mexique, PhD thesis, PMC Paris, France.

Zoback, M.L., Anderson, R.E., & Thompson, G.A., 1981. Cainozoic evolution of the state of stress and style of tectonism of the Basin and Range Province of the western United States: Philosophical Transactions of the Royal Astronomical Society of London, v. **A300**, p. 407– 434.

Appendix A

Table 2. Elemental wt% of electron microporbe analyses of uranium minerals from the Nopal I deposit, Chihuahua, Mexico.
Elemental Weight Percent

Sample	Mineral	Si	U	S	Ti	Fe	Pb	Ca	Al	Th	K	V	Zr	Ba	O	Total	Age (Ma)	1σ (Ma)
PBA-105A-1-1	*Ianthinite*	0.00	79.53	0.01	0.02	0.02	-0.05	0.01	0.00	0.05	0.33	0.00	0.06	-0.03	10.81	90.82	0	0
PBA-105A-1-2	*Uraninite*	0.08	82.86	0.04	0.03	0.03	0.11	0.58	0.01	0.07	0.00	0.01	-0.01	-0.03	11.57	95.41	10	28
PBA-105A-1-3	*Ianthinite*	1.08	78.39	0.05	0.06	0.23	-0.04	0.68	0.13	-0.01	0.33	0.01	-0.03	-0.15	12.39	93.37	0	0
PBA-105A-2-4	*Ianthinite*	-0.02	78.07	0.00	0.02	0.10	0.00	0.01	0.01	-0.04	0.29	-0.03	-0.04	-0.12	10.55	89.05	0	0
PBA-105A-2-5	*Uraninite*	0.12	83.46	0.06	0.01	0.04	0.11	0.30	0.00	-0.13	0.02	0.01	0.00	-0.16	11.55	95.69	9	25
PBA-105A-2-6	*Ianthinite*	1.97	76.13	0.04	0.03	0.09	0.22	2.01	0.00	-0.03	0.01	-0.02	0.02	-0.10	13.38	93.91	21	56
PBA-105A-3-7	*Ianthinite*	-0.03	82.33	0.01	0.02	-0.01	-0.02	-0.01	0.01	0.03	0.17	0.00	-0.03	-0.10	11.08	93.65	0	0
PBA-105A-3-8	*Uranophane-β*	3.98	58.43	0.02	0.01	0.01	0.02	3.74	-0.01	0.01	0.06	0.01	0.03	-0.10	13.92	80.23	2	5
PBA-105A-3-9	*Uraninite*	0.36	82.67	0.06	0.03	0.10	0.09	1.01	0.01	-0.07	-0.01	0.04	0.06	-0.05	12.11	96.54	8	22
PBA-105A-3-10	*Schoepite*	0.08	76.20	0.03	0.02	0.05	0.13	0.13	0.02	-0.02	0.21	0.00	0.01	-0.13	10.51	87.41	13	33
PBA-105A-3-11	*Ianthinite*	0.01	80.97	0.00	0.01	0.03	0.02	0.12	0.00	-0.06	0.22	-0.01	-0.04	-0.08	10.98	92.37	2	5
PBA-105A-4-12	*Uranophane-β*	7.33	61.50	0.02	0.01	0.06	0.05	5.26	0.02	-0.02	0.11	0.00	-0.06	-0.13	18.78	93.14	6	15
PBA-105A-4-13	*Ianthinite*	0.00	82.86	0.01	0.02	0.80	0.02	0.00	0.02	0.01	0.05	0.02	0.03	-0.10	11.56	95.40	1	4
PBA-105A-4-14	*Uranophane-β*	7.08	57.79	0.01	0.02	1.92	0.08	4.56	0.01	0.04	0.07	-0.01	0.03	-0.16	18.53	90.14	10	23
PBA-105A-4-15	*Uraninite*	0.52	81.74	0.08	0.03	0.04	0.12	0.42	0.00	0.10	0.05	0.00	-0.01	-0.09	11.88	94.98	11	30
PBA-105A-5-16	*Uranophane-β*	6.65	59.98	0.01	0.01	0.03	0.19	4.72	0.01	-0.04	0.02	0.00	0.00	-0.01	17.58	89.20	23	54
PBA-105A-5-17	*Uraninite*	1.92	78.55	0.06	0.02	0.06	0.27	1.36	0.03	-0.04	0.02	0.02	-0.01	-0.13	13.44	95.75	24	66
PBA-105A-5-18	*Uraninite*	0.10	79.24	-0.01	0.02	0.27	0.18	2.39	0.01	0.21	0.01	0.02	-0.02	-0.10	11.89	94.34	16	44
PBA-105A-5-19	*D. Schoepite*	0.06	77.74	0.01	0.02	0.00	-0.09	0.02	0.01	0.00	0.29	-0.01	-0.06	-0.03	10.59	88.75	0	0
PBA-105A-7-20	*Uraninite*	0.19	83.37	0.06	0.02	0.16	0.11	0.11	-0.01	0.04	-0.01	-0.03	0.01	-0.07	11.60	95.67	9	25
PBA-105A-7-21	*Uraninite*	1.11	79.15	0.06	0.04	0.06	0.18	1.12	0.01	0.03	0.11	-0.02	0.06	-0.05	12.52	94.44	16	44
PBA-105A-8-22	*Uraninite*	0.13	79.28	-0.01	0.03	0.14	0.30	1.86	-0.01	-0.08	0.26	0.02	-0.04	-0.10	11.67	93.68	27	73
PBA-105A-8-23	*Ianthinite*	0.00	79.50	0.00	0.01	0.80	0.13	0.02	0.04	-0.05	0.09	0.03	-0.04	-0.07	11.11	91.73	11	31
PBA-105A-8-24	*Uraninite*	0.97	77.88	0.06	0.02	0.07	0.16	0.98	0.01	0.01	0.02	0.02	0.04	-0.07	12.11	92.33	14	39
PBA-105A-10-25	*Uranophane-β*	5.59	66.76	0.01	0.01	0.03	0.01	4.42	-0.01	0.01	0.01	0.03	-0.05	0.00	17.13	94.01	1	4
PBA-105A-10-26	*Uraninite*	0.11	84.15	0.08	0.03	0.01	-0.01	0.09	0.00	0.01	0.00	0.01	-0.02	-0.14	11.56	96.05	0	0
PBA-105A-10-27	*Uraninite*	0.58	80.82	0.05	0.03	0.02	0.15	0.82	0.01	0.01	0.06	0.02	-0.01	-0.10	11.96	94.52	13	37
PBA-105A-9-28	*Ianthinite*	-0.02	79.62	0.00	0.00	0.02	0.02	0.02	0.00	-0.12	0.05	0.03	-0.01	-0.07	10.71	90.46	2	4
PBA-105A-11-29	*Uranophane-β*	6.64	60.33	0.00	0.02	0.08	-0.04	4.33	0.02	-0.02	0.08	-0.02	0.06	-0.11	17.47	89.03	0	0
PBA-105A-11-30	*Schoepite*	0.11	75.14	0.02	0.02	0.04	-0.01	0.05	0.02	-0.01	0.09	-0.01	0.01	-0.07	10.32	85.83	0	0
PBA-105A-11-31	*Schoepite*	0.00	76.06	0.01	0.00	0.01	-0.03	0.06	0.00	0.05	0.01	-0.01	-0.03	-0.01	10.25	86.46	0	0
PBA-105A-11-32	*Uraninite*	0.58	81.70	0.05	0.03	0.02	0.22	0.42	0.01	0.02	0.02	-0.02	-0.01	-0.12	11.89	94.97	19	53
PBA-105A-13-33	*Ianthinite*	-0.01	81.80	0.00	0.01	0.04	0.05	0.02	0.01	0.06	0.13	-0.02	-0.07	-0.07	11.01	93.13	5	13
PBA-105A-13-34	*Uranophane-β*	6.65	57.61	0.02	0.02	0.08	0.03	4.80	0.02	0.02	0.20	0.00	-0.04	-0.03	17.36	86.82	4	9
PBA-105A-13-35	*Ianthinite*	0.04	80.80	0.02	0.02	-0.01	0.00	0.12	0.01	0.09	0.19	-0.06	-0.06	-0.10	10.96	92.24	0	1
PBA-105A-13-36	*Ianthinite*	0.84	79.27	0.07	0.02	0.04	0.11	1.05	0.04	-0.06	0.05	-0.01	-0.05	0.02	12.15	93.65	10	28
PBA-105A-15-39	*Uranophane-β*	4.31	57.80	0.00	3.34	0.44	0.03	3.51	0.04	0.10	0.39	0.08	1.25	-4.86	16.58	87.88	4	9
PBA-105A-15-40	*Schoepite*	0.13	72.44	-0.01	0.95	0.09	-0.05	0.27	0.00	0.05	0.34	0.05	0.50	-1.52	10.76	85.57	0	0
PBA-105A-15-41	*Bequerellite*	0.05	78.92	0.01	0.02	0.10	0.16	2.68	0.01	-0.01	0.21	0.03	-0.04	-0.17	11.86	94.06	15	40
PBA-105A-16-42	*Uranophane-β*	6.72	62.84	0.01	0.02	0.04	0.00	4.42	0.00	0.00	0.01	0.00	-0.03	-0.12	17.89	91.95	0	0
PBA-105A-17-44	*Uranophane-β*	5.97	58.50	0.01	0.02	0.01	0.07	2.94	0.02	-0.03	0.00	-0.01	-0.02	-0.06	15.85	83.38	8	19
PBA-105A-17-45	*Schoepite*	0.02	76.25	0.01	0.04	0.01	0.04	0.12	0.03	0.09	0.24	0.00	0.02	-0.23	10.44	87.31	3	9
PBA-105A-18-46	*Uranophane-β*	6.02	58.95	0.01	0.01	3.00	0.00	4.69	0.14	-0.18	0.05	0.00	-0.01	-0.08	18.05	90.92	1	1

Table 2. Elemental wt% of electron microporbe analyses of uranium minerals from the Nopal I deposit, Chihuahua, Mexico.

Elemental Weight Percent

Sample	Mineral	Si	U	S	Ti	Fe	Pb	Ca	Al	Th	K	V	Zr	Ba	O	Total	Age (Ma)	1σ (Ma)
PBA-105A-18-47	*Schoepite*	-0.04	75.16	0.00	0.00	0.22	0.06	0.03	-0.01	0.02	1.22	0.03	0.00	0.08	10.45	87.27	5	14
PBA-105A-18-48	*Ianthinite*	-0.03	80.76	0.01	0.02	0.10	-0.08	0.02	0.00	-0.11	0.11	0.01	0.00	-0.11	10.90	91.93	0	0
PBA-105A-19-49	*Schoepite*	-0.05	75.00	0.00	0.01	0.07	-0.04	0.03	-0.01	0.02	1.28	0.01	-0.03	0.05	10.34	86.82	0	0
PBA-105A-20-50	*Uranophane-β*	5.59	60.92	0.01	0.01	-0.01	0.01	4.17	0.00	0.02	0.06	0.03	-0.03	-0.05	16.26	87.07	2	4
PBA-105A-20-51	*Schoepite*	-0.02	68.76	0.00	0.01	0.40	0.06	0.40	0.01	0.06	0.05	0.02	-0.04	-0.22	9.57	79.33	6	16
PBA-105A-21-53	*Uranophane-β*	4.97	59.43	0.00	0.04	0.01	0.07	3.31	0.00	-0.01	0.01	-0.02	-0.06	-0.07	14.97	82.81	8	20
PBA-105A-21-54	*Uraninite*	0.07	82.05	0.06	0.01	0.02	0.02	0.03	0.01	0.04	0.00	0.00	-0.03	-0.12	11.19	93.50	2	5
PBA-105A-21-55	*Uraninite*	0.28	83.35	0.06	0.01	0.00	-0.04	0.21	0.00	-0.01	0.00	0.02	0.05	-0.10	11.69	95.68	0	0
PBA-105A-21-56	*Uraninite*	1.25	78.82	0.06	0.02	0.05	0.25	1.25	0.00	0.10	-0.01	-0.01	0.01	-0.04	12.64	94.44	22	60
PBA-105A-22-57	*Uranophane-β*	5.24	54.56	0.00	0.01	-0.01	-0.07	4.95	0.01	-0.11	0.10	0.00	-0.03	-0.05	15.29	80.16	0	0
PBA-105A-22-58	*Uraninite*	0.26	81.35	0.07	0.03	0.06	-0.05	0.24	0.00	0.02	0.02	0.01	-0.04	-0.10	11.43	93.48	0	0
PBA-105A-23-60	*Uranophane-β*	6.89	61.10	-0.01	0.02	0.05	0.18	4.86	0.00	0.02	0.03	-0.03	0.05	-0.10	18.03	91.23	22	53
PBA-105A-23-61	*Schoepite*	-0.01	76.28	-0.01	0.00	-0.03	-0.14	0.08	-0.01	0.05	0.90	0.00	0.01	-0.03	10.42	87.74	0	0
PBA-105A-23-62	*Uraninite*	0.91	78.05	0.06	0.04	0.01	0.11	0.71	0.01	0.03	0.04	0.02	-0.03	-0.10	11.92	91.91	11	28
PBA-105A-24-63	*Becquerelite*	0.16	79.15	0.00	0.03	0.09	0.05	0.90	0.01	0.03	0.01	0.03	0.01	-0.05	11.29	91.77	5	13
PBA-105A-25-64	*Uranophane-β*	5.19	58.73	0.01	0.02	0.03	0.03	4.45	0.01	0.04	0.06	-0.03	0.05	-0.01	15.64	84.26	4	10
PBA-105A-25-65	*Ianthinite*	0.00	78.37	0.00	0.02	-0.02	-0.08	0.05	-0.01	0.02	0.14	-0.02	0.03	-0.09	10.57	89.22	0	0
PBA-105A-25-66	*Uraninite*	0.12	79.90	0.05	0.04	0.06	0.05	0.86	0.01	0.02	0.02	-0.02	0.00	-0.01	11.33	92.47	4	12
PBA-105A-26-67	*Schoepite*	0.02	68.47	0.01	0.01	0.01	-0.03	0.04	0.01	0.07	0.23	0.00	-0.06	-0.12	9.30	78.18	0	0
PBA-105A-26-68	*Uranophane-β*	5.84	59.53	0.01	0.01	0.02	0.04	3.92	0.01	0.00	0.03	-0.02	0.00	0.04	16.25	85.69	5	11
PBA-105A-26-69	*Uraninite*	0.23	81.32	0.09	0.02	0.04	0.18	0.36	0.01	-0.01	0.02	-0.02	-0.02	-0.05	11.45	93.71	16	44
PBA-105-1-70	*Ianthinite*	-0.04	79.65	0.00	0.03	0.03	-0.09	0.07	0.01	-0.10	0.39	-0.01	-0.01	0.00	10.78	90.96	0	0
PBA-105-1-71	*Uraninite*	0.06	79.70	0.04	0.03	0.09	0.25	0.48	0.04	-0.02	0.03	-0.05	0.03	-0.04	11.10	91.86	22	61
PBA-105-2-72	*Uranophane-β*	7.02	59.84	0.01	0.01	-0.01	-0.11	4.07	0.00	-0.18	-0.01	-0.01	-0.01	-0.05	17.61	88.56	0	0
PBA-105-2-73	*Ianthinite*	-0.05	78.57	0.00	0.01	0.02	0.00	-0.01	0.00	0.04	0.01	0.00	-0.04	-0.04	10.51	89.15	0	0
PBA-105-3-74	*Ianthinite*	-0.02	79.95	0.01	0.02	0.00	0.04	0.02	-0.01	0.00	0.06	-0.01	0.00	-0.12	10.74	90.83	4	10
PBA-105-3-75	*Uraninite*	0.96	76.58	0.06	0.03	0.11	0.43	1.02	0.01	-0.01	0.03	-0.01	0.07	-0.14	11.97	91.28	40	107
PBA-105-3-76	*Uranophane-β*	6.94	60.15	0.01	0.01	0.00	0.05	4.43	-0.01	0.12	0.03	-0.01	0.00	-0.14	17.78	89.53	6	14
PBA-105-3-77	*D. Schoepite*	0.01	75.19	0.00	0.00	0.02	-0.01	0.00	0.02	-0.07	0.05	0.02	-0.02	-0.03	10.15	85.46	0	0
PBA-105-4-78	*Ianthinite*	-0.03	81.56	0.01	0.01	0.01	0.03	0.01	0.00	0.17	0.06	-0.01	-0.05	-0.03	10.97	92.83	2	6
PBA-105-4-79	*Uranophane-β*	6.10	59.25	0.01	0.02	0.05	-0.09	5.46	-0.01	-0.10	0.03	0.02	-0.01	-0.04	17.13	88.07	0	0
PBA-105-4-80	*Ianthinite*	0.27	79.51	0.02	0.02	0.11	0.05	0.12	0.07	0.00	0.03	-0.03	-0.08	-0.10	11.14	91.34	4	12
PBA-105-5-81	*Uraninite*	-0.02	77.01	0.01	0.00	0.01	0.20	-0.01	0.00	0.11	0.10	-0.02	0.01	0.02	10.38	87.85	18	49
PBA-105-5-82	*Uranophane-β*	7.04	59.73	0.01	0.00	0.59	-0.02	4.41	-0.01	0.16	0.00	-0.03	0.04	-0.01	18.07	90.05	0	0
PBA-105-6-83	*Ianthinite*	-0.03	77.98	0.00	0.01	0.03	-0.05	0.04	0.00	-0.08	0.05	0.01	-0.05	-0.05	10.47	88.59	0	0
PBA-105-7-84	*Ianthinite*	-0.03	79.73	0.00	0.01	0.25	0.09	0.00	0.01	0.13	0.09	0.01	0.00	-0.11	10.84	91.15	8	21
PBA-105-7-85	*Uranophane*	6.84	58.59	0.00	0.01	0.07	0.03	3.87	0.01	0.08	-0.02	-0.01	-0.08	-0.13	17.22	86.72	4	9
PBA-105-7-86	*Uraninite*	0.41	79.43	0.07	0.03	0.07	0.18	0.33	0.00	-0.04	0.03	0.00	0.03	-0.01	11.42	92.00	16	44
PBA-105-8-87	*Ianthinite*	0.01	77.46	0.01	0.00	0.59	0.01	0.06	0.01	-0.03	0.09	-0.01	-0.03	-0.12	10.70	88.93	1	2
PBA-105-8-88	*Uranophane-β*	6.62	59.21	0.03	0.02	0.59	-0.04	4.34	0.05	-0.05	0.01	-0.01	0.02	-0.07	17.57	88.46	0	0
PBA-105-9-89	*Ianthinite*	-0.04	82.36	0.02	0.01	0.03	-0.02	0.03	0.00	0.03	0.07	-0.03	-0.03	-0.19	11.04	93.58	0	0
PBA-105-9-90	*Ianthinite*	-0.04	77.80	0.00	0.01	0.01	-0.07	0.09	0.00	0.12	0.20	0.00	-0.08	-0.10	10.46	88.69	0	0
PBA-105-10-91	*Uranophane-β*	6.06	57.67	-0.01	0.00	0.03	-0.02	4.23	0.00	0.09	0.00	-0.01	-0.03	-0.11	16.33	84.42	0	0

Table 2. Elemental wt% of electron microporbe analyses of uranium minerals from the Nopal I deposit, Chihuahua, Mexico.

Elemental Weight Percent

Sample	Mineral	Si	U	S	Ti	Fe	Pb	Ca	Al	Th	K	V	Zr	Ba	O	Total	Age (Ma)	1σ (Ma)
PBA-105-10-92	*Ianthinite*	0.02	75.88	0.00	0.01	0.00	0.05	0.07	0.02	0.05	0.07	-0.01	-0.03	-0.02	10.28	86.47	5	12
PBA-105-10-93	*Uraninite*	1.33	75.83	0.03	0.03	0.09	0.45	1.68	0.01	0.00	0.05	0.03	0.00	-0.12	12.53	92.07	43	114
PBA-105-11-94	*Ianthinite*	-0.05	75.55	-0.01	0.02	0.00	0.09	-0.01	0.01	-0.05	0.06	-0.03	-0.03	-0.12	10.07	85.80	9	24
PBA-105-11-95	*Uranophane-β*	5.02	56.72	0.00	0.01	0.13	0.05	4.39	-0.01	-0.15	0.00	0.00	0.02	-0.13	15.13	81.47	7	16
PBA-105-11-96	*Becquerelite*	1.65	71.12	0.06	0.02	0.37	0.46	1.78	-0.01	-0.04	0.06	0.04	-0.02	-0.09	12.42	87.97	47	121
PBA-105-12-98	*Uranophane-β*	6.86	58.29	0.01	0.02	0.07	0.00	3.95	0.00	0.02	-0.01	-0.01	-0.05	-0.10	17.25	86.47	0	0
PBA-105-12-99	*Ianthinite*	0.00	78.77	0.00	0.01	0.24	-0.02	0.25	0.02	-0.10	0.29	-0.03	0.01	-0.06	10.82	90.39	0	0
PBA-105-12-100	*Uranophane-β*	5.70	54.49	0.01	0.01	3.47	0.11	3.88	0.21	-0.03	0.02	0.02	-0.05	-0.12	17.06	84.99	15	33
PBA-105-12-101	*Uraninite*	0.87	78.85	0.04	0.03	0.06	0.24	1.20	0.01	0.06	0.12	-0.01	0.00	-0.14	12.19	93.67	22	60
PBA-105-13-102	*Schoepite*	0.00	73.06	0.02	0.01	0.64	0.02	-0.01	0.02	-0.01	0.24	-0.02	0.03	-0.06	10.18	84.23	2	6
PBA-105-13-103	*Ianthinite*	0.19	80.27	0.01	0.01	0.15	0.00	0.05	0.07	0.05	0.09	0.03	0.01	0.01	11.23	92.18	0	0
PBA-105-14-104	*Ianthinite*	-0.04	76.82	0.01	0.01	-0.01	0.03	-0.04	0.00	-0.16	0.05	0.01	0.03	-0.02	10.28	87.24	3	8
PBA-105-14-105	*Ianthinite*	0.10	79.71	0.01	0.03	0.16	0.06	0.16	0.05	0.07	0.44	0.03	-0.03	-0.09	11.15	91.97	6	15
PBA-105-15-106	*Ianthinite*	-0.02	77.20	-0.01	0.03	0.33	-0.01	0.01	-0.01	-0.03	0.12	0.00	0.00	-0.05	10.53	88.22	0	0
PBA-105-15-107	*Uranophane-β*	5.64	61.76	0.02	0.96	0.34	-0.06	3.37	0.00	0.03	0.03	0.07	0.02	-1.48	16.77	89.01	0	0
PBA-105-15-108	*Schoepite*	0.05	71.03	0.01	0.02	3.98	-0.12	0.06	0.05	-0.08	0.13	-0.01	-0.03	0.04	11.40	86.77	0	0
PBA-105-16-109	*Ianthinite*	-0.01	79.49	0.01	-0.01	-0.02	-0.04	0.06	0.01	0.04	0.12	-0.02	-0.05	-0.14	10.67	90.39	0	0
PBA-105-16-110	*Uranophane-β*	6.57	53.54	0.01	0.00	0.67	-0.04	4.12	0.00	0.00	0.05	0.00	0.02	-0.12	16.63	81.61	0	0
PBA-105-16-111	*Ianthinite*	0.00	79.59	0.00	0.01	0.05	0.07	0.01	-0.01	-0.02	0.11	0.02	-0.02	-0.05	10.75	90.62	7	18
PBA-105-16-112	*Schoepite*	-0.04	72.17	0.00	0.02	-0.01	-0.06	0.03	0.00	0.02	0.14	0.05	0.07	-0.06	9.75	82.25	0	0
PBA-105-18-117	*Ianthinite*	-0.04	81.72	-0.01	0.01	0.00	0.06	0.03	0.00	0.10	0.13	-0.02	0.05	-0.07	10.99	93.10	6	16
PBA-105-18-118	*Uranophane-β*	7.26	58.03	0.00	0.02	0.01	-0.03	3.90	-0.01	-0.08	-0.02	0.05	0.02	-0.01	17.67	86.96	0	0
PBA-105-18-119	*Ianthinite*	0.01	78.11	0.01	0.02	0.08	0.00	0.68	0.01	0.16	0.13	-0.04	-0.04	-0.13	10.84	90.06	0	0
PBA-105-19-120	*D. Schoepite*	-0.05	77.34	0.00	0.02	0.00	0.01	0.00	-0.01	-0.12	0.02	0.03	0.02	-0.11	10.35	87.79	1	3
PBA-105-19-121	*D. Schoepite*	-0.02	78.30	0.00	0.00	0.05	0.03	2.43	0.02	-0.10	0.00	0.03	-0.04	-0.09	11.51	92.37	3	7
PBA-105-19-122	*Uranophane-β*	6.41	56.67	0.01	0.00	0.18	0.03	4.29	0.00	-0.01	-0.01	0.01	-0.04	-0.04	16.69	84.27	3	7
PBA-105-19-123	*Schoepite*	0.00	75.46	0.00	0.02	0.48	0.03	0.15	0.03	0.04	0.16	0.00	0.01	-0.14	10.47	86.84	3	7
PBA-105-20-124	*Uranophane-β*	6.74	59.53	0.01	0.01	-0.02	-0.01	4.67	0.00	0.05	-0.01	-0.01	0.00	-0.05	17.54	88.56	0	0
PBA-105-20-125	*Ianthinite*	0.00	79.55	0.01	0.01	0.04	0.00	0.01	0.01	0.05	0.07	0.02	0.07	-0.08	10.79	90.63	0	1
PBA-105-21-126	*Schoepite*	0.04	74.33	0.00	0.02	2.12	0.08	0.05	0.09	-0.09	0.06	0.02	-0.03	-0.01	11.07	87.87	8	20
PBA-105-21-127	*Uranophane-β*	6.98	62.01	0.01	0.01	0.04	-0.12	4.38	0.00	-0.13	-0.02	0.00	-0.01	-0.08	18.02	91.45	0	0
PBA-105-21-128	*D. Schoepite*	-0.01	77.22	-0.01	0.01	0.24	-0.09	0.03	0.02	0.14	0.05	-0.04	-0.04	-0.11	10.47	88.18	0	0
PBA-105B-1-1	*Uranophane-β*	6.69	59.79	0.00	0.03	0.29	0.00	4.04	0.02	-0.06	-0.02	0.01	-0.03	0.05	17.43	88.35	1	1
PBA-105B-1-2	*Uraninite*	0.33	75.91	0.01	0.04	0.10	0.36	1.82	0.17	0.00	0.04	0.01	-0.07	-0.09	11.54	90.33	34	90
PBA-105B-1-3	*Uraninite*	0.18	77.85	0.04	0.04	0.16	1.46	1.24	0.03	-0.03	0.03	0.02	0.34	-0.08	11.56	92.95	133	362
PBA-105B-2-4	*D. Schoepite*	-0.05	77.12	0.01	0.01	0.24	-0.02	0.05	0.02	0.02	0.10	-0.01	0.06	-0.03	10.51	88.15	0	0
PBA-105B-2-5	*Uranophane-β*	6.28	61.30	0.01	0.03	0.10	0.04	4.15	0.01	-0.09	0.04	-0.01	-0.02	-0.05	17.11	89.07	4	10
PBA-105B-3-6	*Ianthinite*	-0.02	78.67	0.00	0.02	0.04	0.13	0.03	0.00	-0.05	0.03	-0.02	0.00	-0.02	10.59	89.52	12	33
PBA-105B-3-7	*Schoepite*	0.01	72.76	0.01	0.02	0.01	-0.08	0.13	0.01	0.01	0.29	-0.02	0.02	-0.12	9.90	83.16	0	0
PBA-105B-4-8	*Ianthinite*	-0.02	78.92	0.00	0.03	0.00	0.02	0.03	0.01	-0.03	0.03	0.04	-0.03	-0.05	10.64	89.73	2	5
PBA-105B-4-9	*Ianthinite*	-0.03	78.20	0.00	0.03	0.04	0.08	0.00	0.01	0.02	0.13	-0.03	-0.01	0.06	10.55	89.12	7	19
PBA-105B-5-10	*Uraninite*	0.07	78.01	0.03	0.00	0.29	0.28	2.26	0.02	0.17	0.01	-0.01	-0.01	-0.07	11.67	92.82	25	69
PBA-105B-5-11	*Uranophane-β*	6.74	63.08	0.00	0.02	0.01	-0.06	4.28	0.00	-0.07	-0.01	0.02	0.04	-0.10	17.89	92.08	0	0

Table 2. Elemental wt% of electron microporbe analyses of uranium minerals from the Nopal I deposit, Chihuahua, Mexico.

Elemental Weight Percent

Sample	Mineral	Si	U	S	Ti	Fe	Pb	Ca	Al	Th	K	V	Zr	Ba	O	Total	Age (Ma)	1σ (Ma)
PBA-105B-5-12	*Ianthinite*	0.03	78.44	0.01	0.02	-0.01	-0.02	-0.01	0.03	0.04	0.05	-0.01	0.01	-0.03	10.63	89.27	0	0
PBA-105B-5-13	*Ianthinite*	-0.03	80.32	0.02	0.05	0.02	0.02	0.01	-0.01	-0.13	0.07	-0.02	-0.01	-0.17	10.79	91.31	2	6
PBA-105B-6-14	*D. Schoepite*	-0.04	76.48	0.01	0.02	0.02	-0.01	0.03	-0.01	0.11	0.50	-0.01	-0.04	-0.11	10.34	87.50	0	0
PBA-105B-6-15	*D. Schoepite*	-0.04	78.59	0.01	0.04	0.00	0.01	0.19	0.00	0.02	0.31	-0.03	-0.05	-0.04	10.65	89.81	1	2
PBA-105B-6-16	*D. Schoepite*	0.02	75.56	0.00	0.02	0.04	-0.06	0.09	0.01	-0.03	0.08	-0.03	-0.01	-0.13	10.23	86.06	0	0
PBA-105B-7-17	*Ianthinite*	-0.03	80.68	0.00	0.02	0.03	0.02	0.03	0.00	0.02	0.48	0.00	0.03	-0.03	10.96	92.28	2	6
PBA-105B-7-18	*Uraninite*	0.36	77.07	0.04	0.04	0.05	0.42	0.62	-0.01	-0.04	0.20	0.03	0.06	-0.18	11.18	90.06	39	105
PBA-105B-7-19	*Uraninite*	0.13	83.33	0.07	0.02	0.05	0.13	0.08	-0.01	-0.05	0.03	0.03	0.02	-0.09	11.51	95.39	11	31
PBA-105B-8-20	*Uranophane-β*	7.06	57.96	0.00	0.01	0.03	0.04	3.46	0.00	0.00	-0.01	-0.02	0.00	-0.05	17.21	85.78	5	11
PBA-105B-8-21	*Ianthinite*	-0.03	80.86	0.00	0.01	0.65	0.17	-0.03	0.00	-0.02	0.06	0.00	0.04	0.00	11.14	92.93	16	43
PBA-105B-8-22	*Uraninite*	0.49	79.45	0.06	0.03	-0.01	0.30	0.68	0.00	-0.11	0.22	0.04	0.11	-0.12	11.69	93.07	27	75
PBA-105B-10-23	*Uranophane-β*	7.06	59.38	0.00	0.01	0.03	0.02	4.79	-0.01	0.07	0.07	-0.03	-0.04	-0.08	17.92	89.36	3	6
PBA-105B-10-24	*Ianthinite*	-0.03	77.75	0.00	0.02	0.01	0.03	-0.01	0.00	0.05	0.02	0.00	0.07	-0.21	10.45	88.41	3	7
PBA-105C-1-1	*Ianthinite*	0.16	79.81	0.01	0.01	0.19	0.06	0.02	0.04	-0.04	0.00	-0.02	0.02	-0.09	11.03	91.35	5	15
PBA-105C-1-2	*Uraninite*	0.38	77.64	0.03	0.05	0.08	0.17	1.14	0.00	-0.03	0.02	0.00	-0.02	-0.09	11.42	90.93	16	42
PBA-105C-2-3	*Schoepite*	0.01	75.54	0.01	0.02	0.15	-0.01	0.08	0.00	0.04	0.36	-0.03	-0.03	-0.12	10.30	86.50	0	0
PBA-105C-2-4	*Schoepite*	0.05	74.36	0.02	0.01	0.31	-0.02	0.13	0.02	0.05	0.43	-0.02	-0.06	-0.08	10.33	85.72	0	0
PBA-105C-2-5	*Uranophane-β*	7.42	59.32	0.01	0.02	0.05	-0.09	4.25	0.00	0.08	0.02	0.01	-0.03	-0.07	18.16	89.33	0	0
PBA-105C-2-6	*Uraninite*	0.20	79.38	0.04	0.04	0.13	0.20	1.30	0.00	-0.03	0.03	0.00	0.02	-0.03	11.56	92.90	18	49
PBA-105C-2-7	*Ianthinite*	0.03	81.04	0.01	0.01	0.02	-0.02	0.02	0.00	0.03	0.02	-0.03	0.01	-0.03	10.94	92.12	0	0
PBA-105C-3-8	*Ianthinite*	-0.03	77.52	0.00	0.01	0.00	0.08	0.03	0.02	-0.04	0.03	-0.02	0.03	-0.03	10.43	88.17	8	20
PBA-105C-3-9	*Uraninite*	0.04	78.36	-0.01	0.01	0.11	0.21	2.28	0.02	0.02	0.00	-0.01	0.08	-0.08	11.59	92.74	19	52
PBA-105C-3-10	*Uranophane-β*	6.91	57.61	-0.01	0.01	0.03	0.08	3.66	0.01	-0.01	-0.01	0.04	-0.03	-0.07	17.11	85.43	9	22
PBA-105C-4-11	*Ianthinite*	-0.02	81.08	0.00	0.01	-0.01	-0.17	-0.02	0.00	0.04	0.04	0.00	0.00	-0.07	10.86	92.02	0	0
PBA-105C-4-12	*Schoepite*	-0.02	72.37	0.00	0.02	-0.04	0.13	-0.01	0.00	0.02	0.03	-0.02	0.02	-0.16	9.69	82.28	12	32
PBA-105C-5-13	*D. Schoepite*	-0.02	79.21	0.00	0.01	0.17	0.13	0.05	0.01	-0.01	0.51	-0.01	-0.01	-0.11	10.83	90.93	12	33
PBA-105C-5-14	*Uranophane-β*	6.43	56.60	0.01	0.01	0.47	0.00	4.17	0.02	0.04	0.00	0.02	0.07	-0.10	16.88	84.73	0	0
PBA-105C-7-15	*Uraninite*	0.15	79.03	0.00	0.02	0.10	0.17	1.52	0.01	-0.02	0.02	-0.01	0.07	-0.15	11.49	92.58	15	41
PBA-105C-8-16	*Schoepite*	-0.02	74.80	0.00	0.02	0.48	0.16	-0.02	-0.01	0.02	0.15	0.00	0.07	-0.11	10.30	85.99	15	39
PBA-105C-9-18	*Schoepite*	-0.05	75.77	0.00	0.02	0.13	-0.11	-0.01	0.00	0.12	0.20	0.00	0.01	-0.11	10.24	86.50	0	147
PBA-105C-11-19	*Soddyite*	2.53	74.22	0.05	0.02	0.04	0.57	2.20	0.01	0.02	0.00	0.00	0.02	-0.11	13.87	93.55	55	16
PBA-105C-11-20	*Uranophane-β*	5.97	57.98	0.00	0.02	-0.01	0.05	4.51	0.01	-0.13	0.03	0.04	-0.04	0.02	16.42	85.03	6	17
PBA-105C-12-21	*Schoepite*	-0.04	73.24	0.00	0.03	0.42	0.07	0.40	0.00	0.00	0.01	0.03	-0.01	0.01	10.18	84.41	7	0
PBA-105C-12-22	*Schoepite*	-0.05	74.25	0.01	0.02	-0.02	0.00	2.31	-0.02	0.01	0.03	-0.04	-0.01	-0.05	10.81	87.43	0	17
PBA-105C-12-23	*Uranophane-β*	5.15	60.66	0.01	0.02	0.55	0.06	3.35	0.00	-0.01	0.19	0.00	-0.07	-0.01	15.65	85.64	7	0
PBA-105C-13-24	*Schoepite*	-0.03	74.03	0.01	0.02	0.02	-0.06	0.00	-0.01	0.00	1.34	0.00	0.05	-0.02	10.23	85.69	0	9
PBA-105C-13-25	*Uranophane-β*	7.12	59.66	0.01	0.03	0.23	0.03	3.77	0.05	0.00	-0.01	0.01	0.03	-0.02	17.82	88.76	4	81
PBA-105C-15-26	*Uraninite*	0.81	77.85	0.04	0.04	0.02	0.37	1.34	0.00	0.07	0.03	0.00	-0.08	-0.09	12.01	92.58	34	1
PBA-105C-15-27	*Ianthinite*	-0.05	80.19	0.00	0.01	0.77	0.00	0.02	0.00	0.06	0.04	0.02	-0.01	-0.14	11.09	92.21	0	13
PBA-105C-16-28	*D. Schoepite*	-0.04	77.01	-0.01	0.02	0.27	0.05	0.02	0.02	-0.02	0.42	-0.02	-0.04	-0.13	10.50	88.32	5	14
PBA-106-1-3	*Uranophane-β*	6.75	59.24	0.01	0.02	0.49	0.04	4.01	0.02	0.06	0.02	0.06	-0.01	-0.04	17.55	88.27	5	43
PBA-106-3-7	*Uranophane-β*	6.94	60.40	0.01	0.02	0.22	0.02	4.29	0.01	-0.04	0.01	0.02	0.00	-0.05	17.86	89.79	2	0
PBA-106-4-8	*Uranophane-β*	6.60	57.19	0.00	0.01	0.07	0.04	3.63	-0.01	-0.15	0.02	0.01	-0.06	-0.04	16.66	84.24	6	18

Table 2. Elemental wt% of electron microporbe analyses of uranium minerals from the Nopal I deposit, Chihuahua, Mexico.

Elemental Weight Percent

Sample	Mineral	Si	U	S	Ti	Fe	Pb	Ca	Al	Th	K	V	Zr	Ba	O	Total	Age (Ma)	1σ (Ma)
PBA-106-7-9	*Uranophane-β*	6.61	57.98	0.00	0.03	0.23	0.14	4.02	0.04	-0.06	0.00	0.02	-0.01	-0.11	17.09	86.15	18	0
PBA-106-8-10	*Uranophane-β*	6.49	56.81	0.00	0.01	0.07	0.01	4.15	0.00	-0.10	0.01	0.02	-0.04	-0.02	16.71	84.27	1	16
PBA-113-9-46	*Uranophane-β*	6.12	60.13	0.00	0.01	0.05	-0.07	4.84	0.00	-0.04	0.29	0.07			17.12	88.64	0	16
PBA-108-1-1	*Uranophane-B*	7.04	62.14	0.02	0.01	0.06	-0.07	3.88	0.01	-0.10	0.00	0.00	-0.01	-0.06	17.94	91.10	0	0
PBA-108-2-2	*Uranophane-B*	7.10	55.28	-0.01	0.01	0.05	0.06	4.46	0.01	-0.01	0.15	0.04	0.04	0.00	17.41	84.61	8	18
PBA-108-2-3	*Uranophane-B*	8.95	57.69	0.03	0.01	0.55	-0.13	4.72	0.19	-0.04	0.09	0.02	0.05	-0.10	20.31	92.63	0	0
PBA-108-4-4	*Uranophane-B*	6.34	56.23	0.00	0.01	0.03	0.06	3.66	0.00	-0.02	0.03	0.00	-0.02	-0.06	16.27	82.65	7	16
PBA-108-5-5	*Uranophane-B*	7.06	57.42	0.00	0.02	0.02	-0.01	3.57	0.01	0.02	0.04	0.03	-0.07	0.02	17.23	85.43	0	0
PBA-108-5-6	*Uranophane-B*	7.24	56.32	0.02	0.01	0.25	-0.02	5.07	0.06	0.03	0.12	0.01	0.00	-0.06	18.07	87.22	0	0
PBA-108-6-7	*Uranophane-B*	6.57	61.84	0.01	0.02	0.03	0.06	4.56	0.01	-0.05	0.21	0.06	0.01	-0.11	17.74	91.13	7	17
PBA-108-7-8	*Uranophane-B*	6.37	56.27	0.01	0.01	0.20	-0.04	3.79	0.06	0.11	0.04	0.30	0.03	-0.06	16.75	83.93	0	0
PBA-108A-1-1	*Uranophane-B*	6.58	57.59	0.00	0.02	0.05	0.06	3.81	0.00	0.08	-0.01	-0.02	-0.03	-0.04	16.77	84.95	7	26
PBA-108A-2-2	*Uranophane-B*	6.34	58.45	0.01	0.01	0.03	0.10	4.42	0.00	-0.19	0.34	0.06	0.01	-0.07	16.97	86.73	11	40
PBA-108A-2-3	*Uranophane-B*	7.16	58.67	0.00	0.00	0.01	0.04	4.52	0.00	-0.01	0.17	0.07	0.00	0.09	17.97	88.72	5	19
PBA-108A-3-4	*Uranophane-B*	6.94	62.20	0.01	0.16	0.09	-0.03	3.83	0.02	0.10	-0.01	-0.02	-0.04	-0.28	17.92	91.27	0	0
PBA-108A-3-5	*Uranophane-B*	7.14	60.46	0.01	0.04	0.10	0.02	4.29	0.02	-0.13	0.00	-0.03	-0.02	-0.14	18.01	90.09	2	7
PBA-108A-4-6	*Uranophane-B*	6.93	61.35	0.01	0.01	0.00	0.00	4.93	0.04	0.06	0.11	0.00	-0.05	-0.06	18.18	91.63	0	0
PBA-108A-4-7	*Uranophane-B*	7.34	58.53	0.02	0.02	0.01	0.11	4.58	0.01	0.23	0.09	0.00	-0.04	-0.16	18.14	89.08	12	44
PBA-109-1-1	*Uranophane-B*	6.52	59.37	0.02	0.00	0.03	-0.01	4.52	0.06	0.19	0.08	0.01	-0.01	0.02	17.35	88.18	0	0
PBA-109-2-2	*Uranophane-B*	6.66	57.20	0.02	0.00	0.04	0.08	4.13	0.04	-0.09	0.81	0.04	0.03	0.25	17.23	86.55	11	41
PBA-109-3-3	*Uranophane-B*	7.46	58.85	0.00	0.00	0.00	0.04	3.64	0.02	0.16	0.16	0.01	0.03	0.09	17.97	88.43	5	18
319B815-1-1	*Weeksite*	20.18	8.05	0.02	0.01	-0.01	0.04	0.57	0.33	-0.01	3.51	-0.02	0.00	0.00	67.34	100.04	34	98
319B815-1-2	*Weeksite*	20.27	8.01	0.00	0.01	-0.01	0.03	0.57	0.34	0.02	3.29	0.03	0.00	0.00	67.44	100.01	24	69
319B915-1-3	*Weeksite*	20.44	8.02	-0.01	0.01	-0.02	0.00	0.42	0.32	0.00	3.36	-0.01	0.00	0.00	67.47	100.04	0	0
319B915-1-4	*Weeksite*	20.25	7.93	0.01	0.01	0.02	0.02	0.49	0.33	0.00	3.66	0.02	0.00	0.00	67.25	100.00	16	46
319B915-1-5	*Uranophane-β*	14.43	11.07	0.00	0.02	0.02	0.01	3.41	0.11	0.01	3.42	0.02	0.00	0.00	67.48	100.00	9	29
319B1015-3-6	*Uranophane-β*	12.06	12.33	0.01	0.01	0.02	0.01	6.68	0.04	0.00	0.46	0.07	0.00	0.00	68.32	100.00	6	19
319B1015-3-7	*Uranophane-β*	11.83	12.61	0.01	0.00	0.00	0.00	5.85	0.03	0.03	1.26	0.08	0.00	0.00	68.30	100.00	2	6
319B1015-3-8	*Weeksite*	20.18	7.86	0.00	0.01	0.02	0.02	0.60	0.40	-0.01	3.89	-0.02	0.00	0.00	67.07	100.03	18	51
319B1015-3-9	*Uranophane-β*	12.02	12.51	0.01	0.02	-0.01	0.00	6.47	0.06	0.01	0.44	0.00	0.00	0.00	68.45	100.01	1	4
319A115-1-10	*Weeksite*	20.31	8.12	0.01	0.01	0.01	0.01	0.46	0.30	-0.01	3.25	-0.01	0.00	0.00	67.53	100.02	11	32
319A115-1-11	*Weeksite*	20.22	8.12	0.00	0.01	-0.01	0.01	0.42	0.41	-0.02	3.41	-0.02	0.00	0.00	67.45	100.05	9	26
319A15-2-12	*Weeksite*	20.39	7.96	0.02	0.00	0.01	0.01	0.48	0.30	0.00	3.41	0.01	0.00	0.00	67.40	100.00	7	19
319A15-2-13	*Weeksite*	20.30	7.86	0.01	0.01	0.03	0.01	0.48	0.26	0.00	3.92	-0.01	0.00	0.00	67.11	100.01	5	13
319A15-3-14	*Weeksite*	20.43	8.03	0.02	0.00	0.04	0.02	0.52	0.34	-0.02	3.06	0.00	0.00	0.00	67.57	100.02	16	
319A15-3-15	*Weeksite*	20.18	8.02	0.00	0.03	0.00	0.02	0.46	0.32	-0.02	3.78	-0.02	0.00	0.00	67.23	100.04	22	44
319A15-3-16	*Weeksite*	20.30	8.03	0.00	0.01	0.03	0.01	0.50	0.32	-0.01	3.41	0.00	0.00	0.00	67.41	100.01	11	62
319A15-4-17	*Weeksite*	20.27	7.99	0.01	0.01	0.04	0.03	0.54	0.36	0.00	3.37	0.00	0.00	0.00	67.39	100.00	27	30
32316-1-5		29.47	24.25	0.63	3.42	0.91	0.23	0.49	0.27	0.17	0.42	0.08	0.00	0.00	42.40	102.74		0
328A16-1-1	*Uranophane-β*	6.65	56.63	0.00	0.01	0.01	0.06	4.91	0.00	-0.13	0.23	0.02	0.00	0.00	21.02	89.56	7	22
328A16-2-2	*Uranophane-β*	6.73	58.04	0.00	0.02	0.00	0.08	4.85	0.00	-0.01	0.22	0.04	0.00	0.00	21.41	91.40	10	31
328A16-2-3	*Uranophane-β*	6.73	58.39	0.00	0.01	-0.01	-0.04	5.03	-0.01	0.03	0.19	0.01	0.00	0.00	21.50	91.89	0	0
328A16-2-4	*Uranophane-β*	6.71	57.87	-0.01	0.02	0.03	0.16	4.94	-0.02	0.01	0.20	0.05	0.00	0.00	21.38	91.36	20	62

Table 2. Elemental wt% of electron microporbe analyses of uranium minerals from the Nopal I deposit, Chihuahua, Mexico.

Elemental Weight Percent

Sample	Mineral	Si	U	S	Ti	Fe	Pb	Ca	Al	Th	K	V	Zr	Ba	O	Total	Age (Ma)	1σ (Ma)
328A16-2-5	*Uranophane-β*	6.56	55.19	0.00	-0.01	0.02	0.05	4.98	0.00	0.01	0.21	0.01	0.00	0.00	20.66	87.72	7	22
328A16-3-6	*Uranophane-β*	6.60	58.31	0.01	0.01	0.04	0.00	4.93	0.00	0.03	0.23	0.04	0.00	0.00	21.37	91.58	0	0
328A16-3-8	*Uranophane-β*	6.89	57.44	0.00	0.03	0.01	-0.02	4.74	0.10	0.00	0.22	0.03	0.00	0.00	21.51	90.97	0	0
328A16-5-9	*Uranophane-β*	6.56	55.68	0.00	0.00	-0.01	0.23	4.96	0.00	0.01	0.20	0.07	0.00	0.00	20.79	88.51	29	90
328A16-5-10	*Uranophane-β*	6.74	58.05	0.00	0.01	0.01	0.15	5.00	0.00	-0.02	0.23	0.00	0.00	0.00	21.45	91.65	19	58
328A16-6-11	*Uranophane-β*	6.37	55.30	0.00	-0.01	-0.03	0.31	4.95	-0.01	-0.01	0.22	0.09	0.00	0.00	20.51	87.77	40	123
328A16-6-12	*Uranophane-β*	6.64	56.75	0.00	0.01	0.00	0.31	4.88	0.00	0.06	0.25	0.08	0.00	0.00	21.10	90.06	40	121
328B16-1-13	*Weeksite*	12.98	42.08	0.00	0.01	0.05	0.05	3.76	2.91	0.00	3.45	-0.03	0.00	0.00	28.07	93.36	9	22
328B16-3-15	*Uranophane-β*	6.57	57.03	0.00	0.03	-0.04	0.00	3.61	0.02	0.04	0.20	0.04	0.00	0.00	20.52	88.06	0	0
328B16-3-16	*Uranophane-β*	8.53	52.33	0.01	0.01	0.02	0.18	4.65	2.60	-0.01	0.20	0.02	0.00	0.00	24.54	93.10	25	74
328B16-4-17	*Uranophane-β*	5.55	52.24	0.01	0.01	-0.01	-0.04	4.83	0.01	0.05	0.28	0.03	0.00	0.00	18.88	81.88	0	0
328B16-4-18	*Uranophane-β*	6.75	59.14	-0.01	0.01	0.02	0.01	4.95	-0.01	-0.03	0.28	0.05	0.00	0.00	21.68	92.89	2	5
31616-1-19	*Uranophane-β*	6.95	57.74	0.00	0.03	0.02	0.02	5.14	0.09	0.03	0.20	0.02	0.00	0.00	21.79	92.04	2	7
31616-1-20	*Uranophane-β*	5.82	57.72	0.00	0.03	0.06	0.03	5.09	0.03	0.06	0.23	0.02	0.00	0.00	20.45	89.53	3	11
31616-1-21	*Uranophane-β*	6.68	57.18	0.01	0.02	0.00	0.03	5.20	0.06	-0.01	0.19	-0.01	0.00	0.00	21.32	90.69	3	11
31616-2-22	*Schoepite*	0.14	72.63	0.00	0.03	0.01	0.27	0.57	-0.01	-0.09	0.32	-0.02	0.00	0.00	15.10	89.07	26	96
31616-2-23	*Soddyite*	4.53	62.67	0.00	0.00	-0.01	0.14	3.55	0.02	0.04	0.29	-0.02	0.00	0.00	19.30	90.55	16	54
31616-5-27	*Soddyite*	6.62	57.77	0.01	0.02	0.03	0.10	5.24	0.00	0.00	0.22	-0.02	0.00	0.00	21.36	91.36	0	0
328A16-3-7	*Uranophane-β*	1.54	69.86	0.01	0.02	0.00	0.23	1.42	0.02	0.17	0.40	0.00	0.00	0.00	16.58	90.26	13	40
328B16-2-14	*no good*	6.72	58.55	0.01	0.02	-0.01	0.05	4.37	0.03	0.15	0.27	-0.02	0.00	0.00	21.31	91.47	24	101
31616-3-24	*Schoepite*	16.13	20.96	0.00	0.01	0.13	0.14	1.46	13.67	0.10	0.06	0.02	0.00	0.00	35.48	88.17	5	20
31616-3-25	*Uranophane-β*	1.04	68.68	0.00	0.03	-0.04	0.08	0.01	1.29	-0.26	0.47	0.01	0.00	0.00	16.28	87.90	47	106
31616-4-26	*Uranophane-β*	5.58	60.55	0.00	0.02	0.02	-0.16	3.88	0.00	0.06	0.19	0.01	0.00	0.00	20.18	90.49	8	34
5-21-328A16-sp2	*Uranophane*	6.29	58.34	-	0.02	0.01	-0.02	4.63	0.56	-0.09	-0.01	0.27	0.02	-0.01	21.34	91.47	0	-
5-21-328A16-sp3	*Uranophane*	7.59	55.15	-	0.01	0.05	0.06	4.73	1.34	-0.04	0.00	0.28	0.00	-0.03	22.93	92.14	8	-
5-21-328A16-sp4	*Uranophane*	6.43	60.20	-	0.03	0.05	0.00	4.64	0.00	-0.10	0.00	0.32	0.03	0.00	21.44	93.14	0	-
5-21-328A16-sp5	*Uranophane*	7.02	57.58	-	0.02	-0.01	0.04	4.57	0.00	0.14	0.00	0.28	0.04	0.02	21.55	91.25	5	-
PBA105B-1	*Ianthinite*	-0.03	74.58	-	0.01	0.10	0.01	-0.01	0.00	-0.02	0.00	0.66	-0.03	-0.01	15.16	90.52	1	-
PBA105B-2	*Ianthinite*	-0.04	77.55	-	0.02	0.03	0.03	0.00	0.00	-0.08	-0.01	0.50	0.00	-0.04	15.70	93.84	3	-
PBA105B-3	*Ianthinite*	-0.03	74.29	-	0.01	0.17	0.01	-0.01	0.00	0.12	0.01	0.92	-0.01	-0.01	15.22	90.74	1	-
PBA105B-4	*Ianthinite*	-0.03	75.90	-	0.02	-0.01	-0.02	-0.01	0.00	0.10	0.01	0.44	-0.01	0.01	15.39	91.87	0	-
PBA105A-11-1	*Colloform*	0.08	53.39	-	0.01	1.01	0.10	0.16	0.03	0.04	0.02	0.48	-0.03	-0.04	11.49	66.81	14	-
PBA105A-9-1	*Uranophane*	4.82	57.53	-	0.01	0.31	-0.03	4.90	-0.01	-0.05	0.02	0.35	-0.02	-0.04	19.23	87.16	0	-
PBA105A-9-2	*Uranophane*	2.89	32.04	-	0.01	0.05	-0.03	2.00	-0.01	0.08	0.01	0.50	-0.02	-0.01	10.68	48.25		-
3165-1	*Uranophane*	7.67	57.54	-	0.01	0.05	0.01	4.80	1.38	-0.03	0.00	0.21	0.00	-0.04	23.54	95.21	2	-
3165-2	*Uranophane*	8.11	53.72	-	0.01	0.01	0.01	4.62	1.80	0.06	0.00	0.32	0.01	0.03	23.62	92.30	1	-
3165-3	*Uranophane*	6.41	56.91	-	0.02	0.02	0.03	4.95	1.00	-0.10	0.00	0.24	0.01	0.00	21.72	91.31	4	-
3161-1	*Uranophane*	11.35	42.33	-	0.05	0.10	0.06	3.47	6.57	0.02	0.00	0.25	0.02	0.01	28.84	93.07	11	-
3161-2	*Uranophane*	7.23	57.32	-	0.01	-0.01	0.01	4.87	0.62	-0.04	0.01	0.35	0.00	-0.02	22.36	92.79	1	-
PBA-108A-5-8	*Uranophane-B*	7.05	61.42	0.01	0.02	0.03	0.12	4.06	0.04	-0.09	0.03	0.11	0.13	-0.11	18.11	91.14	16	-
PBA-108A-5-9	*Uranophane-B*	7.10	57.52	0.00	0.02	0.03	0.04	3.66	0.06	-0.12	0.00	0.05	0.02	-0.13	17.38	85.89	6	-
PBA-108A-6-10	*Uranophane-B*	6.42	57.68	0.00	0.01	0.04	-0.11	3.60	0.02	0.00	-0.01	0.08	-0.07	-0.03	16.57	84.42	0	-
PBA-108A-6-11		0.00	54.55	0.00	0.01	0.04	0.07	4.37	0.00	-0.04	0.09	0.14	0.03	-0.15	9.23	68.55	-	-

Table 2. Elemental wt% of electron microporbe analyses of uranium minerals from the Nopal I deposit, Chihuahua, Mexico.

Elemental Weight Percent

Sample	Mineral	Si	U	S	Ti	Fe	Pb	Ca	Al	Th	K	V	Zr	Ba	O	Total	Age (Ma)	1σ (Ma)
PBA-108A-7-12	*Uranophane-B*	7.58	59.15	0.02	0.03	0.06	-0.04	4.01	0.03	0.10	0.38	0.05	0.01	0.31	18.46	90.20	0	-
PBA-108A-8-13	*Uranophane-B*	8.26	57.12	0.01	0.04	-0.04	-0.10	3.96	0.07	0.04	0.53	0.04	0.07	0.36	18.96	89.46	0	-
PBA-108A(2)-1-1	*Uranophane-B*	6.60	60.97	0.00	0.01	0.03	-0.07	4.06	-0.01	-0.01	0.02	0.06	-0.09	-0.16	17.35	89.11	0	-
PBA-108A(2)-3-2	*Uranophane-B*	6.87	58.42	0.00	0.01	0.02	0.18	3.67	0.02	0.15	0.03	0.07	0.02	0.06	17.29	86.81	25	-
PBA-108A(2)-4-3	*Uranophane-B*	6.81	58.94	0.01	0.02	0.03	0.03	4.97	0.01	-0.11	0.05	-0.03	-0.09	0.00	17.67	88.55	4	-
TS2-1-1	*Uranophane-β*	6.76	61.50	0.01	0.01	0.01	0.06	4.89	0.03	-0.01	0.10	0.01	0.00	0.00	18.00	91.37	7	18
TS2-1-2	*Schoepite*	0.38	72.14	0.00	0.02	0.02	0.04	0.45	0.01	-0.05	0.09	0.01	0.00	0.00	10.36	83.52	4	11
TS2-1-3	*Schoepite*	0.01	73.54	0.00	0.02	0.02	0.01	0.01	0.04	-0.11	0.29	0.02	0.00	0.00	10.02	84.00	1	3
TS2-2-4	*Schoepite*	-0.02	74.60	0.00	0.02	0.03	0.09	0.05	0.02	-0.03	0.80	0.03	0.00	0.00	10.26	85.91	9	22
TS2-2-5	*Uranophane-β*	5.46	63.45	0.00	0.03	-0.03	0.16	0.08	0.31	-0.06	1.61	-0.01	0.00	0.00	15.39	86.50	19	46
TS2-2-6	*Schoepite*	-0.02	71.57	0.00	0.01	-0.04	0.09	0.03	0.03	0.03			0.00	0.00	9.65	81.41	9	3
TS2-3-8	*Uranophane-β*	6.65	59.72	-0.01	0.00	0.27	-0.02	5.10	-0.01	0.04	0.04	-0.02	0.00	0.00	17.75	89.58	0	8
TS2-3-11	*Soddyite*	4.00	71.84	0.00	0.02	0.18	-0.10	0.02	0.11	-0.07	0.01	0.01	0.00	0.00	14.40	90.59	0	0
TS2-3-12	*Soddyite*	4.43	67.60	0.01	0.01	0.05	0.04	0.08	0.47	0.06	0.06	0.01	0.00	0.00	14.66	87.48	4	0
TS2-5-13	*Soddyite*	3.73	72.77	0.00	0.01	0.02	-0.13	0.00	-0.01	0.02	0.05	0.02	0.00	0.00	14.06	90.68	0	11
TS2-5-14	*Ianthinite*	0.13	78.05	0.00	0.02	0.02	-0.03	0.03	0.13	0.00	0.10	-0.01	0.00	0.00	10.79	89.27	0	0
TS2-5-15	*Uraninite*	0.39	82.89	0.07	0.03	0.03	0.24	0.19	0.09	-0.04	-0.01	0.03	0.00	0.00	11.88	95.84	21	0
TS2-5-16	*Soddyite*	3.92	69.99	0.01	0.01	0.02	0.06	0.01	0.01	0.01	0.04	-0.01	0.00	0.00	13.92	87.99	6	55
TS2-6-17	*Uranophane-β*	6.49	59.17	0.01	0.02	0.15	-0.02	5.00	0.01	0.00	0.09	0.01	0.00	0.00	17.47	88.43	0	13
TS2-6-18	*Ianthinite*	0.00	78.41	0.00	0.11	0.04	-0.06	0.06	0.01	-0.07	0.11	0.00	0.00	0.00	10.67	89.42	0	0
TS2-6-19	*Uraninite*	0.26	81.21	0.06	0.03	0.03	0.12	0.18	0.10	-0.09	0.00	0.00	0.00	0.00	11.47	93.46	11	0
TS2-7-20	*Schoepite*	0.51	74.99	0.00	0.02	0.00	-0.04	0.04	0.65	-0.12	0.21	0.01	0.00	0.00	11.31	87.75	0	8
TS2-8-22	*Ianthinite*	0.23	82.16	0.05	0.03	-0.01	0.07	0.20	0.10	-0.04	0.13	-0.01	0.00	0.00	11.56	94.52	6	0
TS2-8-23	*Uraninite*	1.01	80.53	0.06	0.03	0.06	0.15	0.16	0.71	-0.14	0.01	-0.01	0.00	0.00	12.77	95.49	13	18
TS2-8-24	*Uraninite*	0.19	83.34	0.08	0.03	0.02	0.11	0.10	0.24	0.04	0.05	-0.01	0.00	0.00	11.78	95.96	9	36
TS2-9-25	*Soddyite*	3.95	71.28	0.00	0.02	0.04	-0.14	0.00	0.00	0.06	0.03	0.00	0.00	0.00	14.12	89.51	0	24
TS2-9-26	*Uranophane-β*	6.11	60.35	0.00	0.02	0.07	-0.07	4.15	0.11	-0.06	0.04	0.04	0.00	0.00	16.89	87.78	0	0
TS2-9-27	*Uranophane-β*	5.63	64.22	0.00	0.02	0.06	0.03	4.33	0.17	-0.12	0.09	-0.01	0.00	0.00	16.97	91.53	3	0
TS2-9-28	*Ianthinite*	0.02	77.39	0.01	0.04	-0.02	0.05	0.11	0.03	-0.13	0.34	-0.02	0.00	0.00	10.55	88.53	5	9
TS2-9-29	*Uraninite*	0.12	80.10	0.01	0.03	-0.05	0.37	1.37	0.01	-0.01	0.01	0.03	0.00	0.00	11.52	93.56	33	13
TS2-10-30	*Uranophane-β*	5.54	49.19	0.02	0.01	11.14	0.04	4.31	0.26	-0.01	0.15	0.03	0.00	0.00	19.75	90.45	6	74
TS2-10-31	*Ianthinite*	1.08	78.39	0.05	0.02	0.01	0.09	0.83	0.09	-0.03	0.05	0.00	0.00	0.00	12.26	92.87	8	16
TS2-10-32	*Soddyite*	3.98	69.33	0.00	0.03	-0.01	0.03	0.05	0.00	0.00	0.03	0.00	0.00	0.00	13.90	87.35	3	21
TS2-11-33	*Soddyite*	4.02	72.04	0.01	0.01	0.03	0.09	-0.01	-0.01	0.05	0.05	-0.01	0.00	0.00	14.30	90.60	9	7
TS2-11-34	*Uranophane-β*	7.06	57.27	0.00	0.01	-0.01	0.01	5.09	0.34	-0.04	0.11	0.03	0.00	0.00	18.13	88.04	1	21
TS2-11-35	*Uraninite*	0.45	83.76	0.06	0.04	0.01	0.16	0.14	0.04	0.00	0.00	-0.02	0.00	0.00	11.96	96.62	13	3
ST3-1	*Uranophane-β*	6.69	58.32	0.00	0.02	0.18	0.18	4.89	0.00	0.08	0.17	0.00	0.00	0.00	17.57	88.11	22	32
ST3-2	*Uranophane-β*	6.17	59.32	0.01	0.01	-0.03	-0.09	4.07	0.00	-0.05	0.67	0.00	0.00	0.00	16.76	87.01	0	11
ST3-4	*Uranophane-β*	8.28	58.95	0.88	0.02	0.45	0.65	1.83	3.98	-0.12	0.34	-0.02	0.00	0.00	22.79	98.16	75	0
ST3-2-5	*Uranophane-β*	6.12	57.12	0.00	0.01	0.17	-0.02	4.78	0.12	-0.01	0.23	-0.01	0.00	0.00	16.78	85.32	0	178
ST3-2-6	*Uranophane-β*	6.13	59.15	0.00	0.01	0.10	0.04	4.86	0.01	-0.08	0.20	-0.03	0.00	0.00	16.96	87.48	5	0
ST3-2-7	*Uranophane-β*	6.94	54.17	0.01	0.02	1.99	0.03	4.75	0.55	-0.11	0.27	0.02	0.00	0.00	18.50	87.24	4	12
ST3-3-8	*Uranophane-β*	6.45	59.47	0.01	0.02	0.00	-0.02	4.75	0.03	-0.03	0.28	0.01	0.00	0.00	17.34	88.36	0	2

Table 2. Elemental wt% of electron microporbe analyses of uranium minerals from the Nopal I deposit, Chihuahua, Mexico.
Elemental Weight Percent

Sample	Mineral	Si	U	S	Ti	Fe	Pb	Ca	Al	Th	K	V	Zr	Ba	O	Total	Age (Ma)	1σ (Ma)
ST3-3-11	*Soddyite*	4.51	63.13	0.04	0.03	0.45	1.15	3.82	0.05	0.07	0.31	0.01	0.00	0.00	15.62	89.17	40	0
ST3-4-15	*Uranophane-β*	7.20	60.05	0.02	0.01	0.16	0.00	4.50	0.02	-0.04	0.31	-0.03	0.00	0.00	18.22	90.50	0	50
ST3-5-17	*Uranophane-β*	6.42	58.15	0.00	0.03	0.12	-0.05	4.85	0.04	0.09	0.17	0.01	0.00	0.00	17.23	87.12	0	0
ST3-5-19	*Uranophane-β*	6.64	56.72	0.11	0.09	3.03	-0.09	4.53	0.06	-0.02	0.69	0.01	0.00	0.00	18.67	90.55	0	0
ST3-7-22	*Uranophane-β*	6.67	60.82	0.03	0.03	1.67	0.03	4.99	0.08	0.00	0.41	-0.04	0.00	0.00	18.65	93.36	3	0
ST3-8-25	*Uranophane-β*	6.85	58.82	0.01	0.00	-0.04	-0.03	5.19	0.01	-0.08	0.00	0.00	0.00	0.00	17.77	88.66	0	7
ST3-8-26	*Uranophane-β*	5.88	56.01	0.00	0.03	0.06	-0.02	4.44	0.03	-0.12	0.19	0.01	0.00	0.00	16.10	82.74	0	0
ST3-8-27	*Uranophane-β*	6.41	55.90	0.00	0.02	2.25	-0.04	4.92	0.12	-0.02	0.09	-0.02	0.00	0.00	17.86	87.56	0	0
ST3-9-28	*Uranophane-β*	6.02	56.17	0.01	0.05	-0.03	-0.03	4.79	0.02	-0.12	0.05	0.01	0.00	0.00	16.37	83.50	0	0
ST3-10-29	*Uranophane-β*	6.44	57.30	0.00	0.02	0.69	-0.09	5.02	0.03	0.09	0.24	0.02	0.00	0.00	17.46	87.32	0	0
ST3-10-31	*Uranophane?*	5.46	42.21	0.00	0.00	-0.03	0.02	3.66	0.00	-0.03	0.18	-0.02	0.00	0.00	13.37	64.91	4	0
ST3-11-32	*Uranophane-β*	6.63	61.52	0.00	0.00	0.01	-0.01	5.16	0.01	0.02	0.24	0.03	0.00	0.00	17.97	91.58	0	9
ST3-11-33	*soddyite*	3.23	69.08	0.04	0.03	0.23	0.41	3.12	0.06	-0.15	0.33	0.00	0.00	0.00	14.49	91.02	43	0
ST3-12-34	*Uranophane-β*	5.75	47.20	0.00	0.02	0.03	-0.03	3.72	0.02	0.04	0.03	-0.03	0.00	0.00	14.41	71.21	0	93
ST3-14-35	*Uranophane-β*	6.71	55.10	0.00	0.03	0.46	0.02	4.54	0.02	-0.05	0.07	0.00	0.00	0.00	17.11	84.07	3	0
ST3-15-36	*Uranophane-β*	8.90	57.01	0.01	0.01	0.07	0.15	4.29	4.17	-0.04	0.23	-0.04	0.00	0.00	23.29	98.13	19	6
ST3-15-37	*Uranophane-β*	6.72	56.63	0.00	0.01	0.80	-0.04	4.84	0.04	0.08	0.05	-0.02	0.00	0.00	17.59	86.76	0	44
ST3-16-38	*Uranophane-β*	6.39	59.51	0.01	0.02	-0.01	0.09	5.16	-0.01	0.10	0.01	0.05	0.00	0.00	17.41	88.73	11	0
ST3-17-39	*Uranophane-β*	6.62	57.61	0.00	0.01	0.13	-0.08	4.77	0.16	0.01	-0.01	-0.01	0.00	0.00	17.39	86.71	0	24
ST3-17-40	*Soddyite*	4.98	68.65	0.02	0.01	0.05	2.09	0.53	0.28	-0.03	0.38	-0.02	0.00	0.00	15.63	92.62	44	0
ST3-18-41	*Uranophane-β*	6.82	58.83	0.00	0.01	0.01	-0.05	4.91	0.02	-0.03	0.03	0.05	0.00	0.00	17.71	88.39	0	105
ST3-18-42	*Uraninite*	0.98	71.55	0.00	0.01	0.12	6.48	1.28	0.05	-0.03	0.07	0.00	0.00	0.00	11.85	92.37	611	0
ST3-19-43	*Uranophane-β*	6.54	59.48	0.01	0.00	0.01	0.00	5.06	0.00	0.10	0.05	-0.01	0.00	0.00	17.50	88.75	1	1559
ST3-19-44	*Soddyite*	0.94	73.15	0.13	0.05	0.40	0.81	1.53	0.27	-0.08	0.27	-0.01	0.00	0.00	12.19	89.74	80	1
ST3-20-45	*Uranophane-β*	6.47	55.88	0.01	0.01	0.00	0.01	4.64	0.00	-0.01	0.20	0.00	0.00	0.00	16.78	83.99	44	78
ST3-20-47	*Uranophane-β*	2.17	70.08	0.06	0.03	0.80	0.61	2.51	0.17	0.00	0.26	-0.01	0.00	0.00	13.57	90.25	44	112
ST3-21-48	*Uranophane-β*	6.29	59.33	0.00	0.01	0.00	-0.08	4.92	0.00	-0.02	0.03	0.00	0.00	0.00	17.13	87.73	0	106
ST3-21-49	*Uranophane-β*	6.47	58.58	0.00	0.00	0.53	-0.03	5.14	0.02	-0.03	0.00	-0.01	0.00	0.00	17.54	88.28	0	0
ST3-21-50	*Soddyite*	2.09	71.99	0.61	0.07	0.13	0.19	2.41	0.04	-0.02	0.51	-0.01	0.00	0.00	13.87	91.90	19	0
ST3-21-51	*Soddyite*	2.97	68.31	0.33	0.08	0.14	0.16	2.94	0.03	-0.07	0.39	-0.03	0.00	0.00	14.27	89.62	17	52
NOPL-ECP-1-TS1-1-57	*Soddyite*	4.43	69.96	0.01	0.02	0.00	0.06	0.01	0.09	-0.03	0.13	0.04	0.00	0.00	14.62	89.37	6	45
NOPL-ECP-1-TS1-2-58	*Ianthinite*	0.00	76.41	0.00	0.01	0.04	0.05	0.11	0.02	0.13	0.62	0.01	0.00	0.00	10.52	87.90	5	15
NOPL-ECP-1-TS1-4-63	*Soddyite*	3.57	68.09	0.01	1.78	0.19	0.09	0.14	0.03	-0.06	0.07	0.03	0.00	0.00	14.62	88.62	9	11
NOPL-ECP-1-TS1-4-64	*Schoepite*	-0.01	76.39	0.00	0.31	0.01	0.08	0.04	0.07	-0.02	0.15	0.00	0.00	0.00	10.59	87.65	8	25
NOPL-ECP-1-TS1-5-66	*Soddyite*	3.98	71.64	-0.01	0.01	0.00	0.07	-0.02	-0.02	-0.01	0.07	0.02	0.00	0.00	14.18	89.98	7	20
NOPL-ECP-1-TS1-6-69	*Soddyite*	4.21	70.21	0.00	0.02	0.04	-0.03	-0.01	0.04	0.06	0.22	0.02	0.00	0.00	14.36	89.17	0	18
NOPL-ECP-1-TS1-6-71	*Soddyite*	4.07	69.89	0.00	0.00	-0.03	0.05	-0.02	0.00	0.02	0.17	0.02	0.00	0.00	14.08	88.32	5	0
NOPL-ECP-1-TS1-7-74	*Soddyite*	1.72	71.44	0.00	0.02	0.02	-0.01	0.15	0.00	-0.04	0.15	0.00	0.00	0.00	11.67	85.17	0	12
NOPL-ECP-1-TS1-8-75	*Soddyite*	4.11	69.79	0.01	0.03	-0.04	0.02	-0.01	0.13	0.04	0.08	0.01	0.00	0.00	14.22	88.43	2	0
NOPL-ECP-1-TS1-9-79	*Soddyite*	4.09	68.96	0.00	0.02	-0.01	0.04	0.00	0.17	-0.05	0.18	-0.01	0.00	0.00	14.11	87.57	4	6
NOPL-ECP-1-TS1-10-81	*Soddyite*	4.03	70.04	0.00	0.03	0.01	0.04	-0.02	0.00	-0.13	0.12	0.01	0.00	0.00	14.05	88.33	4	10
NOPL-ECP-1-TS1-11-83	*Soddyite*	2.34	68.76	0.00	0.03	-0.01	-0.03	0.01	0.02	-0.06	0.86	0.04	0.00	0.00	12.15	84.21	0	9
TS3-1-36	*Uranophane-β*	6.95	59.96	0.00	0.03	-0.02	0.08	4.95	0.13	-0.02	0.00	-0.02	0.00	0.00	18.07	90.16	10	0

Table 2. Elemental wt% of electron microporbe analyses of uranium minerals from the Nopal I deposit, Chihuahua, Mexico.

Elemental Weight Percent

Sample	Mineral	Si	U	S	Ti	Fe	Pb	Ca	Al	Th	K	V	Zr	Ba	O	Total	Age (Ma)	1σ (Ma)
TS3-1-37	*Schoepite*	0.10	74.79	0.00	0.02	-0.02	0.25	0.31	0.03	-0.06	0.01	0.02	0.00	0.00	10.35	85.88	24	25
TS3-1-39	*Soddyite*	4.04	72.42	0.00	0.02	0.02	-0.03	0.04	0.06	-0.10	0.07	-0.01	0.00	0.00	14.41	91.08	0	61
TS3-2-40	*Soddyite*	4.04	69.30	0.00	0.02	0.09	0.00	0.01	0.01	0.02	0.05	0.02	0.00	0.00	14.02	87.58	0	0
TS3-2-42	*Uranophane-β*	6.56	60.17	0.01	0.00	0.17	0.05	4.56	0.08	0.02	0.09	-0.01	0.00	0.00	17.56	89.26	5	0
TS3-3-43	*Compregnacite*	0.46	69.38	0.01	0.01	-0.02	0.04	0.00	0.02	0.00	1.86	0.06	0.00	0.00	10.30	82.14	4	14
TS3-3-44	*Compregnacite*	0.34	70.07	0.01	0.01	0.00	0.02	-0.01	0.02	0.03	0.93	0.05	0.00	0.00	10.08	81.58	3	10
TS3-3-45	*Uranophane*	7.12	62.92	0.00	0.02	0.06	0.35	0.11	0.17	-0.04	1.36	-0.01	0.00	0.00	17.10	89.21	40	6
TS3-4-46	*Soddyite*	4.07	70.22	0.00	0.02	0.02	0.11	0.00	0.01	-0.04	0.08	-0.02	0.00	0.00	14.11	88.64	11	101
TS3-5-47	*Uranophane-β*	7.20	58.39	0.00	0.01	0.02	0.12	4.33	0.20	-0.09	0.17	0.01	0.00	0.00	18.01	88.46	15	27
TS3-5-48	*Soddyite*	3.95	70.70	0.01	0.01	0.35	-0.01	0.03	0.05	0.08	0.04	-0.01	0.00	0.00	14.24	89.46	0	39
TS3-6-49	*Uranophane-β*	7.00	58.91	0.01	0.02	0.01	0.04	4.76	0.13	-0.10	0.01	0.02	0.00	0.00	17.94	88.82	4	0
TS3-6-50	*D. Shoepite*	-0.03	76.92	-0.01	0.04	-0.03	0.17	0.16	0.00	-0.02	0.09	0.02	0.00	0.00	10.42	87.82	16	10
TS3-6-51	*Compregnacite*	0.16	73.18	0.01	0.02	0.00	0.46	0.22	0.14	-0.04	2.04	-0.01	0.00	0.00	10.69	86.92	45	40
TS3-7-52	*Uranophane-β*	6.98	60.63	0.00	0.02	0.08	0.08	4.21	0.07	-0.08	0.25	-0.03	0.00	0.00	17.91	90.23	9	117
TS3-7-53	*Compregnacite*	0.13	67.84	0.01	0.01	0.57	-0.02	0.01	0.03	-0.07	1.04	0.02	0.00	0.00	9.78	79.44	0	24
TS3-7-54	*D. Shoepite*	-0.03	76.01	0.00	0.02	0.06	0.22	0.25	0.00	0.12	0.05	-0.01	0.00	0.00	10.36	87.09	20	0
TS3-7-55	*Compregnacite*	0.23	75.32	0.00	0.02	0.15	0.07	0.21	0.06	0.09	2.00	-0.01	0.00	0.00	11.02	89.18	7	52
TS3-8-56	*Soddyite*	3.62	62.63	0.00	0.01	1.20	0.14	0.02	0.15	-0.05	0.04	-0.04	0.00	0.00	13.19	81.00	16	17
TS3-8-57	*Soddyite*	4.02	69.63	0.00	0.01	0.08	0.04	-0.01	0.00	0.08	0.03	0.05	0.00	0.00	14.04	87.97	4	40
TS3-8-58	*Soddyite*	3.75	72.17	0.00	0.02	0.07	-0.16	0.02	0.02	0.06	0.06	-0.02	0.00	0.00	14.04	90.21	0	10
TS3-8-59	*Soddyite*	3.98	69.17	0.00	0.02	0.05	0.00	-0.02	0.00	0.03	0.05	0.01	0.00	0.00	13.89	87.20	0	0
TS3-9-60	*Soddyite*	3.88	72.15	0.00	0.02	0.05	0.04	0.02	0.02	-0.08	0.06	-0.02	0.00	0.00	14.17	90.40	4	0
TS3-9-61	*Soddyite*	3.27	60.94	0.01	0.12	7.23	0.03	0.03	0.35	0.12	0.03	0.03	0.00	0.00	15.48	87.63	3	10
TS3-9-62	*Soddyite*	3.95	71.44	0.00	0.02	0.09	-0.02	0.01	0.26	-0.06	0.03	0.01	0.00	0.00	14.40	90.21	0	8
TS3-9-63	*Schoepite*	0.79	75.17	0.04	0.03	0.19	0.50	0.41	0.06	0.03	0.56	0.01	0.00	0.00	11.53	89.30	47	0
TS3-9-64	*Soddyite*	3.91	71.54	0.01	0.02	0.04	0.07	-0.01	0.02	-0.13	0.01	0.02	0.00	0.00	14.12	89.75	7	122
TS3-10-65	*Uranophane-β*	5.70	58.99	0.00	0.02	0.06	0.06	4.96	0.11	0.02	0.05	0.00	0.00	0.00	16.55	86.52	7	18
TS3-10-66	*Soddyite*	3.87	71.76	0.00	0.03	0.03	0.05	0.02	0.04	-0.07	0.06	0.02	0.00	0.00	14.15	90.04	5	19
TS3-11-68	*soddyite*	3.96	70.63	-0.01	0.03	-0.01	-0.01	-0.01	0.02	0.06	0.04	0.03	0.00	0.00	14.06	88.82	0	13
TS3-11-69	*D. Shoepite*	0.69	76.79	0.03	0.03	0.04	0.35	0.32	0.05	-0.05	0.50	0.04	0.00	0.00	11.50	90.32	32	0
TS3-12-70	*Soddyite*	3.95	71.69	0.00	0.01	0.06	0.14	-0.01	0.03	-0.01	0.03	-0.02	0.00	0.00	14.20	90.11	14	88
TS3-12-71	*Uranophane-β*	5.58	56.20	0.00	0.00	3.16	-0.02	4.72	0.21	-0.07	0.03	0.01	0.00	0.00	17.36	87.28	0	36
TS3-12-72	*Uraninite*	0.07	83.14	0.02	0.02	0.00	1.30	0.09	0.25	-0.07	-0.01	-0.02	0.00	0.00	11.61	96.49	111	0
TS3-13-73	*D. Shoepite*	0.11	75.84	0.06	0.04	1.37	0.07	0.16	0.83	-0.05	0.13	0.02	0.00	0.00	11.84	90.47	7	310
TS3-13-74	*Soddyite*	3.91	72.81	0.01	0.04	-0.01	0.10	0.01	0.04	-0.02	0.00	0.02	0.00	0.00	14.33	91.27	10	18
TS3-13-75	*Uraninnite*	0.28	82.91	0.05	0.03	0.00	0.71	0.00	0.18	-0.02	-0.01	-0.02	0.00	0.00	11.73	95.90	61	26
TS3-13-76	*Soddyite*	3.89	71.98	0.00	0.01	0.19	-0.02	0.03	0.11	-0.10	0.03	0.01	0.00	0.00	14.30	90.54	0	161
TS3-13-77	*Uraninite*	0.39	82.95	0.04	0.03	0.01	0.73	0.01	0.11	0.01	0.03	-0.06	0.00	0.00	11.78	96.09	62	0
TS3-14-78	*Soddyite*	4.06	72.30	0.01	0.02	0.01	-0.04	-0.01	0.02	-0.09	0.03	-0.01	0.00	0.00	14.38	90.83	0	167
TS3-14-79	*Uraninite*	0.18	84.89	0.03	0.03	0.06	0.31	0.02	0.09	-0.05	0.00	0.00	0.00	0.00	11.80	97.42	26	0
TS3-14-80	*Ianthinite*	0.06	80.15	0.01	0.02	0.01	0.24	0.08	0.20	-0.07	0.14	-0.01	0.00	0.00	11.11	92.03	21	71
TS3-15-81	*Ianthinite*	0.01	77.70	0.00	0.01	0.01	0.45	0.14	0.12	-0.07	0.15	-0.01	0.00	0.00	10.67	89.25	42	47
TS3-15-82	*Uraninite*	0.05	84.76	0.03	0.02	0.01	0.32	-0.02	0.01	0.11	0.00	0.01	0.00	0.00	11.55	96.88	27	104

Table 2. Elemental wt% of electron microporbe analyses of uranium minerals from the Nopal I deposit, Chihuahua, Mexico.

Elemental Weight Percent

Sample	Mineral	Si	U	S	Ti	Fe	Pb	Ca	Al	Th	K	V	Zr	Ba	O	Total	Age (Ma)	1σ (Ma)
TS3-16-83	*Uranophane-β*	5.21	51.46	0.01	0.02	5.32	0.05	4.41	0.17	0.17	0.06	0.00	0.00	0.00	17.12	84.02	7	69
TS3-16-84	*Compregnacite*	0.88	68.89	0.01	0.01	1.68	0.02	-0.01	0.05	0.04	1.11	0.02	0.00	0.00	11.30	84.02	2	20
TS3-16-85	*Soddyite*	3.98	70.56	0.01	0.02	0.29	0.11	-0.01	0.03	-0.07	0.12	0.02	0.00	0.00	14.23	89.35	11	5
TS3-16-86	*Uraninite*	0.21	84.71	0.05	0.02	0.00	0.26	-0.04	0.02	-0.07	0.02	-0.04	0.00	0.00	11.67	96.96	22	-
TS3-16-87	*Schoepite*	0.18	76.23	0.01	0.01	0.06	0.00	0.19	0.14	0.08	0.16	-0.04	0.00	0.00	10.70	87.77	0	-
NOP-ELP-1-155-1	*Soddyite*	-	70.20	0.00	0.01	0.01	-0.04	-0.01	0.01	-0.06	0.30	0.03	0.00	0.00	14.09	88.65	0	-
NOP-ELP-1-155-2	*Uranophane-β*	-	56.03	0.01	0.01	2.43	-0.05	4.60	0.07	0.04	0.24	0.09	0.00	0.00	17.03	86.18	0	-
NOP-ELP-1-155-2-3	*Uranophane-β*	-	58.69	0.01	0.03	0.02	0.05	4.85	0.35	-0.08	0.06	0.02	0.00	0.00	17.31	87.63	6	-
NOP-ELP-1-155-2-4	*Soddyite*	-	70.41	0.00	0.02	0.00	0.07	0.01	0.02	0.03	0.16	0.02	0.00	0.00	14.10	88.83	7	-
NOP-ELP-1-155-3-5	*Soddyite*	-	69.24	0.00	0.03	-0.03	-0.02	0.00	0.01	-0.05	0.23	0.01	0.00	0.00	13.98	87.55	0	-
NOP-ELP-1-155-3-6	*Soddyite*	-	70.18	0.00	0.02	-0.03	-0.04	0.00	0.01	-0.01	0.21	0.02	0.00	0.00	14.07	88.52	0	-
NOP-ELP-1-155-3-7	*Uranophane-β*	-	58.72	0.00	0.01	-0.01	0.04	4.77	0.35	0.04	0.06	0.02	0.00	0.00	17.98	88.86	5	-
NOP-ELP-1-155-4-8	*Soddyite*	-	70.54	0.00	0.01	0.00	0.08	-0.01	0.00	-0.15	0.11	-0.02	0.00	0.00	14.11	88.93	8	-
NOP-ELP-1-155-4-9	*Uranophane-β*	-	59.51	0.00	0.00	0.03	0.03	4.97	0.11	-0.05	0.04	0.06	0.00	0.00	16.59	87.00	3	-
NOP-ELP-1-155-4-10	*Soddyite*	-	69.31	0.00	0.02	0.00	0.05	0.04	0.11	-0.08	0.06	-0.01	0.00	0.00	14.24	88.04	5	-
NOP-ELP-1-155-5-13	*Soddyite*	-	70.31	0.01	0.01	0.05	-0.01	-0.01	0.03	0.04	0.11	0.00	0.00	0.00	14.11	88.67	0	-
NOP-ELP-1-155-5-14	*D.Schoepite*	-	77.01	0.00	0.01	0.01	-0.02	0.12	0.66	-0.09	0.00	-0.07	0.00	0.00	10.96	88.80	0	-
NOP-ELP-1-155-6-19	*D.Schoepite*	-	73.73	0.01	0.04	0.01	1.34	0.52	0.08	-0.02	0.10	0.02	0.00	0.00	11.44	88.24	129	-
NOP-ELP-1-155-6-20	*D. Schoepite*	-	75.81	0.01	0.03	0.01	0.82	0.11	0.12	-0.02	0.05	0.01	0.00	0.00	10.47	87.46	77	-
NOP-ELP-1-155-7-21	*Soddyite*	-	74.56	0.01	0.03	0.05	0.57	0.07	0.32	-0.03	0.23	0.00	0.00	0.00	13.29	91.60	54	-
NOP-ELP-1-155-7-24	*Soddyite*	-	72.94	0.04	0.02	0.05	0.20	0.67	0.13	-0.04	0.09	-0.01	0.00	0.00	15.92	95.01	20	-
NOP-ELP-1-155-8-25	*Soddyite*	-	71.67	0.01	0.03	-0.02	0.21	0.01	0.22	-0.03	0.03	-0.04	0.00	0.00	14.11	90.04	21	-
NOP-ELP-1-155-8-26	*Ianthinite*	-	82.01	0.06	0.02	0.02	0.35	0.07	0.19	0.12	0.00	-0.05	0.00	0.00	11.99	95.43	30	-
NOP-ELP-1-155-9-28	*Soddyite*	-	70.23	0.01	0.02	0.03	0.08	-0.01	0.07	-0.06	0.16	0.01	0.00	0.00	14.14	88.75	8	-
NOP-ELP-1-155-9-32	*D. Schoepite*	-	75.30	0.03	0.03	0.02	0.10	0.15	0.19	0.06	0.06	0.01	0.00	0.00	11.07	87.56	10	-
NOP-ELP-1-155-10-33	*Soddyite*	-	70.85	0.00	0.03	0.02	-0.15	-0.01	0.02	0.08	0.14	0.01	0.00	0.00	14.06	89.12	0	-
NOP-ELP-1-155-10-35	*Schoepite*	-	69.68	0.02	0.02	0.07	0.01	0.06	0.62	-0.04	0.16	0.01	0.00	0.00	10.72	81.96	1	-
NOP-ELP-1-155-11-38	*weeksite*	-	73.45	-0.01	0.02	0.00	0.12	0.04	0.03	0.05	1.30	-0.01	0.00	0.00	10.28	85.37	12	-
NOP-ELP-1-155-11-39	*Soddyite*	-	69.73	0.01	0.02	0.00	-0.07	0.01	0.01	0.06	0.06	0.03	0.00	0.00	13.97	87.88	0	-
NOP-ELP-1-155-12-44	*Soddyite*	-	69.53	0.00	0.02	-0.02	-0.09	-0.01	0.01	-0.08	0.11	-0.01	0.00	0.00	14.05	87.84	0	-
NOP-ELP-1-155-12-46	*Soddyite*	-	70.00	0.00	0.03	0.03	0.47	0.01	0.00	0.02	0.43	-0.02	0.00	0.00	13.45	87.86	48	-
NOP-ELP-1-155-13-47	*D. Schoepite*	-	77.35	0.01	0.02	0.00	0.01	0.20	0.09	-0.04	0.11	0.02	0.00	0.00	10.66	88.51	1	-
NOP-ELP-1-155-13-48	*Soddyite*	-	71.43	0.00	0.02	0.04	0.08	0.08	0.10	0.08	0.05	-0.01	0.00	0.00	12.76	87.28	8	-
NOP-ELP-1-155-14-51	*Soddyite*	-	70.18	0.00	0.01	-0.01	-0.01	0.02	0.03	0.05	0.06	0.00	0.00	0.00	14.11	88.52	0	-
NOP-ELP-1-155-15-52	*Soddyite*	-	69.93	0.00	0.02	-0.04	0.06	-0.02	0.01	0.00	0.33	0.02	0.00	0.00	14.05	88.42	6	-

Note: All values are reported in wt%.

Appendix B

Table 3. Ion Microprobe U-Pb Data from Selected Uranium Minerals from the Nopal I Deposit

Sample	Mineral	$^{206}Pb/^{204}Pb^{*}$	Error % (1σ)	$^{207}Pb/^{204}Pb^{*}$	Error % (1σ)	$^{207}Pb/^{206}Pb^{*}$	Error % (1σ)
LMNH std	***Uraninite***	***34733.3***				***0.0538***	
7-20-PBA105A11-SP1	*Colloform Ur*	67.3	14	22.5	15	0.3345	1
7-20-PBA105A11-SP2	*Colloform Ur*	93.4	16	29.8	15	0.3189	1
7-20-PBA105A9-SP1	*Uranophane*	56.1	16	3.2	35	0.0558	14
7-20-PBA105A9-SP2	*Uranophane*	67.6	30	3.7	41	0.0516	10
5-15-3165-sp1	*Uranophane*	22.2	18	5.3	29	0.2376	6
5-16-3165-sp2	*Uranophane*	18.0	17	5.1	29	0.2843	3
5-16-3165-sp3	*Uranophane*	36.2	25	8.3	24	0.2298	5
5-16-3161-sp6	*Uranophane*	11.0	11	3.9	32	0.3607	6
5-16-3161-sp7	*Uranophane*	11.5	10	4.2	47	0.3596	0
5-21-328A16-sp2	*Uranophane*	10.0	10	3.7	9	0.3712	2
5-21-328A16-sp3	*Uranophane*	7.4	8	3.7	8	0.5103	15
5-21-328A16-sp4	*Uranophane*	32.1	21	5.5	21	0.1724	7
5-21-328A16-sp5	*Uranophane*	11.2	13	4.0	13	0.3608	3
5-21-328A16-sp7	*Uranophane*	50.5	17	5.5	22	0.1066	10
5-26-PBA105B8-sp1	*Ianthinite*	21.5	6	6.0	7	0.2805	1
5-26-PBA105B8-sp2	*Ianthinite*	21.6	7	6.0	7	0.2782	0
5-26-PBA105B8-sp3	*Ianthinite*	22.9	6	6.0	7	0.2628	1
5-26-PBA105B8-sp4	*Ianthinite*	25.3	7	6.3	7	0.2509	1

*SIMS

Table 4. $^{206}Pb/^{204}Pb$ - $^{238}U/^{204}Pb$ Isotopic Dates Calculated for Uranium Minerals from the El Nopal I

Samples	Mineral	$^{206}Pb/^{204}Pb$	Error% (1σ)	$^{238}U/^{204}Pb$	Error% (1σ)	t_6
LAMNH	***Uraninite***	***4200***		***76364***		***343,649,478***
5-21-328A16-sp7	Uranophane	31.8	17	639662	1	132,466
7-20-PBA105A11-SP1	CollUr	48.6	14	89878	9	2,142,348
7-20-PBA105A11-SP2	CollUr	74.7	16	45615	14	7,906,753
7-20-PBA105A9-SP1	Uranophane	37.4	16	501786	3	240,512
7-20-PBA105A9-SP2	Uranophane	48.9	30	479754	3	406,395
5-26-PBA105B8-sp5	Ianthinite	37.7	25	480260	1	254,401

Modern Day $^{206}Pb/^{204}Pb = 18.7$
All isotopic ratios are common Pb corrected

Table 5. Ion Probe U/U, Th/U and Activity Ratios from Selected Uranium Minerals from the Nopal I Deposit

Sample	Mineral	$^{234}U/^{238}U^{*}$	Error% (1σ)	$^{230}Th/^{238}U^{*}$	Error% (1σ)	$(^{234}U/^{238}U)_A$	$(^{230}Th/^{238}U)_A$	$(^{230}Th/^{234}U)_A$	t
7-20-PBA105A11-SP1	*CollUr*	0.00011989	15	0.000007467	15	0.9	2.1	2.5	0.00
7-20-PBA105A11-SP2	*CollUr*	0.00010579	104	0.000006581	27	0.9	2.0	2.5	0.00
7-20-PBA105A9-SP2	*Uranophane*	0.00005708	12	0.000006748	15	0.5	1.9	4.6	0.00
5-15-3165-sp1	*Uranophane*	0.00002089	34	0.000000062	25	0	0	0	0.00
5-16-3165-sp2	*Uranophane*	0.00005041	12	0.000000177	16	0.9	0.1	0.1	15,819
5-16-3165-sp3	*Uranophane*	0.00003303	12	0.000001041	15	0.6	0.7	1.2	0.00
5-16-3165-sp4	*Uranophane*	0.00005950	10	0.000000083	16	1.0	0.1	0.1	6,275
5-16-3165-sp5	*Uranophane*	0.00005320	10	0.000000974	23	0.9	0.6	0.7	132,299
5-16-3161-sp2	*Uranophane*	0.00005739	10	0.000000875	28	1.0	0.6	0.6	109,645
5-16-3164-sp1	*Uranophane*	0.00005318	12	0.000000975	15	1.0	0.6	0.7	136,435
5-16-3161-sp5	*Uranophane*	0.00005683	10	0.000000855	15	1.0	0.6	0.6	98,735
5-16-3161-sp7	*Uranophane*	0.00005830	6	0.000000766	14	1.0	0.5	0.6	87,084
5-21-328A16-sp1	*Uranophane*	0.00001357	11	0.000000185	15	1.0	0.6	0.6	101,590
5-21-328A16-sp2	*Uranophane*	0.00001419	10	0.000000208	15	1.0	0.6	0.6	108,584
5-21-328A16-sp3	*Uranophane*	0.00001450	8	0.000000044	16	1.1	0.1	0.1	12,473
5-21-328A16-sp4	*Uranophane*	0.00001450	11	0.000000014	15	0	0	0	0.00
5-21-328A16-sp5	*Uranophane*	0.00001383	12	0.000000026	16	1.0	0.1	0.1	6,636
5-21-328A16-sp6	*Uranophane*	0.00001189	17	0.000000039	21	0.9	0.1	0.1	14,733
5-21-328A16-sp7	*Uranophane*	0.00001298	12	0.000000044	17	0.9	0.1	0.1	14,926
5-26-PBA105B8-sp1	*Ianthinite*	0.00004643	17	0.000000547	15	0.8	0.4	0.5	81,324
5-26-PBA105B8-sp2	*Ianthinite*	0.00005313	10	0.000000527	15	1.0	0.4	0.4	57,345
5-26-PBA105B8-sp4	*Ianthinite*	0.00005691	15	0.000000145	17	1.0	0.1	0.1	12,855
5-26-PBA105B8-sp5	*Ianthinite*	0.00005546	12	0.000000141	14	1.0	0.0	0.0	4,180

SIMS*
Secular Equilibrium
$(^{234}U/^{238}U)_A = 1$
t = Ka

Appendix C

U/Pb dates were calculated by using the following equation:

$$\mathbf{t}_6 = \frac{1}{\lambda_{238}} * \ln \left[\frac{(^{206}Pb/^{204}Pb_{cor} - {}^{206}Pb/^{204}Pb_{MD})}{^{238}U/^{204}Pb} + 1 \right] \quad [1]$$

Where $\mathbf{t}_6$ corresponds to time, λ_{238} is the decay rate of ^{238}U ($1.55e^{-10}$), $^{206}Pb/^{204}Pb_{cor}$ is the corrected isotopic ratio for common lead of $^{206}Pb/^{204}Pb$ of the sample, $^{206}Pb/^{204}Pb_{MD}$ is the Modern Day value, and $^{238}U/^{204}Pb$ is the isotopic ratio of the sample.

U-Th disequilibria series methodology of dating was applied to samples whose U/Pb dates were not able to calculate. This methodology consists in correlate values by using several formulas:

$$(\mathbf{^{234}U/^{238}U})_\mathbf{A} = 1 + (\gamma_0 - 1) \times e^{(-\lambda_{234} * t)} \quad [2]$$

$$(\mathbf{^{230}Th/^{234}U})_\mathbf{A} = 1 - e^{(-\lambda_{230} * t)} \quad [3]$$

$$\mathbf{t} = \frac{-1}{\lambda_{230}} * \ln [1 - (^{230}Th/^{234}U)_A] \quad [4]$$

$$\gamma_0 = \left[\frac{(^{234}U/^{238}U)_A - 1}{e^{(-\lambda_{234} * t)}} + 1 \right] \quad [5]$$

Where $(^{234}U/^{238}U)_A$ and $(^{230}Th/2^{34}U)_A$ are the activity ratios of the sample, λ_{234} and λ_{230} are the decay constant of ^{234}U and ^{230}Th respectively ($2.829e^{-06}$ and 9.1933^{-06}, respectively), and **t** is time.